EDGEWOOD
RESEARCH,
DEVELOPMENT &
ENGINEERING
CENTER

ERDEC-TR-060

SOLID AEROSOL PROGRAM

Steven R. Lewis
ISRAEL AEC
Soreq NRC, Yavne, Israel

Alan T. Seitzinger
Eric Knoebel
RESEARCH & TECHNOLOGY DIRECTORATE

April 1993

Approved for public release; distribution is unlimited.

U.S. ARMY
CHEMICAL
AND BIOLOGICAL
DEFENSE AGENCY

Aberdeen Proving Ground, Maryland 21010-5423

Disclaimer

The findings in this report are not to be construed as an official Department of the Army position unless so designated by other authorizing documents.

REPORT DOCUMENTATION PAGE

Form Approved
OMB No. 0704-0188

1. AGENCY USE ONLY (Leave blank)	2. REPORT DATE	3. REPORT TYPE AND DATES COVERED
	1993 April	Final, 92 Feb - 93 Mar

4. TITLE AND SUBTITLE

Solid Aerosol Program

5. FUNDING NUMBERS

PR-10162622A553L

6. AUTHOR(S)

Lewis, Steven R.,* Seitzinger, Alan T., and Knoebel, Eric

7. PERFORMING ORGANIZATION NAME(S) AND ADDRESS(ES)

DIR, ERDEC,** ATTN: SCBRD-RT, APG, MD 21010-5423

8. PERFORMING ORGANIZATION REPORT NUMBER

ERDEC-TR-060

9. SPONSORING/MONITORING AGENCY NAME(S) AND ADDRESS(ES)

10. SPONSORING/MONITORING AGENCY REPORT NUMBER

11. SUPPLEMENTARY NOTES

*Exchange Scientist on sabbatical leave from Israel AEC, Soreq NRC, Yavne, Israel.

(Continued on page ii)

12a. DISTRIBUTION/AVAILABILITY STATEMENT

Approved for public release; distribution is unlimited.

12b. DISTRIBUTION CODE

13. ABSTRACT *(Maximum 200 words)*

Future NBC threats may include solid aerosols as well as vapor and liquids. The goal of this research program is to develop methodology to determine solid aerosol protection factors for enclosures and to express the controlling mechanisms in model calculations. The model program calculates theoretical vapor and size-dependent solid aerosol protection factors for an enclosure with pressure-driven penetration. Current studies of particulate penetration factors and settling rates are included. The model computer program provides an interactive tool appropriate for protection estimation, parameter sensitivity studies, and test procedure design. An experimental system providing real data on the parameters relevant to the calculations has been assembled. The system can be used to produce data for model calibration, verification, and prediction as well as to construct a database of generally applicable parameter values. Together with the model program, the facility will aid in optimizing integrity testing options for shelters and vehicles. When combined with empirical data, model results to date correlate well with observed behavior. Results indicate that size-dependent filtration of particles in apertures will be limited to the millimeter width level at pressure differentials up to only several millimeters water gauge. The extent of turbulent impaction of particles within the enclosure will strongly affect the solid aerosol protection factors.

14. SUBJECT TERMS

Solid aerosols	Protection factor	Enclosures
Shelters	Vehicles	Penetration
Settling	Ventilation kinetics	

15. NUMBER OF PAGES

119

16. PRICE CODE

17. SECURITY CLASSIFICATION OF REPORT	18. SECURITY CLASSIFICATION OF THIS PAGE	19. SECURITY CLASSIFICATION OF ABSTRACT	20. LIMITATION OF ABSTRACT
UNCLASSIFIED	UNCLASSIFIED	UNCLASSIFIED	UL

NSN 7540-01-280-5500

Standard Form 298 (Rev 2-89)
Prescribed by ANSI Std 239-18
298-102

11. SUPPLEMENTARY NOTES (Continued)

**When this work was performed, ERDEC was known as the U.S. Army Chemical Research, Development and Engineering Center (CRDEC), and the authors were assigned to the Research Directorate.

PREFACE

The work described in this report was authorized under Project No. 10162622A553L, CB Defense Assessment Technology. This work was started in February 1992 and completed in March 1993.

The use of trade names or manufacturers' names in this report does not constitute an official endorsement of any commercial products. This report may not be cited for purposes of advertisement.

This report has been approved for release to the public. Registered users should request additional copies from the Defense Technical Information Center; unregistered users should direct such requests to the National Technical Information Service.

BLANK

CONTENTS

LIST OF FIGURES

LIST OF PHOTOGRAPHS

SOLID AEROSOL PROGRAM

1. INTRODUCTION

1.1 Program goals

Future NBC (nuclear, biological and chemical) threats perceived to endanger armed forces on the battlefield may include solid aerosols as well as the more familiar vaporous and liquid compounds. Protection against all such threats is provided most effectively by collective protective enclosures supplied with filtered air at a suitable overpressure, thus preventing contaminants from penetrating against the pressure gradient. The effectiveness of enclosures, whether overpressure-protected or not, in preventing an unsafe level of exposure is clearly dependent on controlling leakage areas through which contaminants may enter.

Exposure is the integral of the threat concentration over time. The measure of protection provided is defined by the protection factor, being the ratio of the exposure one would sustain outside the enclosure to that sustained inside the enclosure for a given time duration. By definition, the protection factor is greater than or equal to one.

The determination of protection factors for enclosures such as vehicles and shelters is based to date on modelling the behavior of chemical agent simulant vapors. The question asked here is what changes may be needed to protection factor models based on vapors to account for size-dependent mechanisms affecting the defense against very small solid particles? Further, if vehicles and shelters need to be tested specifically for solid aerosols, what might be appropriate integrity-testing techniques?

The solid aerosols could conceivably take any of the following forms:

- all possible NBC agent particles (the most threatening in terms of respiratory penetration being in the range 0.5 - 5.0 microns)
- smoke, dust, obscurants, and resuspended particulates

The threatened objects as defined for the research program could involve:

- combat and armored vehicles, static or moving, with or without cannon fire
- fixed or mobile shelter structures
- either leaky or over-pressure protected
- suspect filter and housing integrity
- various leak characteristics (smooth, rough, sticky, greasy, etc.)

The goals of this research program are to develop the methodology needed to determine solid aerosol protection factors for enclosures in the particle size ranges of interest and to express the controlling mechanisms in model calculations. At a later stage of the program, these would be used in developing integrity-testing techniques.

1.2 Program Outline

1.2.1 Objectives

The research reported in this document concerns an exploratory program executed in the framework of the main author's one-year term as an Exchange Scientist with the Ventilation Kinetics group at ERDEC (Edgewood Research, Development and Engineering Center). Given the time limitation, on the one hand, and the generality of the program goals, on the other, there was a need to define objectives likely to be achieved under the constraints of time and knowledge gaps. The objectives which formed the basis for the one-year experimental program are to:

- identify, acquire and test instruments for disseminating and sampling candidate solid aerosols
- generate a theoretical understanding of physical phenomena to enable analysis of experiments
- interact with other individuals and agencies to learn the state of the art and to prevent duplication of efforts
- construct an experimental facility and carry out trials on enclosures to determine vapor and solid aerosol protection factors
- verify the results in light of current theoretical understanding through model calculations

1.2.2 Experimental and Computational Programs

The experimental program was designed to exploit as much of the existing capabilities of the Ventilation Kinetics group as possible while keeping in mind time and logistic constraints. Furthermore, after clarifying the status in the current literature on enclosure protection from solid aerosols, the decision was taken to concentrate on developing the ability to measure the relevant parameters individually. This would lead to a better fundamental understanding of the controlling phenomena than would a program of, say, testing integral exposures of actual vehicles or shelters. This would provide the foundation for future stages of the program once areas both of uncertainty and of special concern were identified and time and logistic constraints could be lifted. This being the situation, an experimental program was constructed with the following guidelines:

- the object of exposure experiments will be a 'dummy' enclosure with a volume on the order of a typical vehicle cabin; maximum control over residual leakage areas should be ensured
- a dedicated test facility should be located close to the laboratories of Bldg. 3161
- for greatest flexibility the powder dissemination system should be designed to produce a cloud of infinitely-variable duration in a confined but open-ended volume
- instrumentation must provide real-time measurement and computerized data acquisition for all relevant physical parameters
- candidate aerosols are to be environmentally acceptable

The program makes use of accumulated experience in the application of gaseous tracers, such as SF_6, in the determination of enclosure air exchange rate and as a vapor challenge simulant. SF_6 is an internationally recognized tracer for air movement and an ideal tool for measuring the protection factors for challenge vapors. This technology provides the basis for incorporation of the solid aerosol mechanisms, since air movement is the carrier of the particulate threat.

The experimental program comprised measurements of external and internal size-dependent solid aerosol count rates and mass concentrations and simulant vapor concentrations as well as the physical parameters needed to characterize the ventilation kinetics of the enclosure. Penetration into the completely sealed enclosure through a well-defined aperture was driven by pressure differential. Measurements to date sufficed to permit calibration and verification of a theoretical model of vapor and solid aerosol protection factors as envisioned by the goals.

Computations and models developed in the research program are performed in several scientific languages for IBM-compatible personal computers acquired especially for this purpose:

- Mathcad 3.1 (Mathsoft, Inc.) mathematical modelling
- ASYSTANT (Asyst Software Technologies, Inc.) numerical calculations and model equation curve fitting
- TableCurve 3.10 (Jandel Scientific) empirical data curve fitting
- Easyest LX (Asyst Software Technologies, Inc.) data acquisition
- Graftool (3-D Visions Corp.) graphical analysis

Several programs were written, primarily in Mathcad to serve the research program as utility codes for repetitive operations. These include:

- background-corrected particle count spectra
- concentration decay rates (for particles and vapors)
- theoretical size-dependent particulate settling rates (calculation and optimization)
- optical sensor size-dependent response calibration
- size-dependent particle penetration ratios

The final product of the computational research program is an interactive Mathcad model for the calculation of the vapor and size-dependent solid aerosol protection factors for a given enclosure and aperture. Penetration dynamics in the model are driven by pressure differential across the well-defined aperture. Measurements of the ventilation kinetic parameters in the experimental system are used to verify the air exchange rate calculated by the model. Theoretical particle filtration and settling rates are calculated based on models published in the literature. Empirical settling rates obtained from the experimental setup can also be used to verify measured protection factors. The model is a flexible tool for the analysis of empirical results, parameter sensitivity studies, testing procedure design, and protection estimation. Results of the model to date correlate reasonably well with measured data when empirical settling rates are used.

1.2.3 Experimental System Requirements

The solid aerosol dissemination system is a critical component of the experimental research system. It is required to continuously disseminate a variety of dry powders in a size range on the order of 0.1 - 10 microns. Energetic de-agglomeration is necessary to ensure reproducible size spectra for the smallest of sizes with as little pre-dissemination treatment as possible. Mass concentrations in the range 1-100 mg/m^3 are required to be maintained outside the test enclosure.

The instrumental setup is required to provide data on the following parameters:

- air exchange rate (SF_6 tracer decay method with one minute resolution)
- pressure differential (to 1 mm Water Gauge)
- air flow rate (10 - 1000 lpm)
- temperature differentials (0.5 degree C resolution)
- external and internal particle mass concentrations (at least 10^3 inside/outside ratio and better than 2 second response time)
- external and internal particle size counts (less than five minutes response time for one spectrum)
- external and internal SF_6 tracer vapor challenge concentrations (at least 10^3 inside/outside ratio)
- environmental conditions (wind speed, humidity, etc.)

1.3 Technical Report Objectives

This report is a compilation of progress achieved during the research program carried out from March 1992 to March 1993 at ERDEC. Starting with the broadly defined goals as stated in the Introduction, the research proceeded systematically in an effort to provide a sound technical base with which to address specific questions in the future. It has been a project of exploration and integration, the open literature concerning enclosure protection from solid aerosols having been found to leave many unanswered questions.

Since only limited practical feedback from potential users of the project at ERDEC has been forthcoming, the results have remained quite general. However, to the extent that the experimental facility and the computational tools which are the final product of the project are to be exploited, the Technical Report will aid the next generation of researchers in absorbing and employing them. The scientific background, gleaned from the literature, is included. Each segment of the experimental setup is described and the nuances of its application, as experienced by the main author, is explained. Computer programs of general value are documented for future applications. Their use requires familiarity primarily with the Mathcad 3.1 scientific programming language, whose use is highly recommended.

It is expected that the fruits of this program will aid threat analysts, operational scientists, simulation and modelling scientists in addressing their questions concerning the solid aerosol challenge with greater focus than previously.

2. LITERATURE SURVEY

2.1 Vapor Challenge Enclosure Protection

The contamination of a 'leaky' enclosure by an external toxic vapor cloud has been treated extensively in the literature (for example: Birenzvige, 1983a,b; Wadden and Sheff, 1983; Chester, 1988; Lewis, 1991). Typical results for some pollutants in indoor air quality studies have been summarized by Engelmann (1990). In general, the enclosure is treated as a well-mixed single compartment system exposed to a constant, spatially uniform threat concentration. Analytical solutions of the contaminant balance for the simplest cases provide useful equations for estimating the efficiency of protective measures. These solutions are often given in terms of an inside to outside ratio (a dose reduction factor) or, interchangeably, an outside to inside ratio (a protection factor).

The vapor protection factor, PF_v, for an enclosure is defined as the ratio of the dose (vapor concentration-time integral) which would result from exposure to an outside concentration during time T to the dose accumulated inside up to some time $t > T$. The governing parameter is volumetric air exchange or infiltration rate, R. The air infiltration rate of a leaky enclosure is determined by a complex combination of factors involving the nature of the enclosure envelope and its interactions with the contaminated environment. It represents the rates both of penetration of vapor and its flushing out after the cloud has passed. The estimation of air infiltration into enclosures in the short and long term is dealt with extensively in the literature of energy conservation, indoor air quality, and environmental health and is well beyond the scope of this discussion.

The degree of mixing within an enclosure is also a complex function of what in many cases may be imponderables unless well-focused measurements support its estimation (Shair, 1974). The existence of dead volumes, channeling, and short circuits may well negate the assumption of ideal mixing Suffice it to say that estimates of the air exchange rate and degree of mixing of the enclosure in question for the time period involved in the analysis of vapor protection are critical. Estimates may possibly derive from tracer gas decay measurement or direct air flowrate when feasible.

Our concern here includes scenarios in which the exposure duration, T, may be short compared to the time during which occupants are exposed to the threat inside the enclosure. Hence the protection factor must account for both time periods. Most analyses in the literature have been concerned with long-term exposures of poorly protected enclosures and ignore the exposure subsequent to passage of the cloud. This scenario toils under the assumption that occupants are instantly aware of the passage of the threat and immediately exit into fresh air, an unrealistic supposition at best. A full derivation of the equation for the vapor protection factor providing the required exposure scenario flexibility is given in Appendix A. For a uniform non-condensing vapor and ideal mixing in a single compartment, the balance equation leads to:

$$PF_v = \frac{R \cdot T}{R \cdot T + \exp(-R \cdot t) \cdot (1 - \exp(R \cdot T))} \quad (1)$$

2.2 Solid Aerosol Challenge Enclosure Protection

Crack filtering and interior surface deposition of particles involve three removal mechanisms: diffusion, gravitational settling and turbulent impaction. If a size-dependent filtering factor, f_p, and settling rate, β_p, are included with the air exchange rate as additional removal terms in the single compartment balance model, a complete expression for the particulate protection factor, PF_p, is obtained (see Appendix A for the full development):

$$PF_p = \frac{R_p \cdot T}{\left(\frac{f_p \cdot R}{R_p}\right)(R_p \cdot T + \exp(-R_p \cdot t) \cdot (1 - \exp(R_p \cdot T)))} \quad (2)$$

where:

$$R_p = R + \beta_p \quad (3)$$

A search of the open literature relevant to sheltering from particulate matter revealed few comprehensive treatments of the problem. The work performed by Engelmann (1992a,b) concerning sheltering effectiveness of buildings and vehicles defines a dose reduction factor, the inverse of the protection factor, in terms of particulate removal phenomena. Here equilibrium dynamics for a monodisperse challenge were studied, but underlying size-dependent mechanisms were not investigated. In the following sections published works are discussed which deal with these mechanisms separately and which are here subsequently integrated into a comprehensive model for calculating the size-dependent particulate protection factor for an enclosure given in Equation 2.

2.3 Air Exchange Rate

The rate of air exchange in a single well-mixed compartment, R in equations (1) and (2), is estimated ideally by the ratio of the air flowrate through the enclosure to the volume of the enclosure:

$$R \equiv \frac{Q}{V} \quad (4)$$

Standard methods for measuring the air exchange rate when the infiltration flow, Q, is not measurable are given in ASHRAE (1981). A practical method is by tracer gas dilution, covered in ASTM Standard E 741-80. Tracer gas concentration response analysis is also useful for detecting the numerous aberrations from ideal mixing which may occur (Nauman, 1981).

When considering a well-defined aperture as the sole source of infiltration into an enclosure, the crack flow equation can be used to estimate the air flow (ASHRAE 1981). With differential air pressure across the aperture as the driving force for penetration, the air flowrate is:

$$Q = C \cdot A_e \cdot (dp)^n \qquad (5)$$

where dp is the differential pressure, n is the characteristic flow exponent which varies between 0.5 and 1.0 depending on the Reynold's number (Kreith and Eisenstadt, 1957), C is a discharge coefficient and A_e is the 'effective' leakage area. It should be kept in mind that the effective leakage area is defined by the above relationship between the pressure differential and the flowrate. It will not in general equal the geometric area of the aperture opening, especially if the aperture is thick, narrow, rough or any combination of these factors.

2.4 Stirred Settling of Particles in Enclosures

Solid aerosol settling in enclosures with convective stirring has been researched widely, with several efforts at verifying model equations through controlled chamber tests seen in the open literature. Activity in this area has appeared in many fields: nuclear safety, fine powder processing, aerosol sampling, indoor air quality, and tropospheric photo chemistry.
Earlier works strove to give theoretical meaning to the observed exponential decay in the particle count concentration in small chambers:

$$dC(t)/dt = -\beta_p C(t) \qquad (6)$$

where the decay rate comprises uncoupled stirred settling (β_d) and diffusive deposition (β_d) components (Van de Vate, 1972; Harrison, 1979). Their analysis led to the expression:

$$\beta_p = \beta_s + \beta_d = \frac{v}{h} + \frac{S \cdot D}{V \cdot \sigma} \qquad (7)$$

where v is the terminal particle settling velocity, h is the chamber height, S the surface area, V the volume, D the particle diffusivity, and σ the diffusion boundary layer thickness at the wall.

Crump and Seinfeld (1981) later derived a more general formula for the turbulent deposition and gravitational settling of particulates in arbitrarily shaped chambers which couples the two components of the settling coefficient to the shape of the chamber and gives explicit expression to turbulent eddy diffusivity for a stirred chamber, similar to the results of Corner and Pendlebury (1951).

Crump and Seinfeld's equation for a rectangular chamber, of particular interest for our project, is, as expressed by Chen et al. (1992a) :

$$\beta_p \equiv \frac{2 \cdot U_t}{X_1}\left(\frac{1}{l}+\frac{1}{w}\right)+\frac{U_t}{h}\coth\left(\frac{X_1}{2}\right) \quad [1/\text{sec}] \qquad (8)$$

where l, w and h are the length, width and height, respectively, of the enclosure; U_t is the particle settling velocity, and:

$$X_1 = \frac{\pi \cdot U_t}{n \cdot \sin\left(\frac{\pi}{n}\right)\left(k_e \cdot D_B{}^{n-1}\right)^{1/n}} \qquad (9)$$

where D_B is the Brownian diffusion coefficient and k_e and n are related to the turbulent energy dissipation rate (and, hence, to the rate of power consumption/unit mass of air) due to all sources. The turbulent eddy diffusion coefficient, which does not appear explicitly in the model, has been defined as:

$$D_e = k_e \cdot Y^n \qquad (10)$$

where Y is the distance from the wall. The model of Crump and Seinfeld has been adopted here for use in the model calculations of settling in the stirred enclosure.

It will be seen later that the two parameters, k_e and n, are critical to the determination of the particulate settling rates. Several attempts to quantify and correlate them with empirical data were seen in the literature. Okuyama et al. (1986) reported experimental observations of particle settling in stirred tanks under various conditions of turbulent energy input. Results were compared to the theoretical results of Crump and Seinfeld in terms of particle size and turbulent intensity. The exponent n has a theoretical value of 2 according to Crump and Seinfeld, but Okuyama's data indicated a value of 2.7.

Chen, et al (1992a) used solid particle decay data in an environmental reaction chamber to determine both k_e and n as a function of vertical temperature gradients. Although the data of other researchers, which Chen, et al (1992a) analyzed, yielded best fits for n in the range 1.85 - 3.5, his results showed n=2 to be the best value, as Crump and Seinfeld proposed. However, the wide discrepancies in the published experimental values of the k_e-n pair of parameters sheds considerable doubt on the generality of their conclusion.

2.5 Crack Filtration of Solid Aerosols

The literature provides little comprehensive data on the size-dependent infiltration of solid aerosols into structures although several efforts have been made in the past to quantify this factor (Megaw, 1962; Cristy and Chester, 1981; Roed and Cannell, 1987). For example, based on early results Engelmann (1990), when calculating dose reduction factors, assumed that particles below 2 microns are not filtered during penetration into buildings. Much work is being in recent years on penetration of fine particles through orifices (Sutter, et al, 1980; Mitchell, et al, 1990; Fletcher and Verkouteren, 1992), although under larger pressure differences than interest

us here, and through respirator facepieces (Hinds and Kraske, 1987; Hinds and Bellin, 1987; Holton et al, 1987; Chen, et al, 1992b).

A review report by Schwendiman and Sutter (1977), concerning the transport of particles through gas leaks, summarized equations for the three controlling mechanisms: deposition by molecular diffusion, impaction by turbulent eddies and gravitational settling. Deposition by molecular diffusion is controlled by the diffusion coefficient, aperture length and the air flow rate. Empirical equations, verified for diffusion batteries by Sinclair, et al (1976), were presented. Eddy transport of particles to the aperture walls is determined by the inertial properties of the particles in the turbulent field. The fraction lost to turbulent impaction, F_T, is defined by:

$$F_T = 1 - \exp\left(-\frac{P \cdot K \cdot l_a}{A \cdot V}\right) \qquad (11)$$

where P is the aperture perimeter, A is the cross sectional area, l_a is the length of the aperture path, V is the average velocity and K is the true deposition velocity. Lacking sufficient experimental data for the very narrow apertures of interest to Schwendiman and Sutter (and to us) required to correlate K with particle size, Reynold's number and surface roughness, the terminal settling velocity is used, resulting in a minimum wall loss.

An approximation for the fraction lost by gravitational settling in a rectangular aperture, stipulating a uniform velocity profile, is given by:

$$F_G = \frac{l_a \cdot U_t}{V} \qquad (12)$$

2.6 Survey Conclusions

The nature of the research program was determined after reviewing the 'state of the art' regarding protection of enclosures from solid aerosol threats. Given the absence of any comprehensive treatment of a size-dependent particulate protection factor, the decision was taken to integrate available knowledge of the relevant physical mechanisms into a flexible mathematical model which would become an analytical tool to serve the program goals. In parallel with the modeling effort, the experimental system would be designed to provide real data on all the parameters required to calculate the protection factors for both vapors and solid aerosols. Data on actual protection factors would serve to verify the model for the exposure scenarios of greatest interest.

This approach was chosen over other options, such as direct measurements of integral vehicle exposures or equilibrium level exposure of enclosures (see Engelmann, 1992b), not just for short term logistic reasons, but primarily to provide a tool which would advance the fundamental understanding of physical mechanisms which combine to determine the protection factor for any scenario. It was felt that direct application of published parameter values without a firm scientific basis could yield 'blind' results of limited validity and, hence, worth.

The main equations for the protection factor model as applied to vapor and particles, with variable threat duration and exposure time, are shown in Appendix A as derived by the main author. They may be fed either theoretically derived parameter values or, alternatively, any combination of empirically obtained values. This includes as well either calculating the air exchange rate from the pressure-driven flow through the aperture or measuring the air exchange rate by tracer gas decay.

The model equation of Crump and Seinfeld for particulate decay in a rectangular enclosure as given by Chen et al. (1992a) has been adopted in the overall model program. The model has both k_e and n as independent parameters. In view of the wide discrepancies seen in the literature regarding these parameters, it was clear that the investment of considerable effort in obtaining specific experimental values of the decay rates is certainly justified.

Schwendiman and Sutter's (1977) report served as the basis for a sub-model to calculate the size-dependent total transport fraction, f_p in Equation (2), of particles through a well-defined aperture. Using this approach the theoretical results could be compared to measurements on a real aperture and provide viable verification of the theory before applying it to broader questions. Again, this is as opposed to the option of attempting to study penetration on a complex system such as a real vehicle. Although the equations are relatively simple, ignoring such possible complications as electrostatic charges, aperture clogging, surface roughness, and tortuosity, they do appear robust enough to provide first-order approximations.

3. DISSEMINATION FACILITY

3.1 Cloche Construction

Since the original goal of the program is to investigate solid aerosol penetration into vehicles, some kind of field testing facility was envisioned. Since the research would be exploratory in nature and difficult to execute on a scheduled basis, the facility would preferably be independent and dedicated to the program. Logistically speaking, its proximity to Bldg. 3161 would be preferable, allowing use of its laboratories. An enclosure of sufficient dimensions to house vehicles would aid in confining a particulate cloud around them and ensuring uniformity and relative independence from the vagaries of wind conditions. One possibility that was explored initially is construction of a maintenance tent such as those used by the Vehicle Recovery Unit on post. Such a tent has been ordered and eventually could be raised at the grenade range or even at M-Field at a later date.

Since this particular solution would not come to be in the short time required by the program, an open-ended agricultural cloche structure identical to one existing behind Bldg. 3161 has been erected. which permits controlled dissemination of solid aerosols and simulant gases and exposure of small enclosures. The cloche is made of semi-circular metal arches 2 meters high, 4.3 meters wide, covered with polyethylene sheeting to a length of 18 meters. Plasticized nylon tarps provide shade over the work areas at either end. A black sun-screen netting covers the rest

of the cloche between the ends. The cloche is anchored on the concrete pad area adjacent to the southern end of bldg. 3161. The cloche is intended for use on soil surfaces by simply driving 2" metal pipes into the ground to support the arches. One side was constructed as intended, along the edge of the concrete pad. The other side had to be anchored onto the concrete. For this purpose, specially-made metal plates with sections of the original pipes welded to them were produced and anchored to the pad with 3/4" bolts. A photograph of the completed cloche facility is provided in the Appendix.

The dimensions of the cloche were intended to permit dissemination of a solid aerosol cloud at the western end and exposure of a chamber or small vehicle (a HMMWV vehicle can enter the cloche) at the eastern end. It was expected that the 18 meter length would suffice to guarantee development of uniform concentrations in the vicinity of the target enclosure with a properly designed dissemination system.

The facility receives electric power from an external receptacle and compressed air from the laboratory compressor through a 1/2" plastic pipe leading from the air supply receptacle on a nearby room. Metal link connectors are attached to the plasticized tarp at the western end permitting an additional tarp to be hung there as a rain shield.

The facility is intended to provide for dissemination of particulate clouds of varying duration, from short pulses of about one-half minute to extended exposures of even one half hour. Hence it is operated with both ends open so that the dissemination fan system also flushes the facility after the passage of the cloud. If so desired in the future, the ends can be closed by tarps to trap the cloud and produce extended stable exposure times.

3.2 Solid Aerosol Dissemination System

The dry powder dissemination system is required to produce a controlled, continuous stream of particles which have been de-agglomerated to the fullest extent possible. It would potentially be used for primary particles in the range 0. 02 - 30 microns, hence utmost flexibility in operating conditions is necessary.

Discussions with Mr. R. Doherty of the Obscuration Sciences Branch led to the suggestion to use a similar component to that which produces particle clouds for that Branch's aerosol chamber facility - the SRI sonic velocity nozzle (hereafter referred to as the sonic nozzle). The component is simple and effective as a de-agglomerating apparatus. Its application is well documented in the literature (Withal and Gates, 1983). A spare unit, whose schematic diagram is provided in Figure 1, was adopted for use in the dissemination facility.

The sonic nozzle uses air flowing at the speed of sound to produce a region of high shear force where the powder enters the air stream. The flow of air past the opening of the powder feed tube causes a suction which draws particles into that region where the shear forces and pressures caused by fluid drag then act to break apart agglomerates comprised of the primary particles. Van der Waals forces are the primary adhesive mechanism forming agglomerates in dry powders. The energy available at the point of pressure drop outside the nozzle divides between

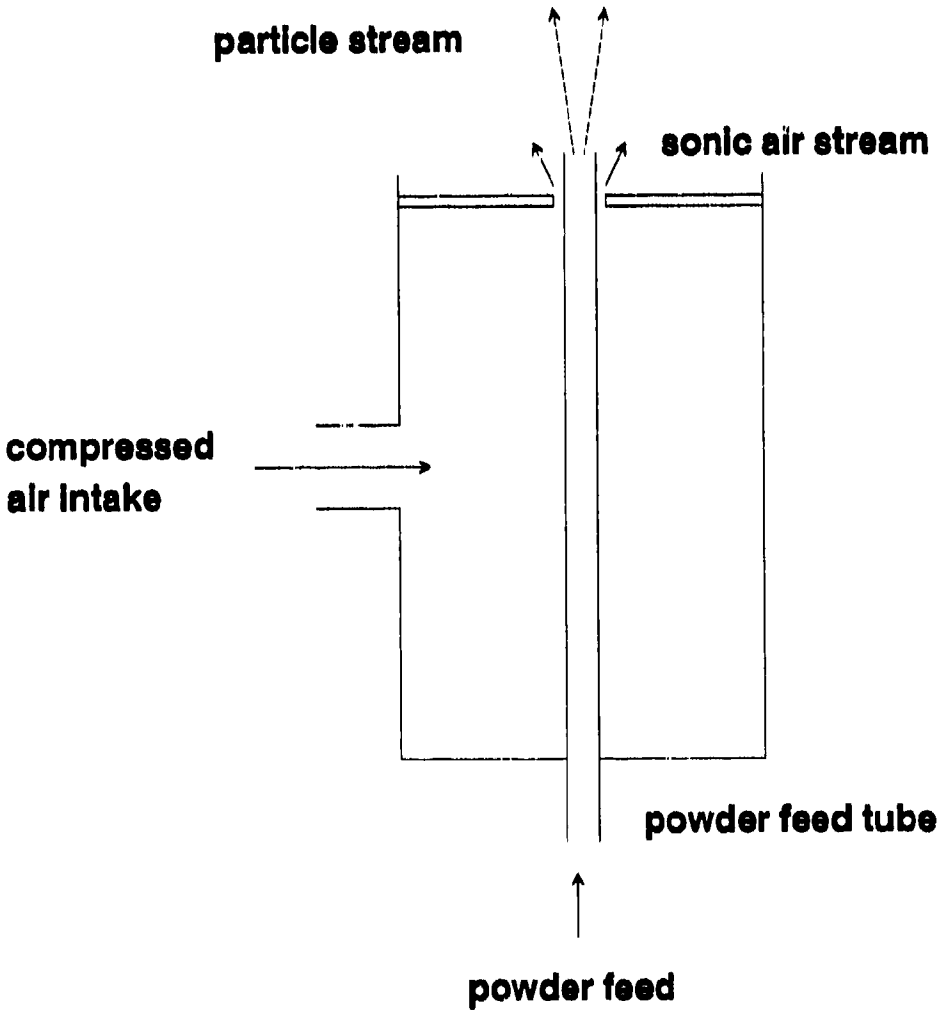

Figure 1: SRI Pneumatic Nozzle Schematic

suction and de-agglomeration of the powder drawn into the region. Operation of the nozzle requires a compromise between the two mechanisms to suit the needs of the application.

At this point it remained to obtain some apparatus for controlled continuous feeding of powder to the sonic nozzle feed tube. The solution was found in a Metronics Associates, Inc. Fluorescent Particle Aerosol Generator (Model 10), also provided by the Obscuration Sciences Branch. This apparatus is intended to provide a continuous release of dry powder particles into the atmospheric environment as simulants for the transport and dispersion of airborne particulate contaminants. Powder is fed from a stirred hopper by a rotating toothed wheel into the intake of a high speed centrifugal blower. The feed rate is controlled by the rotational speed of the wheel. Two alternative wheels with different tooth spacings are available, providing two broad ranges of feed rates. The hopper has about a 2 liter capacity. Since the toothed wheel feeds powder by discrete increments, the mechanism is not truly continuous but pulsed. This was not expected to be of concern even at low feed rates since the powder stream would be further dispersed by the turbulent means.

The final dissemination system is then comprised of the aerosol feeder coupled to the pneumatic nozzle, the blower having been removed (see Figure 2 and the photograph in Appendix). The nozzle's powder feed tube is connected to a smooth tygon tube to a funnel attached to the underside of the powder feeder. The nozzle is fed by the laboratory air compressor operating at 70 psi with a 3 psi differential range. About 20 inWG suction develops at the powder input so that as each parcel of powder drops from a gear tooth into the funnel it is drawn rapidly into the nozzle and disseminated. The air flow ratio between nozzle output and powder input is about 50:1, so the shear force de-agglomerating mechanism is considerably energetic.

The powder feed apparatus is located on a table at the head of the cloche together with its control console. The nozzle is situated on a small table in front of the feeder at 1.25 meters above the ground. Behind it are three 24" fans in a row facing down the length of the cloche. A 12" fan situated in front of the nozzle faces into the stream of disseminating particles, spreading the stream across the plane of the larger fans and facilitating its uniform crosswise mixing (see photographs in the Appendix). The system produces a 1-1.5 m/s breeze at a distance of 15 meters from the fans near the far end of the cloche. Particle mass concentration measurements later showed that deviations of only 10-20% from a mean value across the area of the cloche at that distance may be achieved. Cloud concentrations up to several tens of mg/m^3 can be produced, depending on powder composition, feed rate, and fan power level.

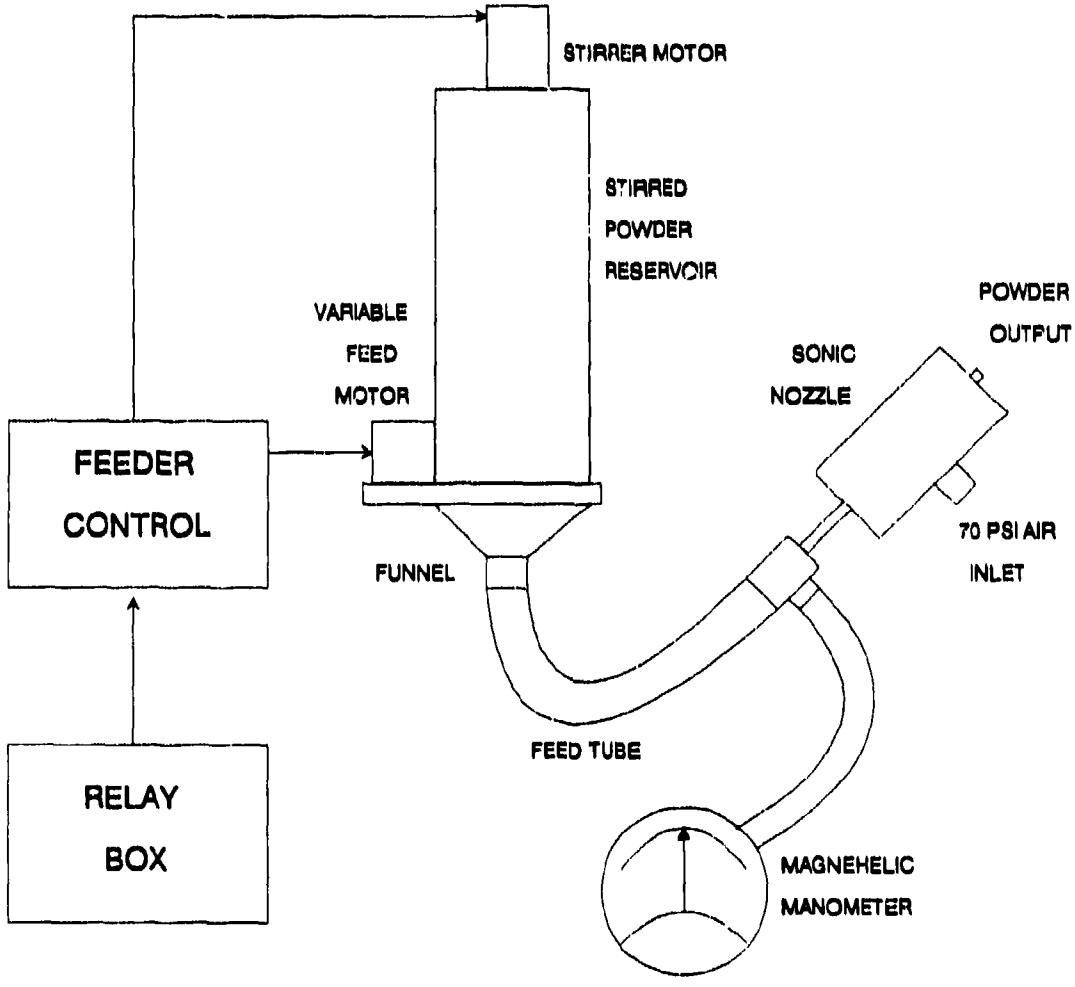

Figure 2: Dissemination System Schematic Diagram

3.3 Tracer Gas Dissemination

SF_6 gas is used universally as a tracer for air movement and the transport of vapor and gasses in general. Its use as a means for measurement of air exchange rates is well documented and standardized (ASHRAE,1981).

The gas is supplied liquefied under a vapor pressure of about 20 atmospheres. Hence, it is disseminated under its own pressure through a regulator and flowmeter of some sort. A bottle of SF_6 is located near the particle dissemination system when the penetration of vapors is to be investigated with the SF_6 simulant. Dispensing the gas through a rotameter and fine hypodermic needle as a controlling orifice has proved sufficient for our purposes. The needle is situated near the outlet of the sonic nozzle so that the gas experiences the same amount of turbulent dispersion as do the particles.

4. TEST CHAMBER

4.1 Chamber Construction

The exposure testing enclosure is a reconstructed gas mask testing chamber made of fiberglass and having several Plexiglas windows (see photograph in Appendix). The airlock wall was left out to make a volume of 4.43 m^3, sufficient to represent a small crew compartment. The chamber lies on its side on a small wheeled carriage for ease in movement. All joints were sealed with 1/4" x 2" rubber stripping to ensure air-tightness. Provisions were made for several signal cables and air sampling tubes.

One window, facing toward the dissemination system, has been replaced by two 10 mm thick plates of perspex held to the rubber seal by 16 quick-release clamps. The 85 cm. long plates can be separated using spark plug feeler gauges to provide a well-defined, controlled leak into the chamber. Additional perspex strips are added at the interface to provide leak thicknesses up to 5 cm. as desired.

4.2 Instrumentation Description

Figure 3 provides a schematic outline of the instrumentation system constructed to collect and analyze all the parameters related to investigating vapor and particulate protection of the exposure test chamber. The chamber is instrumented to measure inside and outside particle mass concentrations and size count and vapor concentrations as well as air flow, temperature and pressure differences, and relative humidity.

A 100 cfm centrifugal blower at the far end of the cloche is connected to the chamber through 3.5" plastic tubing to provide over-pressure or under-pressure as needed. The blower output is connected to a metal iris which permits continuous adjustment of the flowrate into or out of the chamber. A Kurz Model 505 mass flowmeter located with its control box on

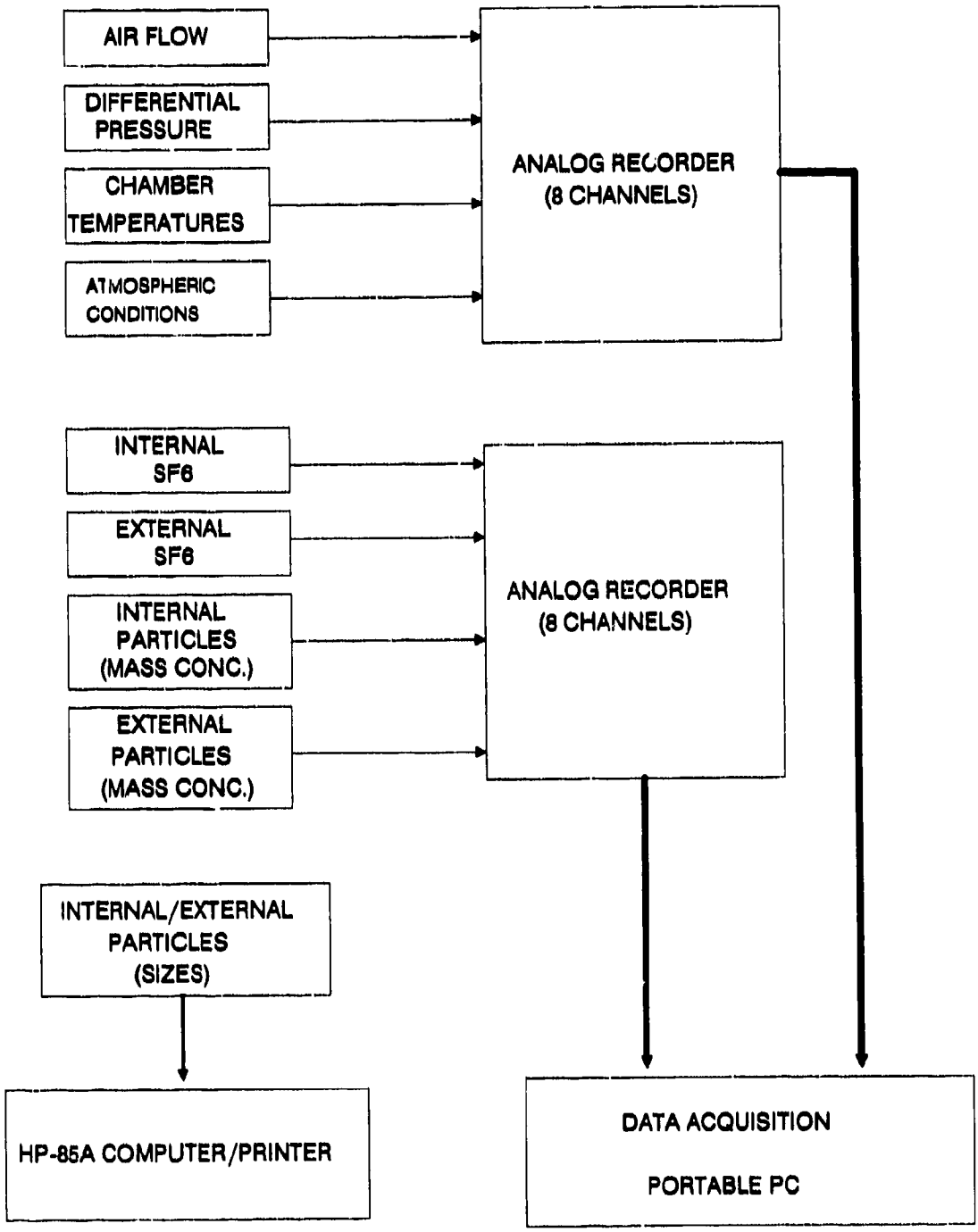

Figure 3: Solid Aerosol Instrumentation System

the flow line near the control table measures air flowrate. The pressure differential between the chamber and the environment is measured by an Endevco 8510B (1 psi full scale) piezo-resistive transducer located with its amplifier inside the chamber. The blower produces pressure differentials of several mmWG only. If higher pressure differentials are required, a 400 cfm blower is available, but structural limitations of the fiberglass construction and the rubber strip sealing of the windows must be considered.

Three MIE, Inc. RAS-2 Real-time Aerosol Sensors situated around the chamber obtain cloud mass concentration data in the range 0.01 - 100 mg/m^3 with a 0.2 second response time. The RAS-2 sensors are light-scattering nephelometers providing analog signals linearly proportional to mass concentration. The sensors are provided with both open (free convective) chambers and closed (pumped) chambers. Experience showed that the closed chamber option maintained the sensor windows cleaner than in the open chamber option, especially when disseminating talc or titanium dioxide powders which tend to stick to the glass windows of the sensors in humid weather. The three sensors' chambers are connected by tygon tubing to a manifold and a 10 lpm diaphragm pump which pulls air through the chambers. Valves on each arm of the manifold allow balancing of the air flow from each of the sensors. The flow is adjusted to about 2 lpm through each sample chamber.

Inside the enclosure an MIE, Inc. RAM-1 Real-time Aerosol Monitor measures the penetrating particle mass concentration in the range 0.001 - 200 mg/m^3 with response time down to 0.5 second. This monitor uses the same detector system as the RAM-2 sensor but provides digital readout of the concentration as well as analog output, internal reference calibration, and continuous flushing of optical surfaces.

A Particle Measuring Systems LAS-X Laser Aerosol Spectrometer inside the enclosure collects particle size count spectra. The LAS-X provides 64 bins in four ranges in the region of 0.12 - 7.5 microns. The LAS-X contains a precision He-Ne laser-illuminated optical mirror system which permits single particle sampling by collecting the light scattered from each particle which is then sensed by a solid state photodetector. The instrument is calibrated by the manufacturer based on diameter using spherical latex particles. The data output is sent by standard RS-232C interface signal to an HP-85A portable computer for processing and later analysis. A TSI APS 3300B particle sizer is also available for particle sizes up to 30 microns but has not yet been put to use since concern to date has been with the 0.1 - 5 micron range.

The LAS-X spectrometer input is connected through a tygon tube to the outside wall of the enclosure when the external cloud spectrum is to be obtained. In this configuration the LAS-X is linked to a TSI Model 3302 Diluter to provide lower countrates and prevent saturation in the lowest channels. The maximum countrate in channels 1-16 noted by the manufacturer is 7.0 KHz/channel. Since the sampling flowrate is only 5-10 cc/sec, use of the TSI 3302 diluter necessitated construction of a special flow-matching arrangement to provide isokinetic sampling by the LAS-X. This apparatus is discussed in Appendix E.

The data provided by the RS-232C output are processed in the HP-85A computer by a dedicated program written for this purpose at Los Alamos National Laboratory (Soderholm,

1984). The program output provided on the HP-85A's printer summarizes information relevant to each run. These include a plot of the bin count data for each of the four ranges, a chart of the run parameters, and a listing of particle counts for each of the 16 bins in all the four size ranges. Since the size ranges are overlapped and not of equal bin width, analysis of the data may be confusing. The program calculates a best-fit log normal distribution of the data and plots it with the original counts on the output graph. This calculation is useful only if the data are not bimodal with the background spectrum, in which case the data must be analyzed separately by first subtracting the background spectrum. Manipulation of the LAS-X data will be discussed further in Appendix C.1. A sample of the data output of the program for ambient background is provided in Figure 4. The data plot and parameter chart are shown.

Several options exist for the measurement of SF_6 tracer gas concentrations inside and outside the enclosure. A MIRAN-1A Infrared Gas Analyzer can be situated inside the enclosure to monitor tracer concentration during air exchange rate measurements of the sealed system or when the rate is relatively slow. Fast response measurements, such as for vapor penetration testing and short air exchange rates must be done using an electron capture gas chromatograph and automatic sampling system. Such a system has been acquired from HNU, Inc. but has yet to be adapted to the overall system. Pending its inclusion in the experimental setup, the available S-Cubed, Inc. (now Lagus Associates) portable SF_6 Gas Chromatographs have been used. The columns have been changed from molecular sieve to alumina, permitting more rapid analysis of SF_6. The SF_6 peak follows the oxygen peak and clears the systems in less than one minute. For trial runs the injection cycle has been hand operated from the instrument panel. A 10 lpm diaphragm pump at the control table samples air from the chamber in a closed cycle while the sampling loop of the gas chromatograph is permitted to bleed off the required flow during the sample injection cycle. The vented sample air is returned to the return air line to the chamber, thus preventing even the slightest effect on the measured air exchange rates.

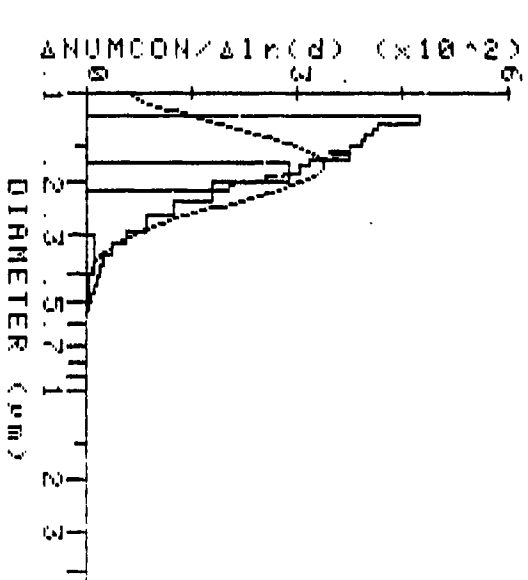


```
DATE YY/MM/DD   TIME 160516   PSLF
MAX CNTS/SEC=   1232   SEC=      8
R:0-3 TRUN   0 BINS    5.00 ML/SEC
DILUTION RATIO          = 1.000E+000
TEMPERATURE          (C)= 2.200E+001
ATM PRESSURE (mm Hg)= 7.600E+002
REL HUMIDITY         (%)= 5.000E+001
A PARAMETER             = 0.000E+000
B PARAMETER             = 0.000E+000
C PARAMETER             = 0.000E+000
NUM CONC  (NUMB/cm3)= 2.510E+002
GEOM MEAN DIAM   (μm)= 1.746E-001
GEOM STANDARD DEV    = 1.348E+000
MASS CONC     (mg/m3)= 1.879E-003
UNDIL MASSCON(mg/m3)= 1.879E-003
MAX CNTS/SEC            = 1.232E+003
PEAK DIAMETER (μm)   = 1.230E-001
FIT NUM CONC (#/cm3)= 0.000E+000
FIT GEOM MN DIA (μm)= 1.000E-008
FIT GEOM STAND DEV   = 1.000E+002
FIT UNDIL M0 (mg/m3)= 0.000E+000
```

Figure 4: Sample LAS-X Data Output for Ambient Air

5. SOLID AEROSOL PROTECTION FACTOR MODEL

The protection factor model program is written in the Mathcad 3.1 scientific programming language. This is an interactive tool operated in the Microsoft Windows environment which permits model equations, text, and graphs to be written in the same program as if on a scratchpad. As described earlier, the model calculates particle size-dependent parameters for the solid aerosol protection factor in Equation (2). For comparative purposes, it also calculates Equation (1) for the vapor protection factor. The program is also provided experimental data for particulate settling rates and calculates a semi-empirical result for comparison to the fully theoretical results.

After presenting the size-dependent protection factors in a two-dimensional matrix for several pressure differential values, the results can be weighed either by a given experimental size spectrum or by a log normal distribution spectrum defined by user-supplied geometric mean and standard deviation parameters. The log normal weighted results can be displayed with both the theoretical settling rates and the experimental settling rates alongside the vapor protection factors.

Since the program links text and model equations in the same framework, a sample run of the program is presented in Appendix B in the original Mathcad code with explanatory text included.

The parameters required for the particulate protection factor calculation include enclosure dimensions, aperture dimensions, differential pressure (five values are used simultaneously to provide immediate sensitivity results), turbulent mixing parameters (ke and ne in the program), challenge and exposure durations and challenge size spectrum within a 0.1-10 micron range. The parameters used for the sample run shown in the Appendix are as follows:

- enclosure dimensions: l = 213 cm. h = 117 cm. w = 167 cm.
- aperture dimensions: l = 80 cm. h = 0.015 cm. w = 4 cm.
- cloud duration (T): 5 minutes exposure time (t): 30 minutes
- particle density: 2.7 g/cm^3 (Talc)
- log normal parameters: geometric mean 1.2 Standard deviation: 2.284
- flow exponen (n): 0.5
- turbulent dissipation: ke = 1000 ne = 2.038 (approx. small fan operating)
- pressure differentials: -1, -1.5, -2, -2.5 and -3 mmWG (simulating wind)

These parameters were chosen to demonstrate a situation in which significant filtration of the larger particles in the narrow and deep aperture should be assured. The low air exchange rates expected from the small pressure differentials assure sufficient time for pronounced particulate settling to occur.

The general features of the results correlate well with expected behavior. Particle filtration in the aperture (fig. 5) increases sharply at 1 micron. As the pressure differential

increases (higher curves), the filtration decreases as more and larger particles are pulled through the aperture. The particle settling rates (fig. 5) show a minimum at the junction of the diffusional and gravitational mechanisms at about 1.5 micron in this case. The particulate protection factors given in Figure 7 along with the vapor protection factors (straight lines) show pronounced size-dependence with some improvement at the smallest sizes and sharp improvement at the larger sizes. This behavior is a combination of the higher decay rates at the smallest sizes and high filtration and settling rates of the larger sizes. The weighted protection factors in figure 6 for the log normally distributed spectrum shown in Figure 8 are, of course, correlated with the vapor protection factors but exhibit higher values due to the particulate removal mechanisms. As the differential pressure increases, the increased air exchange rate reduces both the vapor protection and the advantage obtained by particle filtration.

The same functional form of the size-dependent protection factors is to be expected in all instances. Their values can only be larger than those for vapors due to removal mechanisms. The extent to which these mechanisms influence the protection for a given scenario in comparison to the vapor protection depends on the solid aerosol size spectrum. The example shown in Figures 9 relates to the broadly polydispersed threat shown in Figure 8. Figures 10-15 demonstrate the effect on the weighted protection factors of hypothetical relatively monodisperse spectra. The spectrum in Figure 10 with a geometrical mean size of 4 microns yields the weighted factors shown in Figure 11. Note the sharp rise compared to the polydisperse spectrum of Figure 8. The influence of the differential pressure is also accentuated as the larger particles are more strongly filtered at the lower pressures. The 1 micron particles of Figure12 track the vapor protection factor closely. They are not influenced by the change in pressure as the filtering factor is close to 1. Their factors are the closest to those of the vapor as expected by their minimum settling rate. The smallest particles, shown in Figure 14, show the effect of higher settling rates in Figure 15.

After the veracity of the theoretical model is shown to be confirmed through experimental verification in the coming chapters, further sensitivity analyses will demonstrate the usefulness of the model program as a tool in prediction of solid aerosol protection and in designing of integrity tests.

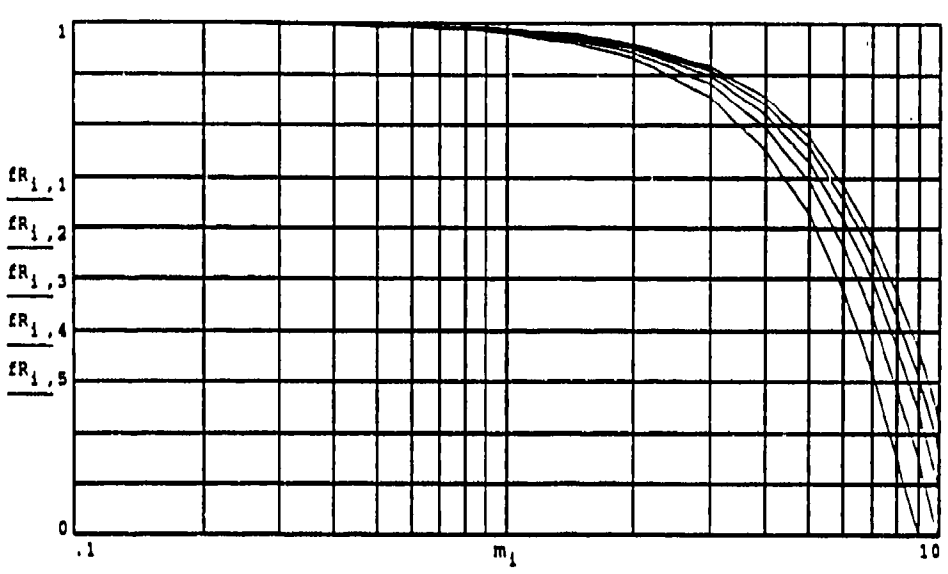

Figure 5: Total Transport Fraction

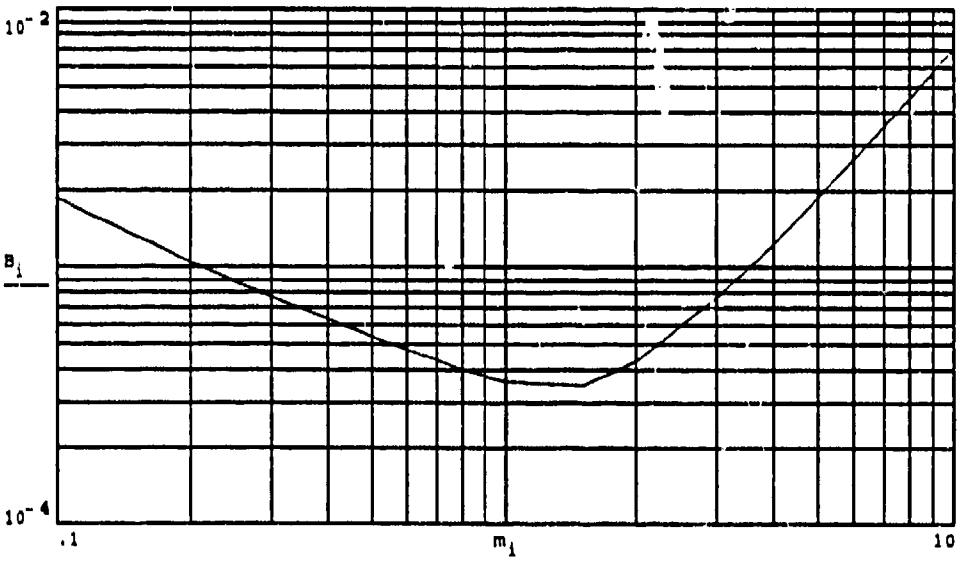

Figure 6: Theoretical Particle Settling Rates [1/sec]

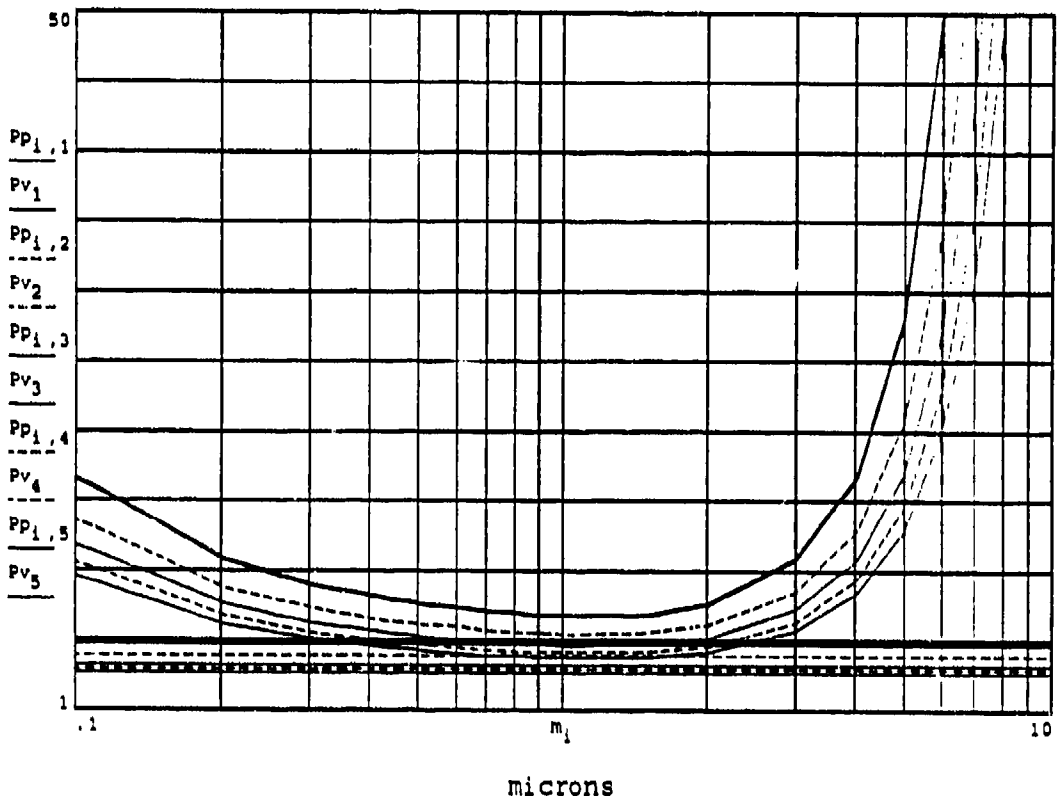

Figure 7: Size-dependent Particulate and Vapor Protection Factors

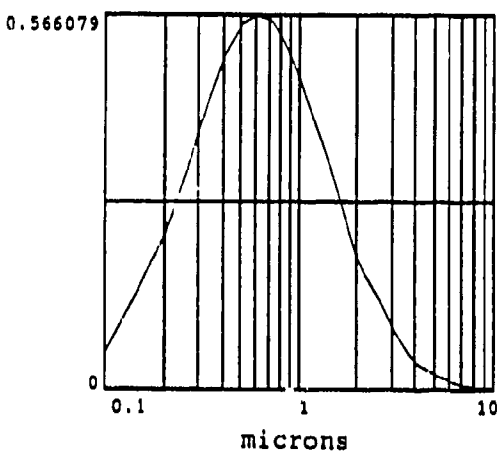

meanG = 1.2

sigG = 2.284

Figure 8: Log Normal Challenge Spectrum

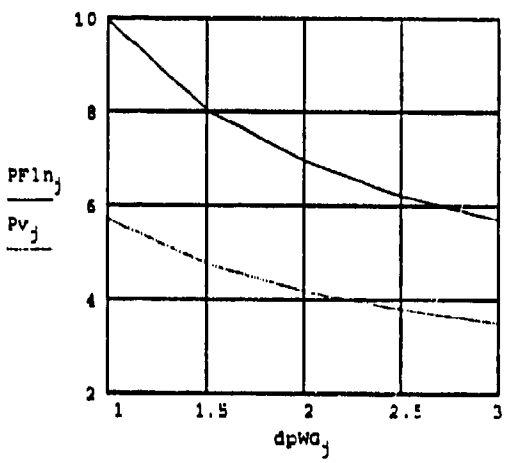

Figure 9: Theoretical Weighted Protection Factors

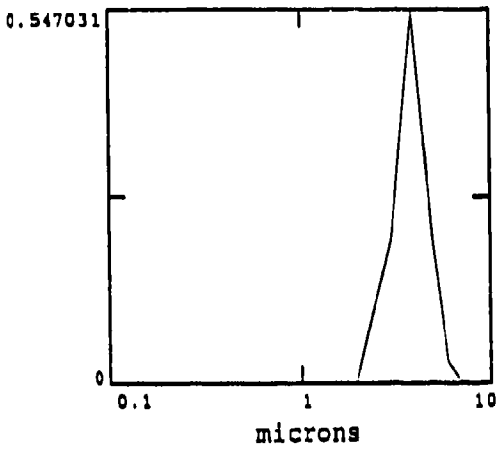

Figure 10: Log Normal Spectrum
$d_g = 4$ $Sigma_g = 1.2$

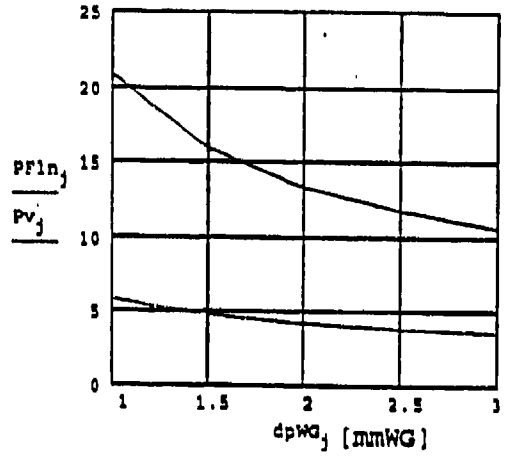

Figure 11: Theoretical Weighted Protection Factors

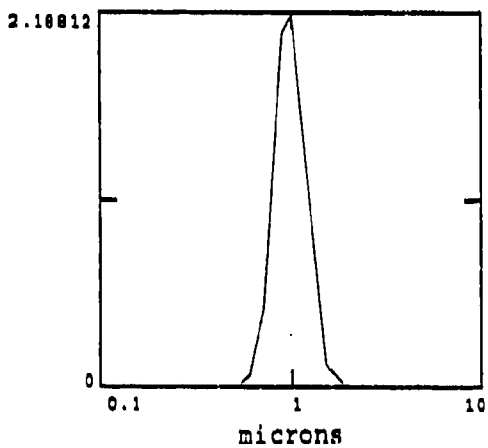

Figure 12: Log Normal Spectrum
$d_g = 1$ $Sigma_g = 1.2$

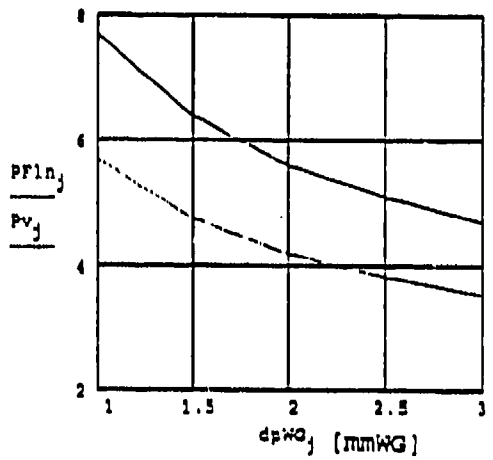

Figure 13: Theoretical Weighted Protection Factors

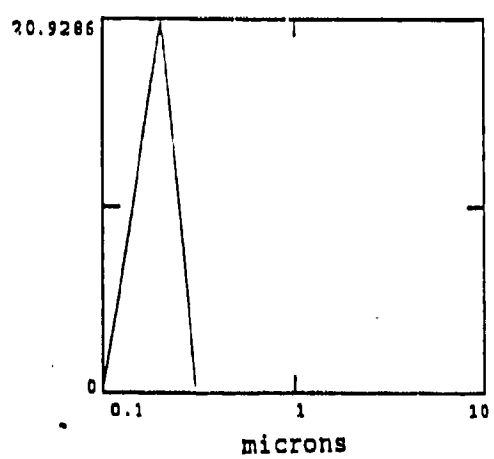

Figure 14: Log Normal Spectrum
$d_g = 0.2$ $Sigma_g = 1.1$

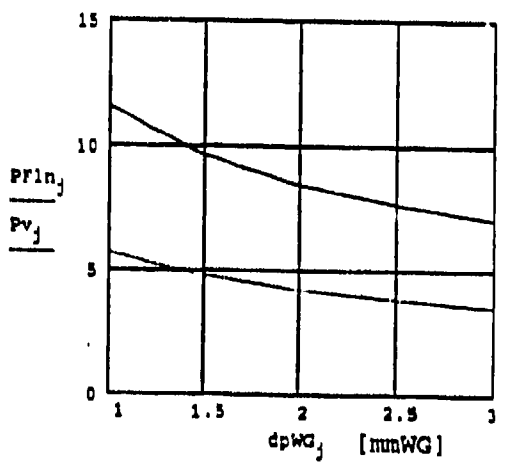

Figure 15: Theoretical Weighted Protection Factors

6. EXPERIMENTAL MEASUREMENTS

6.1 Fine Particle Spectra

Several candidate simulant powders were examined for their ease in dissemination and usefulness as test particles within the 0.1-10 micron range. Pending more specific criteria in choosing threat-specific candidate simulants, only powders whose use in the open air is acceptable by environmental safety standards were considered. Those tested include:

- Asbestos-free Talc
- Aluminum oxide
- Titanium dioxides
- Hydrite MP clay
- Hydrophobic Aerosils (DeGussa fumed silicas)
- Hydrophobic Sipernats (DeGussa precipitated silicas)
- Coarse Arizona road dust (AC dust)
- Cabosils (Cabot fumed silicas)

A main concern is the efficiency of the powder feeder and sonic nozzle in de-agglomerating and disseminating bulk candidate powders. Powders have been tested for flow ability in the feeder system and their disseminated size spectra. As discussed above, the addition of scraper arms on the stirring rod greatly improved the efficiency of the powder feeder apparatus except for the most agglomerated powders on damp days. Example size spectra for bulk candidate powders following dissemination through the nozzle and transport over a distance of 15 meters are shown in Figure 16. These spectra were obtained from LAS-X data by subtracting background counts in a dedicated Mathcad program which will be explained further on in the Report. It was hoped that a wide repertoire of solid aerosol spectra could be constructed with as little preliminary powder preparation as possible. Both narrowly- and broadly-dispersed spectra should be available in a wide specific mass range.

The Aerosils, Cabosils and Sipernats have primary particle sizes in the 7 - 20 nm range, although supplied as agglomerates of varying sizes. The hydrophobic Aerosils are basic fumed silicas which have been treated with silane to produce varying levels of hydrophobicity, depending on the primary particle size. As a result of their hydrophobicity, they are very readily disseminated and can be excellent candidates for simulating solid aerosols under 0.2 micron. It should be kept in mind that the lower limit of detection of the LAS-X is 0.12 micron, so that it is not known if particles are produced from the Aerosils and Cabosils.

Certain agglomerate spectra may be tailored somewhat by changing the nozzle energy or by bypassing it if larger sizes are needed. In that case the original blower of the Metronics Aerosol Generator is used. The measure of de-agglomeration achieved in the nozzle for Aerosils and Sipernats is shown qualitatively in Figures 17 and 18. In Figure 17 the Aerosil 812 spectra for dissemination through the original blower of the Metronics system is shown in comparison to that obtained from the sonic nozzle. Essentially all the agglomerates above 0.2 micron have been separated. by the nozzle. In Figure 18 Sipernat D-11 spectra are shown where, in addition, the spectrum obtained by simply dispersing the bulk powder in front of the large fans is also shown. Agglomerates up to 4 microns have all been de-agglomerated to less than 0.5 microns. The Sipernat D-11 is supplied as a nominal 4 micron agglomerate.

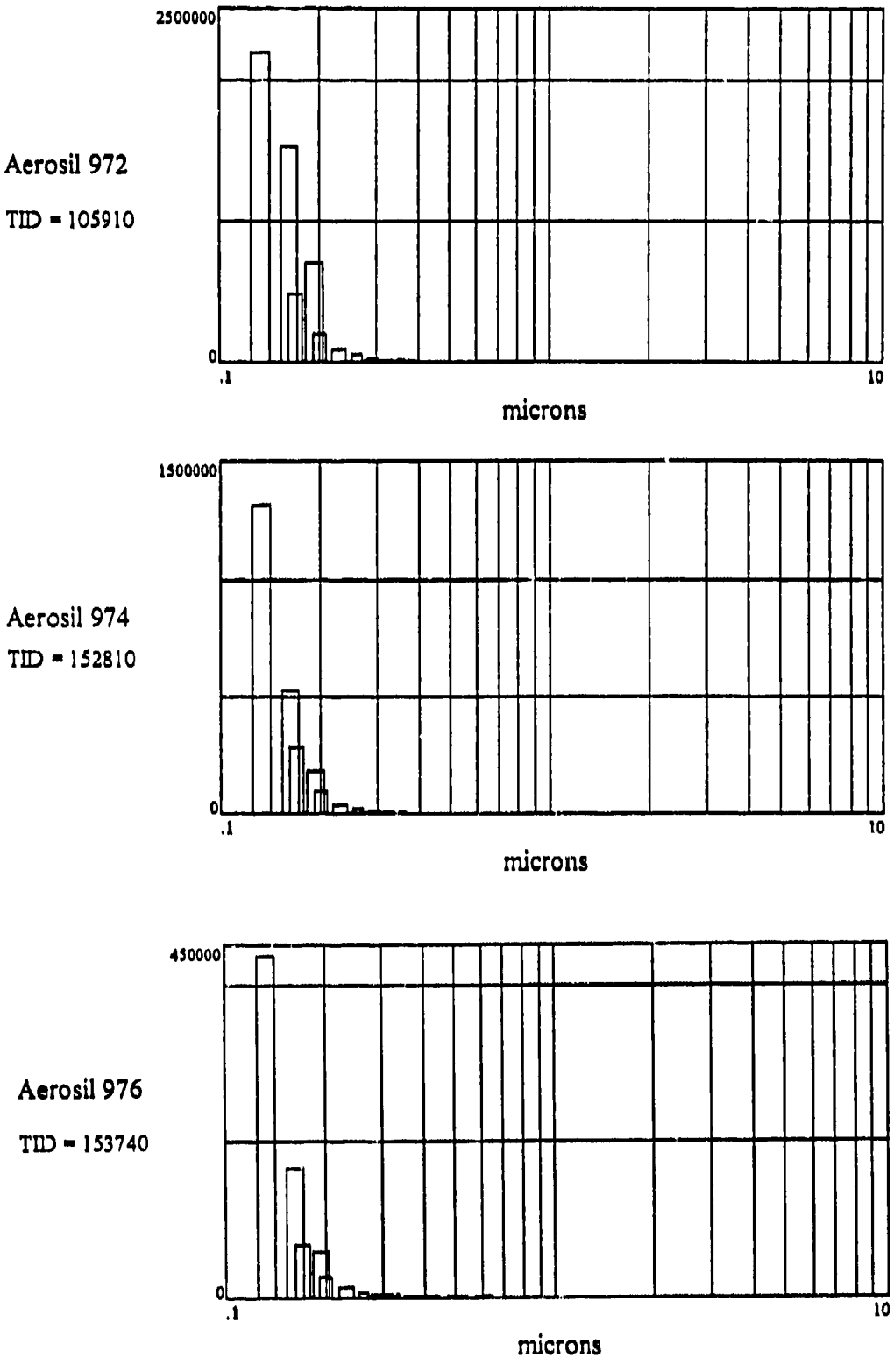

Figure 16: Fine particle spectra from sonic nozzle dissemination

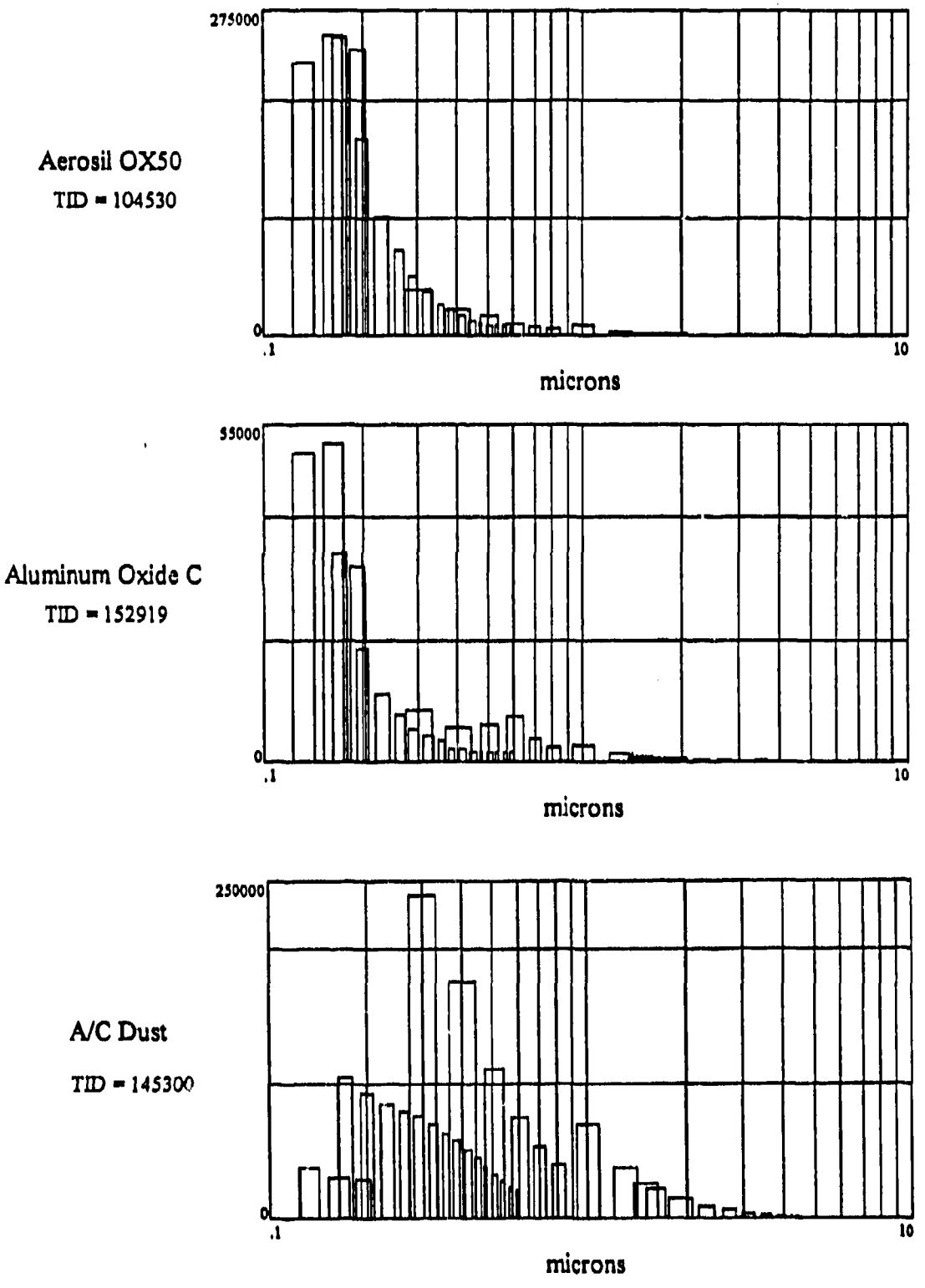

Figure 16: Fine particle spectra from sonic nozzle dissemination (continued)

Cabosil EH-5

TID = 151620

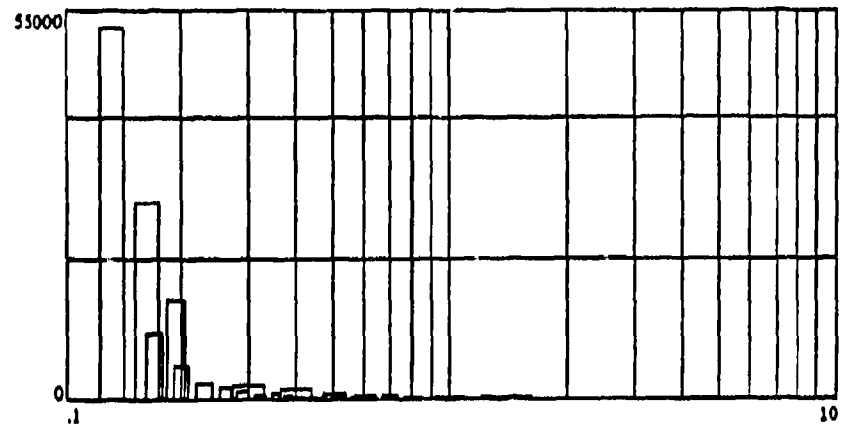

Cabosil M -5

TID = 150750

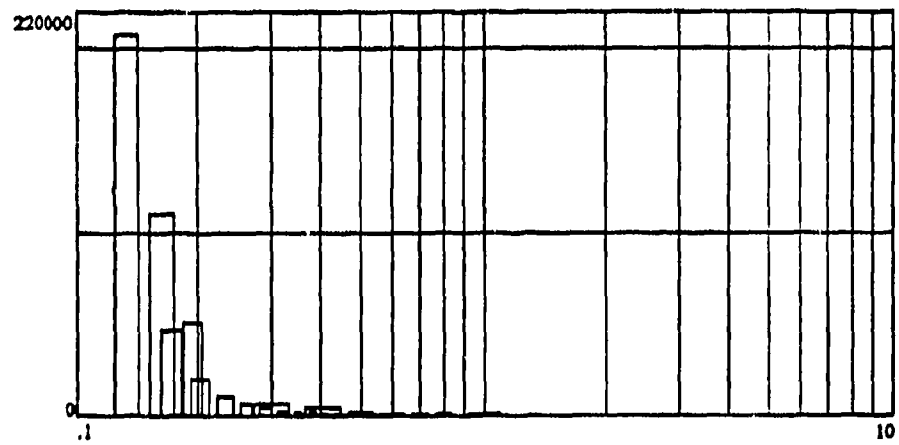

Cabosil TS 530

TID = 150250

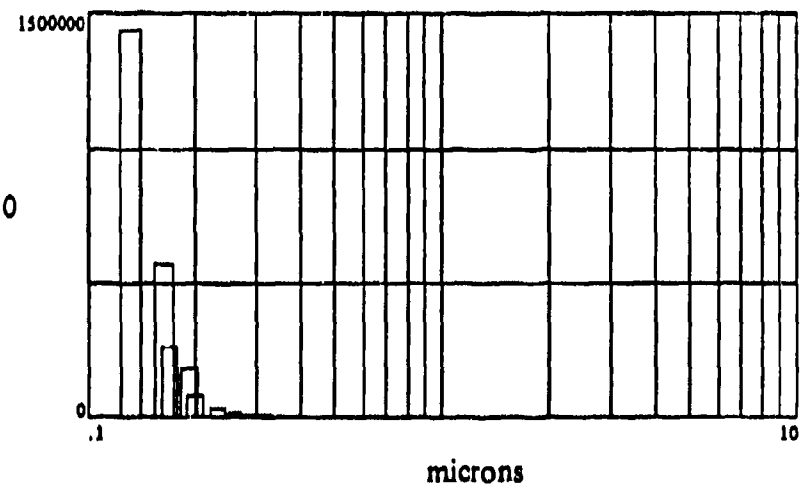

Figure 16: Fine particle spectra from sonic nozzle dissemination (continued)

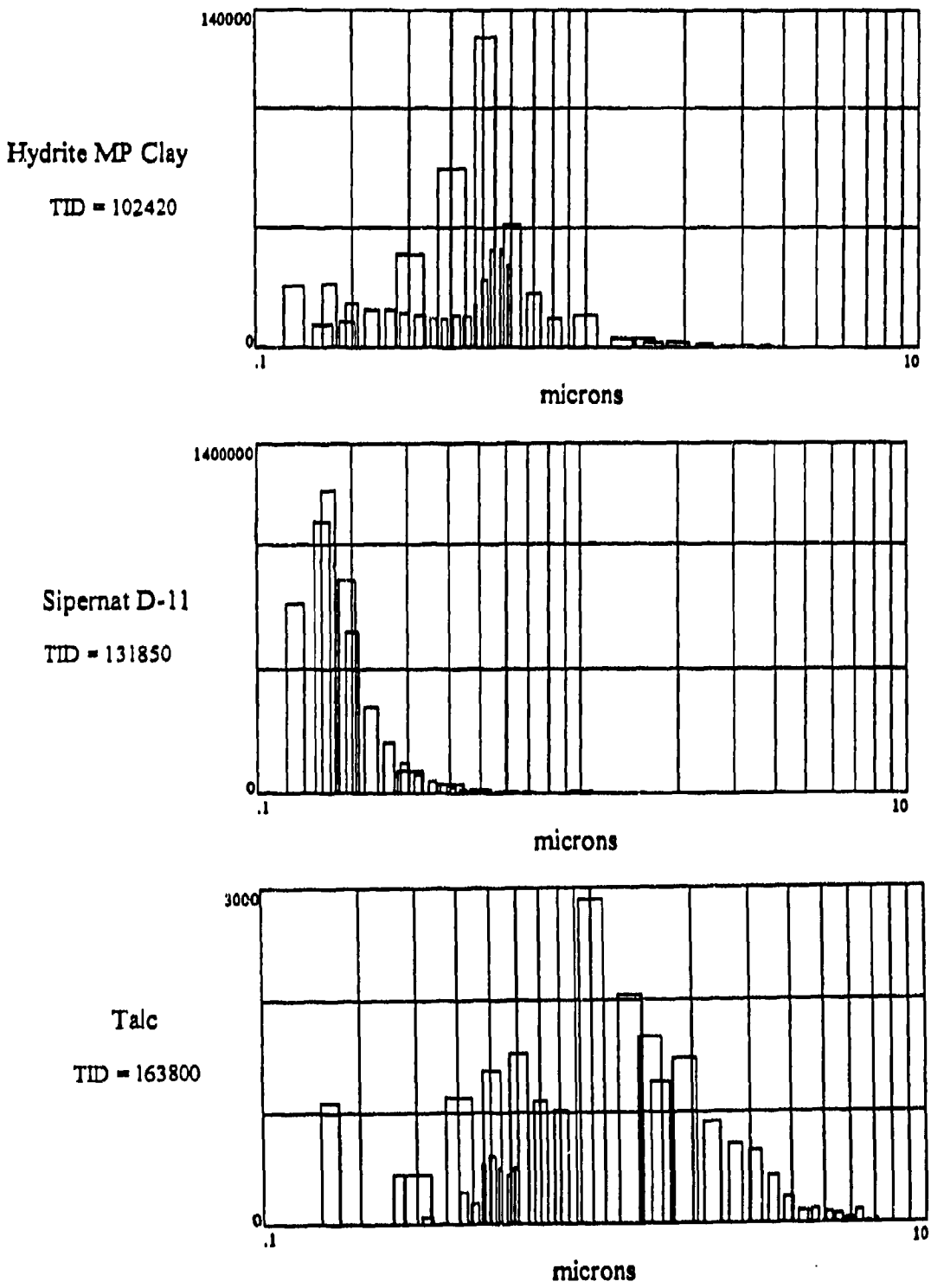

Figure 16: Fine particle spectra from sonic nozzle dissemination (continued)

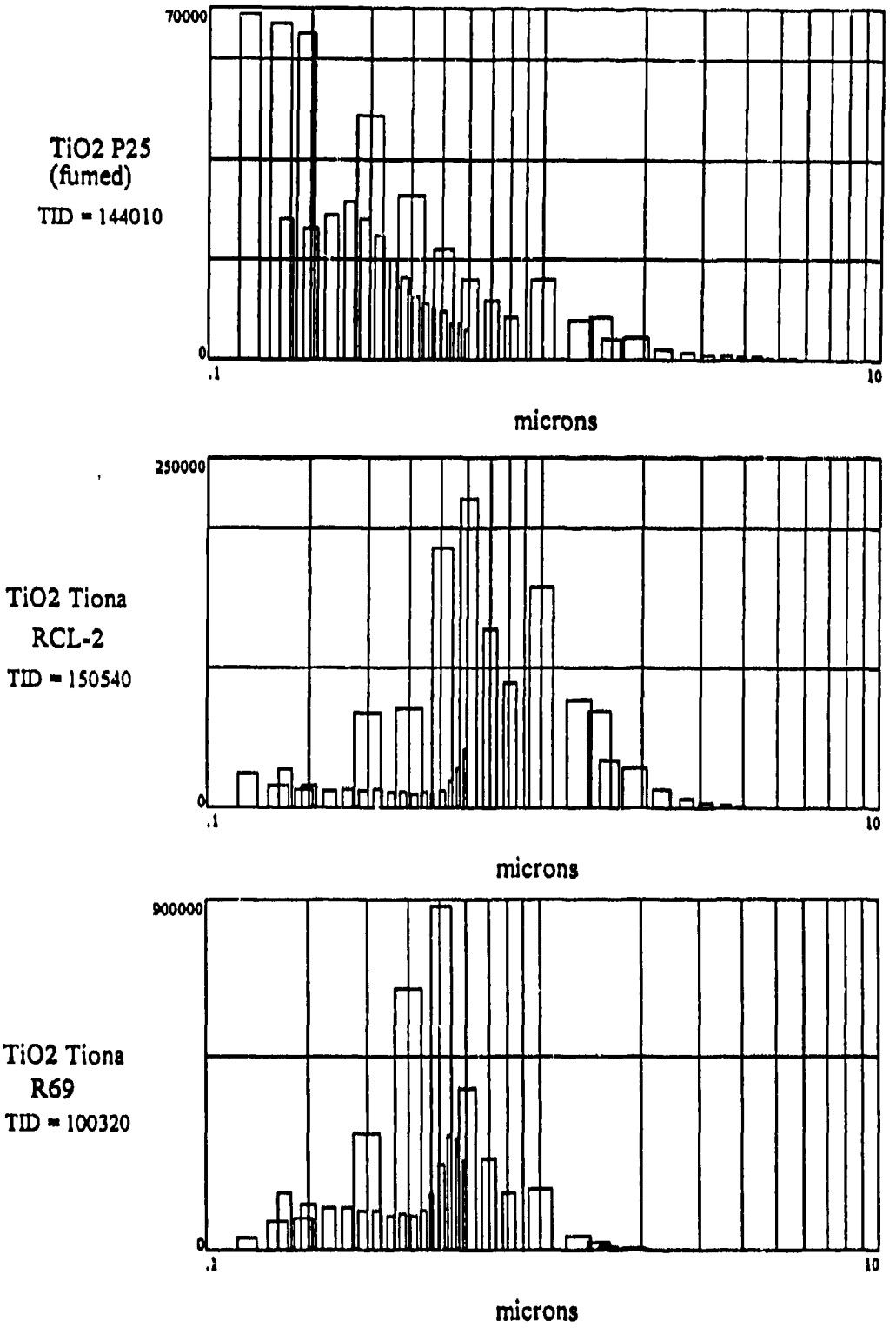

Figure 16: Fine particle spectra from sonic nozzle dissemination (continued)

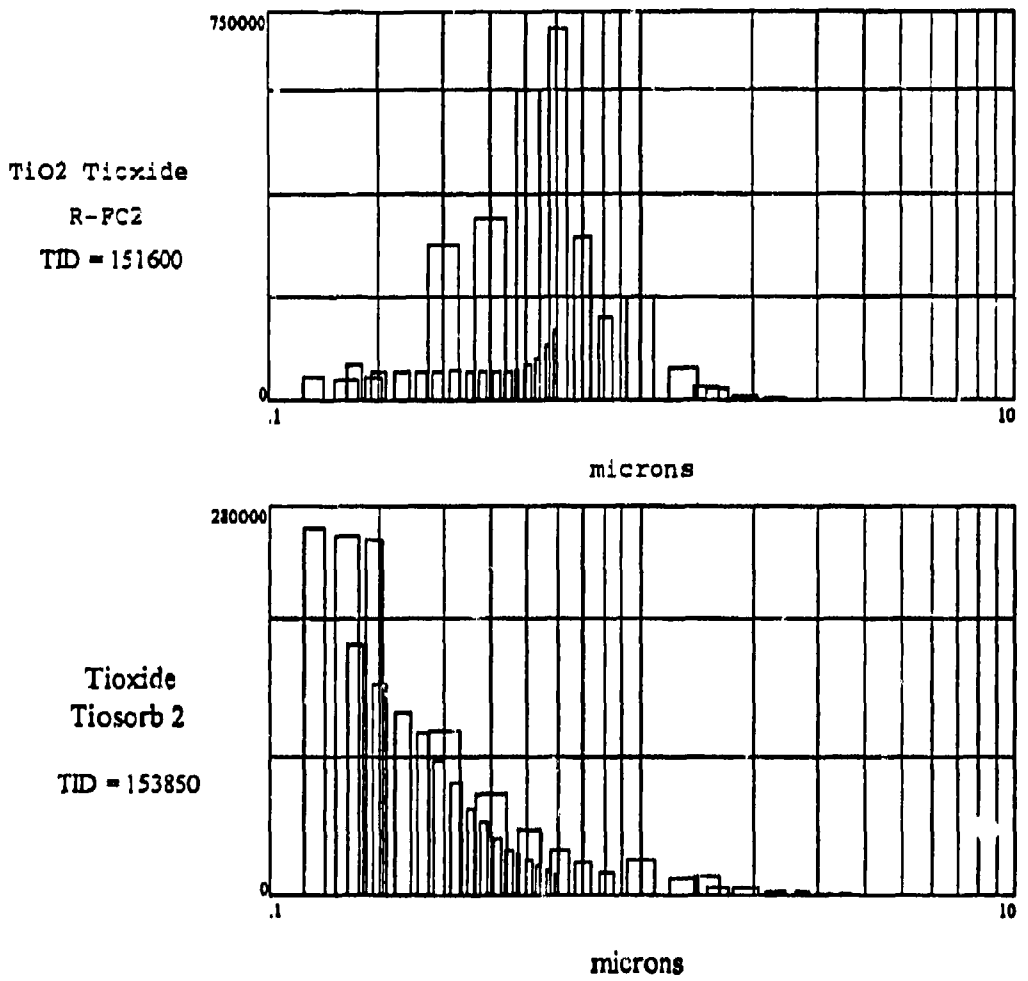

Figure 16: Fine particle spectra from sonic nozzle dissemination (continued)

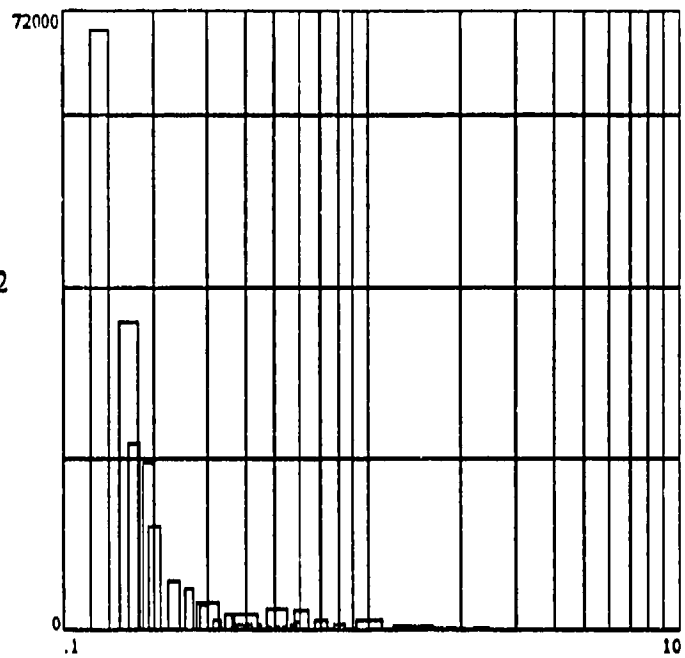

Aerosil R812

BLOWER

TID = 120020

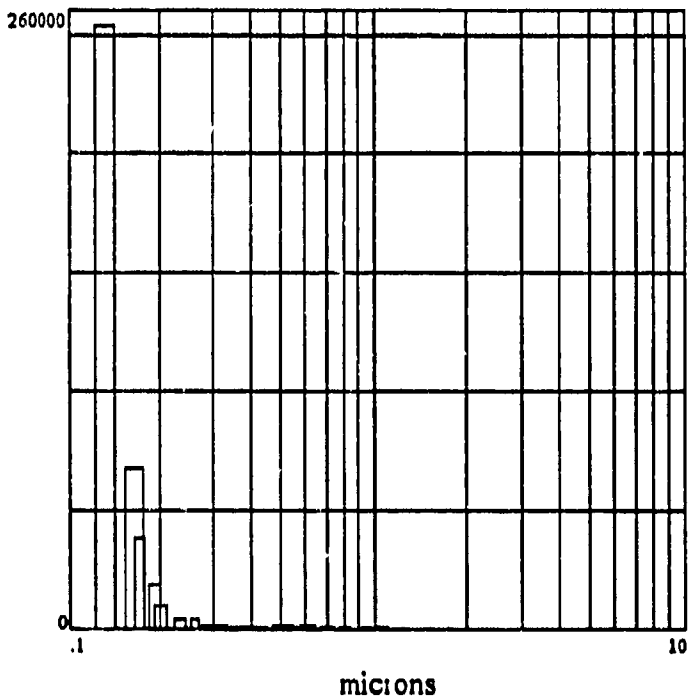

Aerosil R812

NOZZLE

TID = 111810

Figure 17: Aerosil R-812 Dissemination

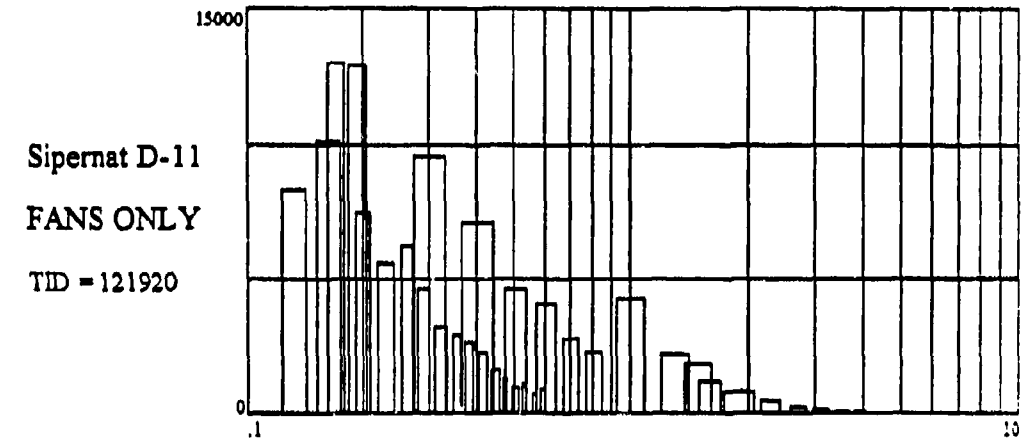

Sipernat D-11

FANS ONLY

TID = 121920

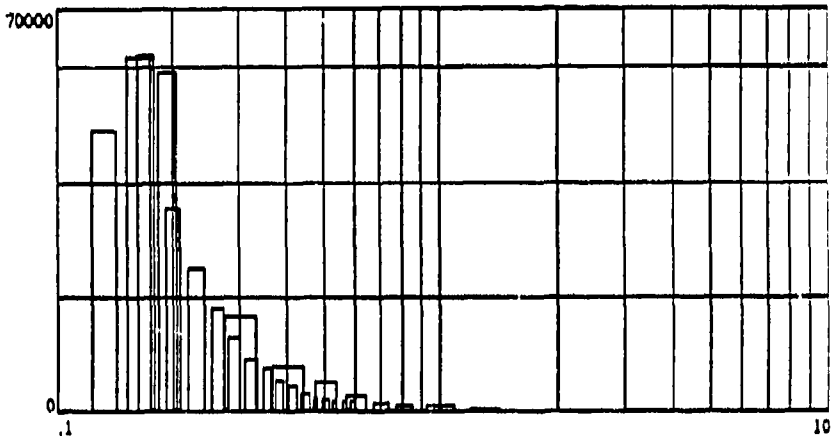

Sipernat D-11

BLOWER

TID = 121400

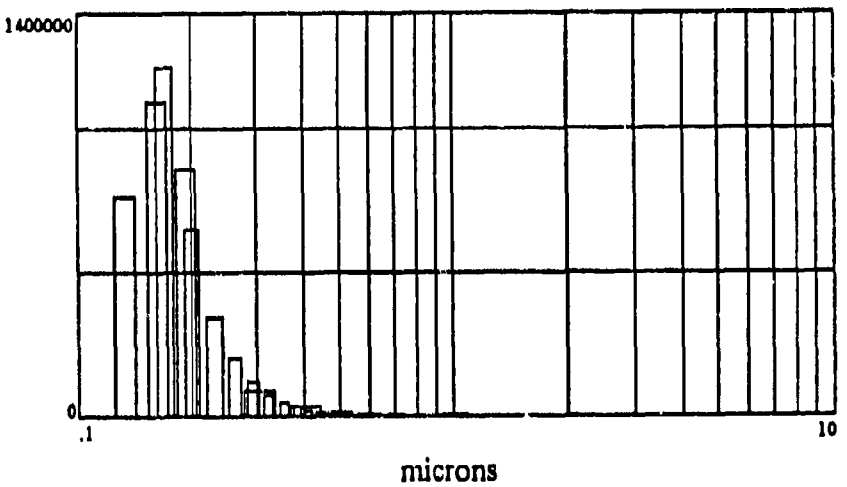

Sipernat D-11

NOZZLE

TID = 131850

Figure 18: Sipernat D-11 Dissemination

Several different forms of titanium dioxide were available for testing. Being also environmentally benign, the TiO_2 is an attractive candidate for mid-range size simulation. Primary particle sizes of the Tiona RCL-2 and R69 (SCM Chemicals) and Tioxide R-FC2 (Tioxide, Inc.) are in the range 0.2-0.3 micron. Their spectra from sonic nozzle dissemination show median size counts at 0.4-0.5 micron indicating reasonably efficient de-agglomeration. It should be noted that these powders are very hygroscopic and, hence, difficult to disperse. The addition of vertical arms to the stirring rod, however, was sufficient to overcome most of these problematic candidates. The narrow spectra achieved can be useful especially as the protection factor model program indicates this size range as particularly problematic from the protection aspect.

Titanium dioxide P-25 is a fumed product with an average primary particle size of 21 nm. Tiosorb 2 (UFO2) is a microfine product of Tioxide with 18 nm primary particle size. Unlike the hydrophobic Aerosil products, these are not well de-agglomerated through the sonic nozzle and are not beneficial candidates for further testing.

Talc and GM Arizona Road Dust provide a useful broad spectrum ranging from 0.2 to 7 microns. Little difference was observed between the spectra from the nozzle and that from the fans only. The two powders appears to exist originally as primary particles, whereas the nm range primary particles of the Aerosils and Sipernats experience more considerable adhesive forces, hence their agglomerate natures.

6.2 Solid Particle Settling Rates

The considerable variances between theory and measurements of solid aerosol settling rates noted in the literature survey and the uncertainty of determining turbulent energy dissipation parameters for stirred enclosures necessitated a series of measurements specific to the chamber itself. Settling rate tests are carried out by exposing the chamber interior to a continuous cloud of disseminated powder and then resealing it. This can be done by removing one perspex plate from the window during passage of the cloud. The mass concentration is monitored to ensure reasonable count rates before spectra are collected by the LAS-X each four minutes for an extended time . Total sampling time is dictated by the slowest settling rates of the size bins of interest. Measurements can be stopped when bin counts reach statistically insignificant levels. Various stirring scenarios can be examined by operating small fans inside the chamber. If a true quiescent state, barring temperature differences within the enclosure space, is of interest, the LAS-X must be situated outside the chamber and its sample tube inserted through an opening in the wall. It has been observed that its circulation fan alone has a significant effect on the settling rates. In all cases the chamber must be completely sealed in order to reduce to a minimum particle losses due to air exchange. It should be noted that results are relevant to an enclosure with smooth, non-conducting walls. Effects such as electrostatic charging and rough surfaces, which may be encountered in practical situations, should be considered for investigation as well.

Data are analyzed by a semi-logarithmic optimization of the background-corrected particle counts in individual size bins vs. time to yield best values of the decay rates:

$$\frac{dC(t)}{dt} = -\beta_p \cdot C(t) \qquad (13)$$

In the Appendix Mathcad utility programs needed for background subtraction of LAS-X data and calculation of settling rates from this data are described. In all measurements to date the decay rates in the chamber have fit the single exponential function with a correlation coefficient better than 0.9. These results could indicate that electrostatic forces are not interfering with the mechanical mechanisms of settling. Such interference would be expected to cause a more rapid initial decay of small particles and possibly a time-dependent hastening of the larger particle decay. Since results of settling measurements have been consistent over several months and under varying environmental conditions, it does not appear that electrostatic charges affect the results. Such influences would be expected to vary with changes in humidity at the very least.

Shown in figure 19 are settling rates plotted against particle size for talc, which spectrum provides a convenient tool for simultaneous, polydisperse measurements. The effect of turbulent mixing intensity, increased between the runs by operating a small muffin fan in the chamber, expresses itself in the settling rate curves which uniformly shift to higher levels. Measurements with other, less polydispersed powders yielded similar results consistent with density differences. These data can be used directly in the protection factor model as calibration parameters. They are useful also in estimating empirical values for the coefficient and exponent of the eddy dissipation equation (10). This topic will be treated separately later.

6.3 Solid Aerosol Protection Factor Tests

Several series of experiments were carried out with the objective of investigating the penetration of particles in the range 0.1-5 microns into the chamber with a ventilation dynamic scenario which should force a significant difference between the protection factors for vapor and solid aerosols. Their purpose is to verify the results of the model given the same scenario. The procedures followed are applicable in general.

The chamber ventilation kinetics are established by first fixing the aperture width with two widely separated feeler gauges. The gauges must remain in the aperture throughout the test to prevent its collapse when a negative pressure differential is applied. The perspex plates will be sucked against the rubber seal and the aperture geometry may be compromised. For very narrow apertures care must be taken that the surfaces are clean and the plates are pressed together against the feeler gauges before final clamping. The door of the chamber must be tapes with duct tape around its entire perimeter to ensure complete sealing. Make sure that all instruments are operating and zeroed before doing this.

The desired negative pressure differential is established by operating the blower situated near the control table. The mechanical iris installed on the air pipe must be used to limit

a - Spectrometer fan and muffin fan on in chamber
b - Spectrometer fan on in chamber
c - No fans in chamber

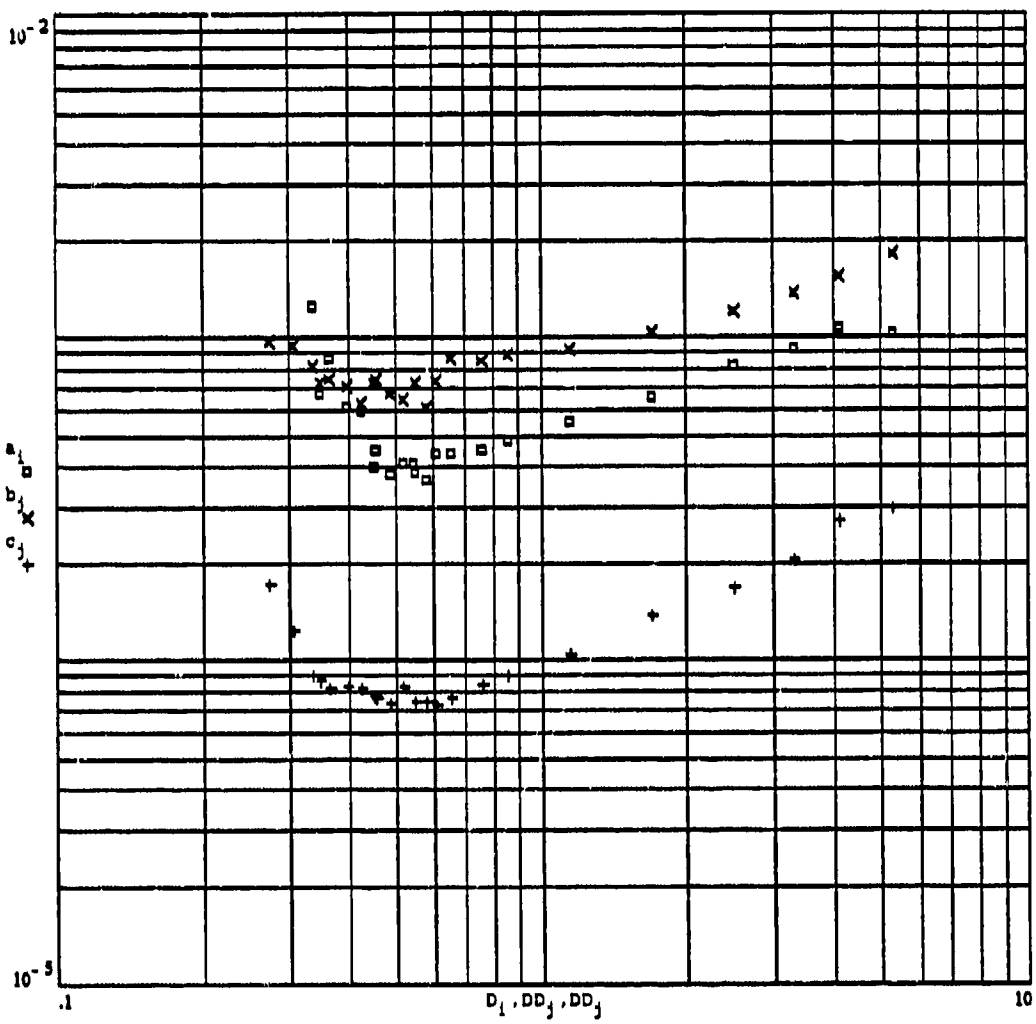

Figure 19: Talc Particle Settling Rates

suction on the chamber. Start with a completely closed iris and with lowered voltage on the Variac transformer which controls the blower. Slowly raise the voltage back to 120 volts and open the iris slightly to fix the desired negative pressure as indicated by the reading of the piezoresistive transducer. Note that for very low pressure differentials, the influence of the 'wind' impacting on the chamber is measurable and significant. Hence, in the case of differentials of only a few mmWG the final adjustment should be done with the fans operating. Pressure and airflow should be recorded continuously during the final adjustment and an average pressure calculated.

The air exchange rate can be established either by measurement directly with tracer gas (SF_6) or by estimation using the measured airflow rate and assuming uniform mixing of the chamber. This assumption is generally valid when any air mover is operating in the chamber or a temperature differential exists across the chamber. In borderline quiescent tests, this assumption should be verified through a tracer test.

Unless a specific exposure time scenario is dictated ahead of time, it may be worthwhile to make a dry run test with the candidate powder to determine release and total exposure time sufficient to produce statistically significant readings and proper instrument range settings. At low air exchange rates and narrow aperture settings the penetration fractions of some powders may be too low for very short exposures.

Once all the sensors are calibrated and ready for operation, the powder may be released for the chosen duration. The LAS-X spectrometer, controlled by software from the HP-85 computer, should begin accumulating data at the moment the cloud appears at the chamber, as seen by the RAS-2 sensor readings. The LAS-X can record repeat spectra at a minimum 4 minute interval. Hence, if spectral data inside the chamber are required, synchronization with the cloud will ensure capture of the initial penetrating particles. Spectra should be accumulated continuously following passage of the cloud and as long as statistically significant data are obtained from the bins of interest. These data will later provide size-dependent particle decay data:

$$R_p = R + \beta_p$$

The approximate empirical protection factors, defined as the outside dose to the inside dose ratio over a given exposure time, are calculated from the analog mass concentration records. The Size-dependent RAS-2 sensor responses are corrected by the log-normal parameters of the challenge spectrum and the internal RAM-1 monitor response by the penetrating particles initial spectrum using the appropriate Mathcad utility program (MIE.MCD) to be described later. The inside dose value is somewhat inaccurate for long exposure times since size composition of measured mass concentrations is time-dependent, the particles decaying in accordance with the decay rate distribution. Hence, the monitor response is time-dependent. Results based on mass concentrations are considered first-order approximations unless the more detailed data from the spectrometer are analyzed for their time-dependent content.

In one series the same ventilation kinetics were maintained while different powders were disseminated. All disseminations were of 0.5 minute duration, simulating the shortest exposure time of interest in this exploratory series. The major parameters are as follows:

- disseminated mass: 1 gram,
- slit width: 0.1 mm (determined by feeler gauges)
- slit depth: 40 mm
- pressure differential: -1 mmWG

Results for the first series showed the expected phenomena. Protection factors were highest for the largest threat size spectra as the large particles are apparently filtered through the slit and decay most rapidly. These effects are seen most clearly by comparing the plots of Sipernat D11 (<0.4 microns) penetration with those of talc (0.3-10 microns) shown in figure 20. The upper pair of plots is the Sipernat test. The 0.5 minute exposure shown for two sensors yielded a well-developed, long-lived contamination of the chamber. The lower two plots show a series of three consecutive talc disseminations, each of 0.5 minute, on the same time scale as the plot above. The chamber concentrations are erratic at best and die out very shortly. Clearly, penetration of the talc, with a mass median diameter about 8 microns, is restricted in comparison to the much smaller Sipernat particles.

The following table gives the measured protection factors for 1/2 minute pulses. The exposure times used in the calculations reflect the relative speeds of disappearance of the major mass fractions for each powder:

number	test powder	PF_p	exposure time (min.)
1	Sipernat D11	16	20
* 2	Talc	70	1.5
3	Arizona dust	5	25
4	Talc	60	4.5
5	TiO_2 RCL3	6	40
** 6	Arizona dust	12	10

Notes: * poor statistics; ** 10 grams released during 10 minutes

The higher protection factors measured for talc exposure could indicate both considerable particle filtering in the aperture and rapid decay of the high mass particles. However, the short exposures did not permit the accumulation of sufficient particle counts to allow comparison of the size-dependent transport fractions from the LAS-X data.

For similar exposure times, the high protection factor for the Sipernat D11 compared to Arizona Road Dust may be a consequence of the rapid settling rate of the smallest particles. Arizona Road Dust has a large portion of its mass in the 0.5 to 2 micron region in which the settling rates have been seen to be the slowest, hence the protection factors are lowered

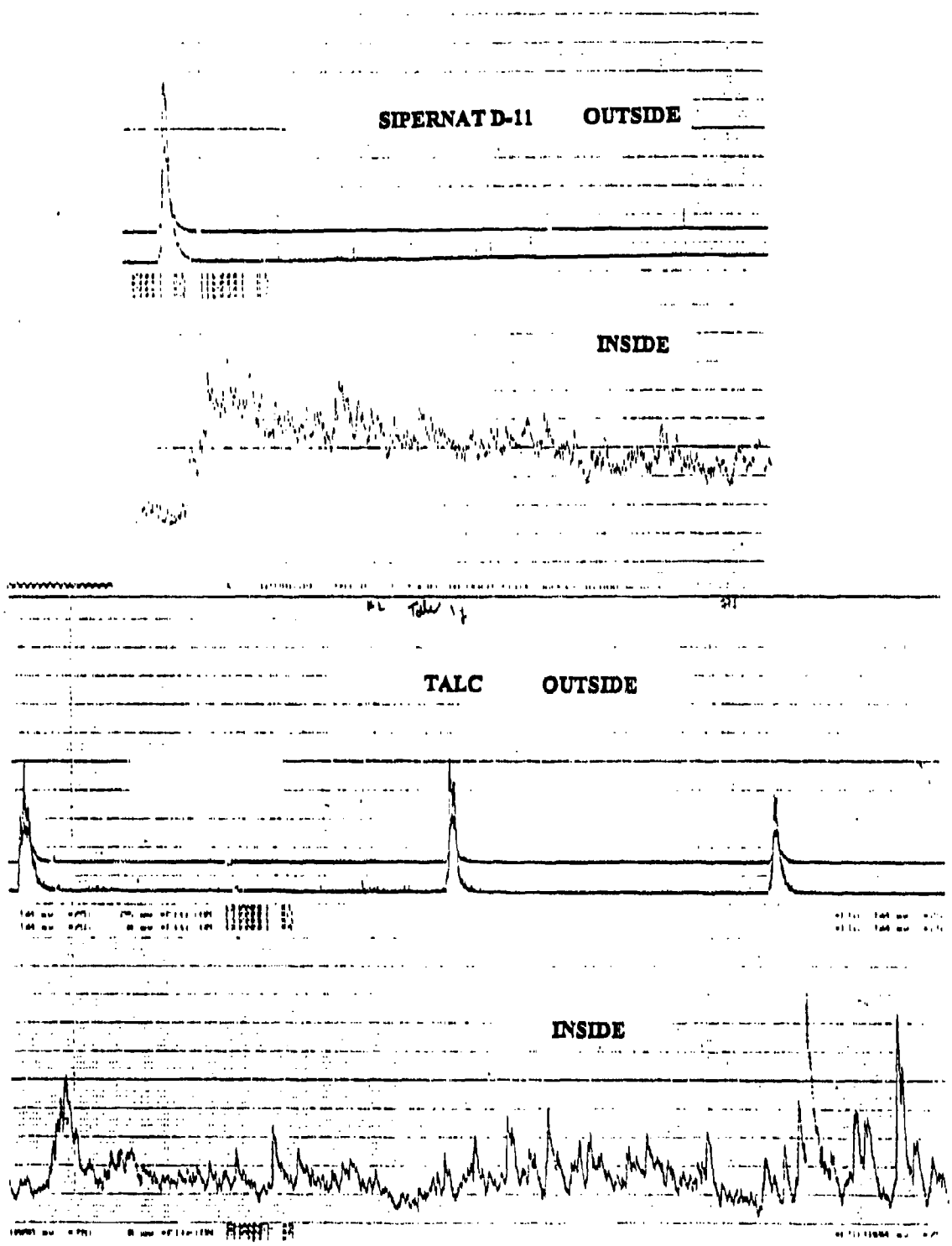

Figure 20: Solid Aerosol Penetration

by the ongoing exposure to these particles. A similar result occurred with the TiO_2 whose spectrum is in the problematic mid-range.

The presentation of results from the first series is qualitative in nature since only the integral exposure data are being considered and compared to expectations from our understanding of the powders used in the tests. The results will be compared to model calculations in the next chapter.

The second series of tests was designed to emphasize the size differentiation during particle penetration as a function of the differential pressure across the aperture using a talc exposure of longer duration to ensure statistically significant results. Three runs were performed at pressure differentials of -1, -2 and -3 mmWG with the same aperture. Results of the measurements are as follows:

Differential Pressure	Exposure Times		Protection
[mmWG]	T [min.]	t [min.]	Factor
-1	11	34	27
-2	11	29	15
-3	17	35	10

As expected, the protection factors measured fall sharply as the pressure differential increases. This is in part due to the increased air exchange rate which flushes particles out more rapidly. The extent to which particulate penetration itself was affected will be investigated further. Note again that at this point only gross integral information is provided by the mass concentration sensors. The results will later be compared to model predictions.

6.4 Solid Particle Penetration Factors

The extent of particle filtering in the aperture as a function of pressure differential was investigated by comparing the shapes of the particle size spectra of the cloud and of the penetrating fraction for the test at -1 mmWG and at -3 mmWG differential pressure. Data from the LAS-X spectrometer provided counts of the initial penetrating fraction. The spectrum of the threat cloud was obtained by the LAS-X prior to the test by sampling through the enclosure wall. In figure 21 are the inside/outside ratios of counts in each size bin for the two differential pressures. The vectors ratio0, ratio1, and ratio2 cover the range for which differentiation is expected, between 1 micron and the maximum size at about 7 microns . The square symbols show these ratio values on the semi-log plot. The sharp cutoff between 6 and 7 microns at -1 mmWG correlates well with the model results for the total transport fraction. Note that the ratio at 7.1 microns is statistically invalid, being based on single counts only. The transport fractions at -3 mmWG in the lower part of Figure 21 show less pronounced filtration, as would be expected from theory. There is no cutoff size. About 40-50% of the particles at 6-7 microns still penetrate the aperture.

The statistical fluctuations of the real data make it difficult to clearly compare the ratios for the different tests. The solid lines shown are the inside/outside ratios calculated from

TOTAL TRANSPORT FRACTIONS FOR -1MMWG PRESSURE DIFFERENTIAL

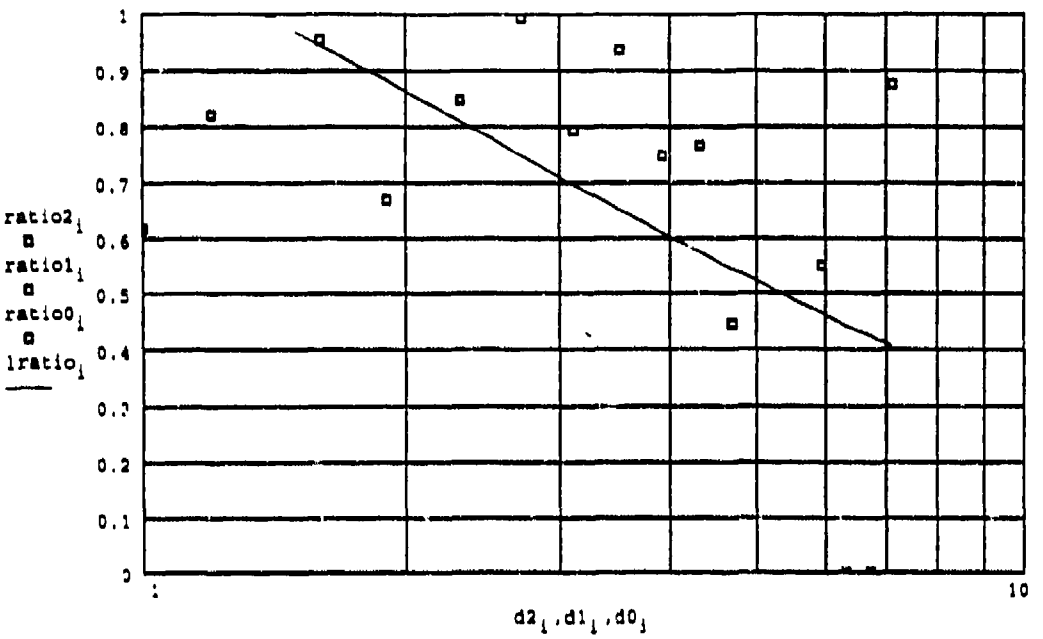

MICRONS
(Note cutoff at 6-7 microns)

TOTAL TRANSPORT FRACTIONS FOR -3MMWG PRESSURE DIFFERENTIAL

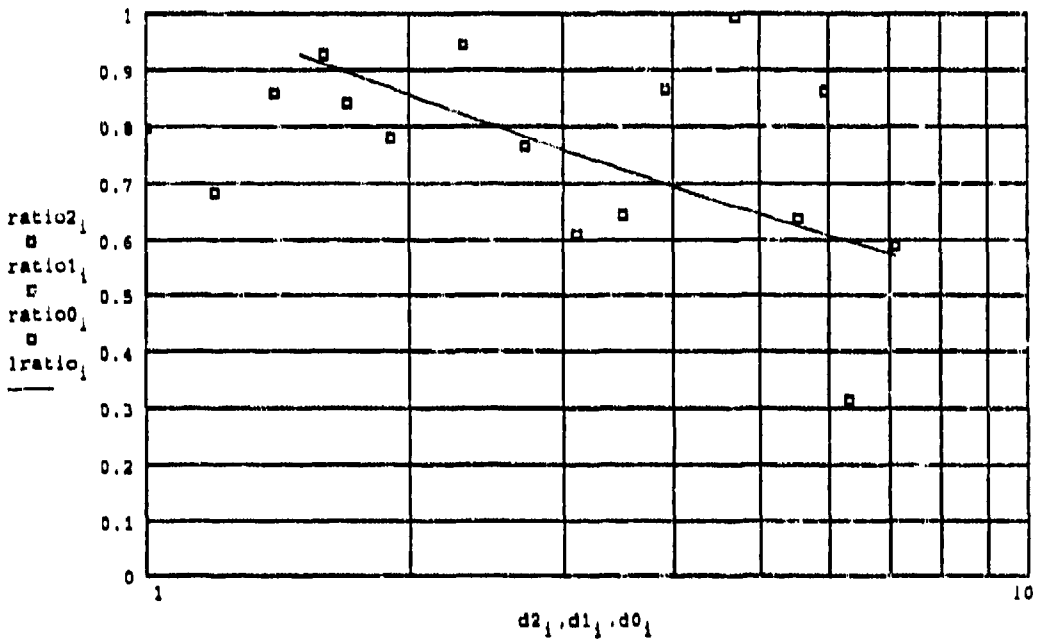

MICRONS

Figure 21: Solid Particle Penetration Factors

log normal distribution parameter estimates obtained from each data spectrum. The lines are not extended further since the theoretical distributions are asymptotic and the real size spectra are, of course, not. The ratios for the test at -3 mmWG pressure differential clearly show reduced filtering in comparison to the test at -1 mmWG. These results compare favorably with the model results shown in Figure 1 for the same range of pressure differentials.

6.5 Aperture Flow Characteristics

Solid aerosol dynamics are intimately linked to the ventilation kinetics of the enclosure. The air exchange rate is a major parameter controlling the particle balance. If the assumption of ideal air mixing is valid, the equation R=Q/V can be applied. This, of course, requires measurement of air flowrate and enclosure volume. In cases in which this is not feasible, the tracer decay method, discussed earlier, allows direct measurement of the air exchange rate.

The model program is constructed to calculate the airflow directly from the characteristics of the aperture and the pressure differential using equation 5. This is not essential to the protection factor calculations if other estimates of the air exchange rate are available. If so, this calculation may be bypassed. It is instructive, however, to get a feeling for flow characteristics by testing the aperture dynamics against theory and estimating the empirical parameters. This has been done for the 40 mm deep aperture at 0.1 mm height with -1 mmWG pressure through precise measurement of the air flowrate and pressure differentials. The flow exponent (n in equation 5) and the effective leakage area (and, hence, effective height) were then estimated by a Mathcad utility program designed for this purpose. A sample run of the program for this calculation is given in the Appendix.

Pressure differentials in the range 0.4 to 0.8 mmWG were measured with the Endevco piezoresistive transducer and recorded continuously on the strip-chart recorder. Air flowrate at the blower output was measured with the Gilian Instrument Corp. Gilibrator Primary Flow Calibrator. The Gilibrator can handle flows up to 30 lpm only, hence limiting the range of application. However, its being a primary calibration gave the advantage of reduced uncertainty.

Estimation of the best-fit parameters for Equation 5 using five data points yielded a correlation coefficient of 0.993. The flow exponent value for the nominal 0.1 mm aperture is 0.52 and the effective height of the aperture is 0.15 mm. The difference between the nominal and the effective aperture height is reasonable, considering the roughness of the height measurement using only feeler gauges. Extrapolation of the characteristic curve to -1 mmWG yielded a flowrate of 29 lpm which was also observed by direct measurement.

7. SOLID AEROSOL PROTECTION FACTOR MODEL CALIBRATION AND VERIFICATION

7.1 Model Calibration

Results of the model program given earlier were based solely on theoretical calculations of the parameters determining solid aerosol behavior in the enclosure. These include the air exchange rate R, the size-dependent settling rate β_p and filtration factor f_p. Calibration of the model prior to verifying it against solid aerosol protection factor measurements requires consideration of the validity of calculated parameter values.

As stated, the air exchange rate can either be calculated theoretically or estimated from measurement. The current version of the model uses the crack flow equation and, hence, empirical values of the relevant parameters (effective height and flow characteristic exponent, n) have been used to calibrate this segment of the model since their validity has been assured.

The theoretical model for the size-dependent particle settling rates (Equation 8) does not produce a satisfactory fit to the experimental data for the enclosure (the rate of change of settling rates with particle size for particles larger than 1 micron is lower experimentally than the theoretical value) although it does reproduce published results of other researchers who have used it to fit their empirical data. Attempts to find best-fit parameter values using the Asystant scientific programming language's curve-fitting algorithm found the problem to be rather ill-conditioned. The settling rate model was programmed as a nested user function and run through the optimization algorithm with many initial parameter values. The solutions, graphs of which are shown in Appendix C.4 along with the functions, showed the fitting function to be too insensitive to the turbulent energy intensity to be of value. A sampling of the results is given here:

Turbulent intensity (k_e)	Exponent (n)	Goodness of fit (R^2)
1000	2.038	0.9335
5000	2.222	0.9359
10000	2.301	0.9361

Since no reasonable combination of parameters succeeded in reproducing the observed settling rates at higher sizes, empirical data were adopted to calibrate the model. The form of the size-dependency was found to be identical for several powders tested to date so only a weighting factor was seen to be required in the model to adjust the calculation for different powder densities.

The transport of particles through the aperture appears to be modeled well enough at this point to permit use of the theoretical equations in the model. Of course, further runs with additional powder challenges are recommended, but there is no objective reason to reject the model as it stands in view of the positive results of the penetration tests at low differential pressures.

7.2 Model Output Verification

The model was run with the calibrations described in the previous section included and with parameters identical to those of the test experiments described previously, including the actual exposure times used to calculate the protection factors from the mass concentrations. The model results for both particles and vapors are compared to the experimental results in the following table. Recall that these runs were designed to accentuate the difference between the two protection factors by using minimum pressure differential (-1 mmWG) and a very narrow (0.1 mm) and deep (40 mm) aperture. The model calculations in the table include log-normal weighting with the known challenge spectrum in each case and the mass concentration ratios comprising the measured PF_p include sensor corrections in accordance with the same spectra..

#	Test Powder	d_g [microns]	Exposure Time [mins.]	PF_p(measured)	Model Results PF_p(solid)	Model Results PF_v(vapor)
1	Sipernat	0.18	20	16	13	8
*2	Talc	1.7	1.5	70	140	114
3	Arizona dust	0.7	25	5	10	6
4	Talc	1.7	4.5	60	50	34
5	Titanium dioxide	0.6	40	6	6	4
**6	Arizona dust	0.7	10	12	21	16

Notes: * poor statistics; ** 10 grams during 10 minutes

The numerical comparison between measured and calculated values of PF_p is reasonably good considering the brevity of the experiments. The 0.5 minute pulses led to poorer statistics than could be obtained with more extended exposures. However they do show that the experimental system can handle the desired span.

Note that the differences between the vapor and particulate protection factors are also as expected by the model. The smallest difference is for titanium dioxide, which has a narrow size spectrum in the 0.3-1 micron range. From Figure 3 we would expect the least difference between the factors in this region. Sipernat, with an narrow spectrum near 0.2 microns, produced a factor 2 difference between the solid and the vapor protection factors, again as expected from the model results. Also according to expectations, the broad Arizona road dust spectrum below 1 micron did not produce a significant difference. A most clear difference occurred with the talc exposure in test 4. The talc spectrum includes a significant portion of particles over 1 micron and, hence, according to the model results, a large difference between PF_p and PF_v is expected. The talc run in test 2 does not appear to be representative as the measured exposure inside the enclosure was too short to ensure statistically significant results. For this reason the next set of runs was done with longer challenge duration to ensure a fully developed inside exposure. Note that these brief experiments were carried out far from the equilibrium exposure levels. At the low exchange rates used, equilibrium exposure levels would have been reached only after several hours.

The next set of experiments investigated the influence of the pressure differential in determining the particle protection factor. Three runs were carried out with talc, the challenge with the largest expected differences in the factors. Three pressure differentials, again in the very low range expected to still show some size differentiation, were used. Challenge durations were extended sufficiently to effect a fully-developed inside exposure. The previously shown results of these tests, along with the model calculations are given in the following table.

			Model Results	
Pressure [mmWG]	Exposure Time [min.]	PF_p(measured)	PF_p(solid)	PF_v(vapor)
-1	11	27	18	5.5
-2	11	15	15	7
-3	17	10	12	3.6

The model results compare reasonably well with experiment for the solid aerosol protection factors, keeping in mind the uncertainty due to the time dependency of the sensor responses. The decrease in vapor protection with increasing pressure differential is obvious as the air exchange rate increases. The solid aerosol protection factors tracked the expected decrease as the increasing pressure differential pulls more and larger particles into the enclosure.

7.3 Sensitivity Analysis

Having seen that a reasonable correlation between the expected and the measured results is obtained, the model may be then used for parameter sensitivity testing. Such numerical testing helps, for example, to determine under what circumstances a significant difference between the vapor and the solid aerosol protection factors may occur or what must be done to prevent particles with a given size distribution from penetrating an enclosure.

In the model runs used for Figure 22, all the parameters are those previously used in the verification runs for a talc challenge. Only the aperture height is changed between the diagrams. In each diagram three sets of protection factors are plotted against the differential pressure: vapor, solid aerosol with quiescent mixing and solid aerosol with more turbulent mixing conditions (two small fans operating in the chamber). As seen in the experimental results, a 0.15 mm slit width with turbulent mixing particularly improves the solid aerosol protection at all pressure differentials as large particles are filtered out during penetration and the remainder decay to the surfaces more rapidly . This influence of turbulent impaction is sharply accentuated in the curve for quiescent mixing as the solid aerosol protection factors approach those of the vapor. The decay rates of the particles have slowed drastically and they are flushed out more nearly at the rate of the vapor molecules.

With a 1.0 mm slit width the filtering of particles is already insignificant and the solid aerosol protection factors are rapidly approaching those of the vapor, being kept higher primarily by turbulent impaction. With a 2.0 mm slit width the difference between the vapor and the particulate protection factors is inconsequential for all practical purposes.

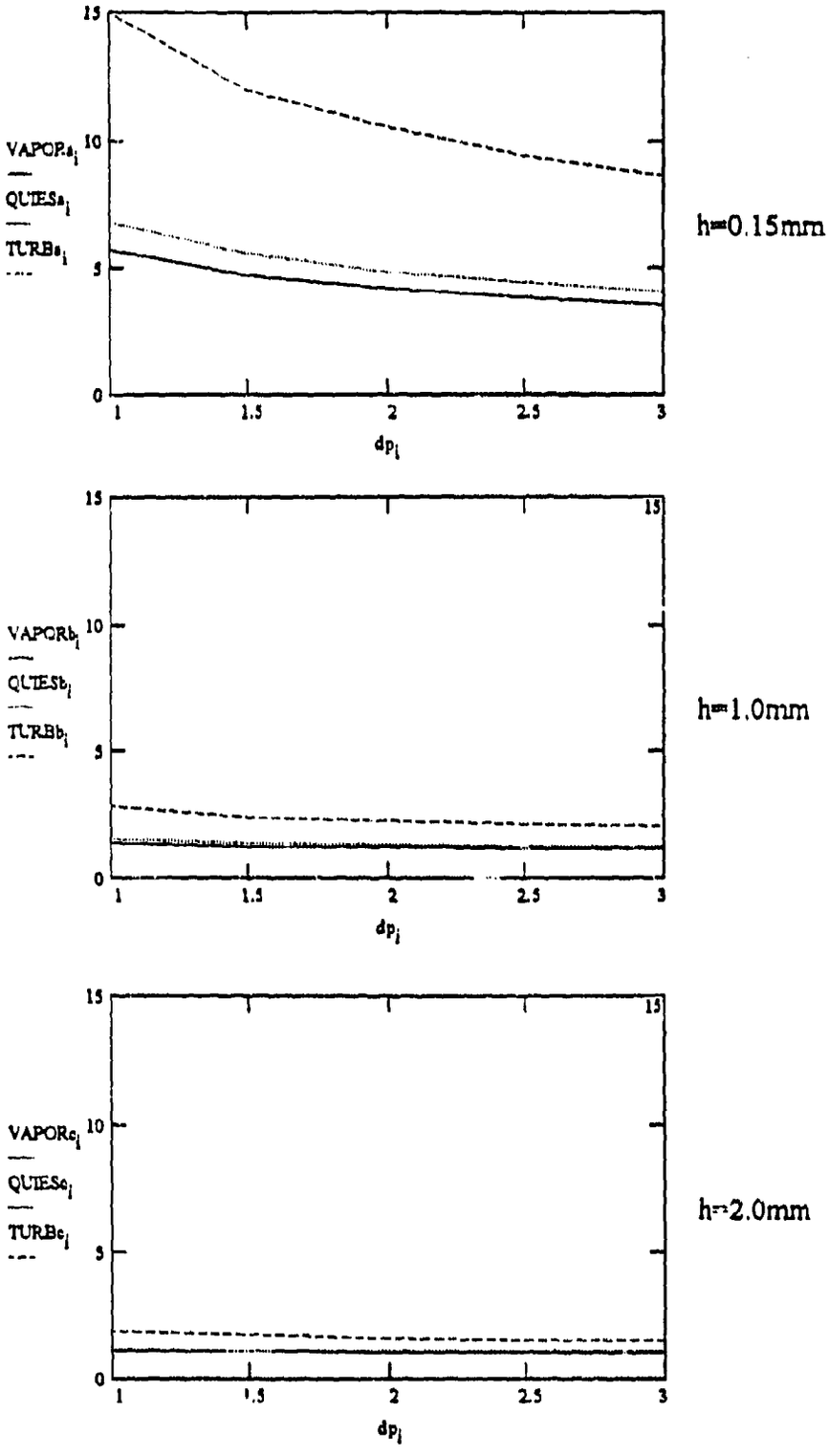

Varying slit height (h): vapor, quiescent and turbulent particle decay

Figure 22: Parameter Sensitivity Analysis

8. CONCLUSIONS

The primary goal of the research program was to develop the methodology needed to determine solid aerosol protection factors for enclosures and to express the controlling mechanisms in model calculations.

A model program has been constructed which calculates theoretical vapor and size-dependent solid aerosol protection factors for an enclosure with pressure-driven penetration. The model integrates the most current studies of particulate penetration factors and settling rates into the theoretical equation for the protection factor of a well-mixed enclosure. The model program is written in the Mathcad scientific language, providing an interactive tool appropriate for protection estimation, parameter sensitivity studies, and test procedure design.

An experimental system has been assembled which can provide real data on the parameters relevant to the calculation of solid aerosol protection factors for enclosures. The system can be used to produce data for model calibration, verification and prediction as well as for construction of a database of generally applicable parameter values. Together with the model program the facility will aid in optimizing integrity testing options for shelters and vehicles.

When combined with empirical data, model results to date correlate well with observed behavior. It appears that size-dependent filtration of particles in apertures will be limited to the millimeter width level at pressure differentials up to only several millimeters water gauge. The extent of turbulent impaction of particles within the enclosure will strongly affect the particulate protection factors. However, further work is needed to provide better characterization of particle settling in a stirred chamber in terms of the turbulent energy content before the effect can be satisfactorily quantified. It must be stressed that the sensitivity of the model output to the settling rates and the wide variance in the turbulent dissipation parameter values seen in the literature warrants caution in their application. Filtration of specific particles in rough apertures, phenomena such as possible electrostatic charges, surface effects, resuspension, and agglomeration will have to be characterized if the phenomena determining the protection factors for various challenges are to be fully understood..

9. RECOMMENDATIONS

The limited timeframe of the program and the onset of inclement weather precluded implementation of a comprehensive series of tests. Therefore, the tests performed were designed to accentuate the mechanisms which should lead to differentiation between the vapor and the particulate protection factors. This having been done and the results having demonstrated the ability of the system to provide quantitatively significant information, it is felt that there is now a basis for specific threat-oriented questions to be treated.

The analytical scheme adopted for the exploratory phase of the program has made use of direct particle size count data and integrated mass concentration data. It does not address other ways of looking at particulate data, such as the mass spectral distribution of polydisperse

threats. It is assumed that, further along, those concerned with specific threat scenarios will adopt the most appropriate definitions and make the conceptual link to the particulate protection factor.

The model is based on the assumption that the settling process is a perfect sink. Particles reaching the walls are lost to the system and do not pose a further threat. Thought should be given to more practical aspects of particles in a confined enclosure, such as in a crew compartment, which may be mechanically resuspended and pose a recurrent threat.

The shift from studying a well-defined enclosure/aperture system to testing an entire vehicle or shelter will have to be done with caution. So far, candidate powders of opportunity were used to help accentuate size-dependent phenomena. Calibrated monodisperse particles should be adopted also to reduce the complexity of the mass concentration sensor responses, especially in situations where experimental uncertainty is already high due to the gross integral nature of a whole-vehicle test. Considerable care will have to be taken also to ensure uniform exposure of a vehicle to the threat cloud in static scenarios, preventing erroneous conclusions due to spatial variances in the test concentration. Even more critical will be the need to produce and characterize realistic exposure profiles in complex dynamic scenarios, such as moving vehicles traversing a transient particulate cloud.

In order to provide a basic heuristic tool, the model constructed for this program involved the most simplistic mass balance assumptions and the experimental setup upon which its verification is based simulates this. It cannot be emphasized too strongly that the solid aerosol dynamics are driven first by the ventilation kinetics of the system. These should always be delineated by means of empirical tracer gas methods before the air/particle/enclosure system can be considered fully characterized.

It was the intention at the outset of this program to assemble a broad, flexible, state of the art instrumentation and computational system capable of independently providing reliable data and analyses to answer as many questions as may arise in the future regarding the protection of vehicles and enclosures from both vapor and solid aerosol challenges. It is the intention of this Technical Report and its Appendices to aid the next users of the system in its successful application. The key words here are likely to be flexibility and interaction. Instrumental components should be configured to answer specific questions and reconfigured again when results raise further questions, as so often happens. Model and utility programs developed so far should be altered, upgraded or discarded in accordance with their usefulness. They are designed to be changed readily and deleted just as readily. However, the user is cautioned not to rely only on what is offered here, rather to familiarize himself thoroughly with the instrument manuals, programming codes and literature references as well. Analysis of solid aerosol data can often be complex at least, open to subjective interpretation at best, and downright tricky at worst. Hence, the importance in applying the right methods to the right questions. It is hoped that some groundwork for flexible responses has been achieved here.

LITERATURE CITED

ASHRAE (1981) Handbook of Fundamentals, Chap. 23, Infiltration and Ventilation, Am. Soc. of Heat., Refrig., and Vent. Eng., Inc., N.Y.

Behnke, W. et al. (1988), "A Smog Chamber for Studies of the Photochemical Degradation of Chemicals in the Presence of Aerosols", Atmospheric Environment, 22#6, pp. 1113-1120.

Birenzvige, A. (1983a), "A Model to Predict the Threat of Exposure to Chemical Warfare Agents in Enclosed Spaces", ARCSL-TR-82093, Chemical Systems Laboratory, Aberdeen Proving Ground, MD.

Birenzvige, A. (1983b), "On the Vulnerability and Protectability of Facilities Against Penetration of Chemical Warfare Agents", ARCSL-TR-83037, Chemical Systems Laboratory, Aberdeen Proving Ground, MD.

Chen, B.T. et al (1992a), "Evaluation of an Environmental Reaction Chamber", Aerosol Science and Technology, 17, pp. 9-24.

Chen, C.C. et al (1992b), "Aerosol Penetration Through Filtering Facepieces and Respirator Cartridges",Am. Ind. Hyg. Assoc. J., 53#9, pp. 566-574.

Chester, C.V. (1988), "Technical Options for Protecting Civilians From Toxic Vapors and Gases", ORNL/TM-10423, Oak Ridge National Laboratory, Oak Ridge, TN.

Corner, J. and Pendlebury, E.D. (1951) Proc. Phys. Soc. B64, p. 645.

Cristy, G.A. and Chester, C.V. (1981), "Emergency Protection from Aerosols", ORNL-5519, Oak Ridge National. Laboratory, Oak Ridge, TN.

Crump, J. G. and J.H. Seinfeld (1981), "Turbulent Deposition and Gravitational Sedimentation of an Aerosol in a Vessel of Arbitrary Shape", J. Aerosol Science, 12#5, pp. 405-415.

Crump, J.G. et al. (1983), "Particle Wall Loss Rates in Vessels", Aerosol Science and Technology, 2, pp.303-309.

Engelmann, R.J. (1990), "Effectiveness of Sheltering in Buildings and Vehicles for Plutonium",DOE/EH-0159T, U.S. Dept. of Energy, Washington, D.C.

Engelmann, R.J. (1992a), "Sheltering Effectiveness Against Plutonium Provided by Buildings", Atmospheric Environment, 26A, pp. 2037-2044.

Fletcher, R.A. and Verkouteren, R.M. (1992) "Progress Report: Clean Air, Aerosol and Particle Transport Through Orifices: Preliminary Measurements", NIST, Gas and Particulate Science Div., Gaithersburg, MD.

Harrison, A.W. (1979), "Quiescent Boundary Layer Thickness in Aerosol Enclosures under Convective Stirring Conditions", J. Colloid and Interface Science, 69#3, pp. 563-570.

Hinds, W.C. and P. Bellin (1987), "Performance of Dust Respirators with Facial Seal Leaks II. Predictive Model", Am. Ind. Hyg. Assoc. J., 48#10, pp. 842-847.

Hinds, W.C. and G. Kraske (1987), "Performance of Dust Respirators with Facial Seal Leaks I: Experimental", Am. Ind. Hyg. Assoc. J., 48#10, pp. 836-841.

Holton, P.M. et al (1987), "Particle size-dependent Leakage and Losses of Aerosols in Respirators", Am. Ind. Hyg. Assoc. J., 48#10, pp. 848-854.

Kreith, F. and R. Eisenstadt (1957), "Pressure Drop and Flow Characteristics of Short Capillary Tubes at Low Reynold's Numbers", ASME Trans. 79, pp. 1070-1078.

Lewis, S.R., (1991), "Protection Factors Against Toxic Vapors for Leaky Enclosures", Internal Communication, Israel AEC, Nahal Soreq Nuclear Research Center.

Megaw, W.J. (1962), "The Penetration of Iodine into Buildings", Int'l. J. Air Water Pollut. 6, pp. 121-128.

Mitchell, J.P. et al. (1990) "The Penetration of Aerosols Through Fine Capillaries" RAMTRANS, 1#2, pp. 101-116.

Nauman, E.B. (1981), "Residence Time Distributions and Micromixing", Chem. Eng. Commun., 8, pp. 53-131.

Okuyama, K. et al. (1986), "Particle Loss of Aerosols with Particle Diameters between 6 and 2000 nm in Stirred Tank", J. Colloid and Interface Science, 110#1, pp. 214-223.

Roed, J. and Cannell, R. J. (1987), "Relationship Between Indoor and Outdoor Aerosol Concentration Following the Chernobyl Accident", Rad. Prot. Dosimetry. 21(1/3), pp. 107-110.

Schwendiman, L.C. and S.L.Sutter (1977), "Transport of Particles Through Gas Leaks - A Review", BNWL-2218.

Shair, F.H. and Heitner, K.L. (1974), "Theoretical Model for Relating Indoor Pollutant Concentrations to Those Outside", Environ. Sci. and Technol.ogy, 8, pp. 444-451.

Sinclair, D. et al. (1976), "Experimental Verification of Diffusion Battery Theory:", Air

Pollution Control Assoc. J., 26#7, pp. 661-663.

Soderholm, S.C. (1984) "Documentation for the Program: LAS-X Data Analysis", Los Alamos National Laboratory, Los Alamos, NM (in LAMAPP manual).

Sutter, S. et al (1980), "Depleted UO_2 Powder Flow Through Very Small Openings", NUREG/CR-1099, Battelle Pacific Northwest Laboratory, Richland, WA.

Van de Vate, J.F. (1972), "The Thickness of the Stagnant Air Layer in Aerosol Containments and the Aerodynamic Diameter of Aggregates of Small Spheres", J. Colloid and Interface Science, 41#2, pp. 194-197.

Van Dingenen, R. et al. (1989), "Molecule and Aerosol Particle Wall Losses in Smog Chambers Made of Glass", J. Aerosol Science, 20#1, pp. 113-122.

Wadden, R.A. and Scheff, P.A. (1983), Indoor Air Pollution and Control, Wiley, NY.

Witham, C.L. and R.W. Gates (1983), "Dry Dispersion with Sonic Velocity Nozzles", in Proc. Symp. Dissemination Techniques for Smoke and Obscurants, A. Deepak Publ., Hampton, VA., pp. 11-28.

BLANK

APPENDIX A

Protection Factors for Vapor and Solid Aerosols

The following provides a brief and simplified derivation of equations (1) and (2) in the text which define the protection factors for vapor and solid aerosol penetration into leaky enclosures. The major addition here is that the exposure resulting from continued occupation of the enclosure after the outside challenge has passed is taken into account.

The analysis assumes spatially uniform exposure of all leakage areas to the challenge concentration outside. It is further assumed that the infiltrating air carries with it the true outside concentration of challenge material at the enclosure boundary. This ideally ignores any possible boundary layer effects which could arise under various circumstances. The vapor is non-condensing and non-depositing.

The enclosure is characterized by an infiltration rate, R, in units of air changes/hour, determined by the ventilation dynamic scenario (wind speed and stability, thermal gradients, leakage areas, etc). Assume the enclosure to be exposed to a "square" cloud of contaminant in which the concentration, CE, increases abruptly to a value CO and then decreases abruptly to zero after finite time T. The rate of change of the inside concentration will be:

$$\frac{d}{dt}CI(t) = R\cdot\left(CE(t) - CI(t)\right)$$

This has the solution, for $0 < t < T$ when CE=CO:

$$CI_1(t) = CO\cdot\left(1 - \exp(-R\cdot T)\right)$$

and, for $t > T$ when CE=0:

$$CI_2(t) = CI(T)\cdot\exp\left(-R\cdot(t-T)\right)$$

Hence:

$$CI_2(t) = CO\cdot\left(\exp(R\cdot T) - 1\right)\cdot\exp(-R\cdot t)$$

We require the concentration-time integrals in order to calculate the dosages outside and inside the enclosure. At time t=T the outside dose is: $DO = CO\cdot T$

Inside the enclosure, for $0 < t < T$:

$$DI_1 = \int_0^T CI_1(t)dt$$

$$DI_1 = \frac{CO}{R}\cdot\left(R\cdot T - \left(1 - \exp(-R\cdot T)\right)\right)$$

For $t > T$:

$$DI_2 = \int_T^t CI_2(t)dt$$

Hence:

$$DI_2 = \frac{CO}{R}\cdot\left(1-\exp(R\cdot T)\right)\cdot\left(\exp(-R\cdot t)-\exp(-R\cdot T)\right)$$

The protection factor is defined as the ratio of the dose which would result from exposure to the outside concentration to the dose accumulating in the enclosure up to time t > T:

$$PF = \frac{DO}{DI_1 + DI_2}$$

Hence:

$$PF_v = \frac{R\cdot T}{R\cdot T-\left(1-\exp(-R\cdot T)\right)+\left(1-\exp(R\cdot T)\right)\cdot\left(\exp(-R\cdot t)-\exp(-R\cdot T)\right)}$$

Reducing this yields equation (1):

$$PF_v = \frac{R\cdot T}{R\cdot T+\exp(-R\cdot t)\cdot\left(1-\exp(R\cdot T)\right)}$$

Note the special case in which the cloud passage time equals exactly the inside exposure time, i.e., the occupants exit the enclosure immediately:

$$PF_v = \frac{R\cdot T}{R\cdot T-\left(1-\exp(-R\cdot T)\right)}$$

Addressing now a solid aerosol challenge, two effects that influence the interior dosage and, hence, the derivation of the protection factor, are the filtering of particles as they pass through the enclosure's leakage areas (cracks, seams, apertures, outlets, etc.) and the deposition of particles on interior surface areas. Resuspension of particles can also conceivably affect the overall balance at a later time as can evaporation of condensed vapors, but is not considered here. Both phenomena are particle-size dependent and as such cannot be characterized completely for a challenge scenario on the basis of ventilation dynamics alone without knowing the characteristics of the challenge. We look at the basic balance equation for the enclosure with the filtering factor, f_p, which reduces the penetrating particle concentration, and the decay rate, β_p, which contributes to the removal of particles:

$$\frac{d}{dt}CI_p(t) = f_p\cdot R\cdot\left(CO_v(t)-CI_p(t)\right)-\beta_p\cdot CI_p(t)$$

We can combine the two removal terms into one effective term (see Engelmann, 1992a):

$$R_p = R + \beta_p$$

Hence:

$$\frac{d}{dt} CI_p(t) = f_p \cdot R \cdot CO_p(t) - R_p \cdot CI_p(t)$$

Solving the equation of the form

$$\frac{dX}{a + b \cdot X} = dt$$

yields:

$$CI_p(t) = \frac{f_p \cdot R}{R_p} \cdot CO_p(t) - \frac{const.}{R_p} \cdot \exp(-R_p \cdot t)$$

with the given boundary conditions for 0<t<T:

$$CI_{p1}(t) = \frac{f_p \cdot R}{R_p} \cdot CO_p \cdot \left(1 - \exp(-R_p \cdot T)\right)$$

Solving for t>T:

$$CI_{p2}(t) = \frac{f_p \cdot R}{R_p} \cdot CO_p \cdot \left(1 - \exp(-R_p \cdot T)\right) \cdot \exp(-R_p \cdot (t - T))$$

Again, we require doses for the two time periods:

$$DI_{p1} = \int_o^T CI_{p1}(t)dt \qquad \text{and} \qquad DI_{p2} = \int_T^t CI_{p2}(t)dt$$

$$DI_{p1} = \frac{f_p \cdot R}{R_p} \cdot CO_p \cdot \left(T - \frac{1}{R_p} + \frac{\exp(-R_p \cdot T)}{R_p} \right)$$

$$DI_{p2} = \frac{f_p \cdot R}{R_p} \cdot CO_p \cdot \left(1 - \exp(R_p \cdot T)\right) \cdot \frac{1}{R_p} \cdot \left(\exp(-R_p \cdot t) - \exp(-R_p \cdot T)\right)$$

By definition we have: $PF_p = \dfrac{DO_p}{DI_{p1} + DI_{p2}}$ where $DO_p = CO_p \cdot T$

Combining and reducing terms yields equation (2):

$$PF_p = \frac{R_p \cdot T}{\frac{f_p \cdot R}{R_p}\left(R_p \cdot T + \exp(-R_p \cdot t) \cdot \left(1 - \exp(R_p \cdot T)\right)\right)}$$

Appendix A

BLANK

APPENDIX B

Protection Factor Model Program

The model program for protection factor calculation is written in the Mathcad programming language. The language combines equations, graphics and text in the same document. Equations are written directly into the program as they would be written by hand and are solved sequentially. Text and graphs are included and results are displayed as desired so that the actual program has the form of a report. The model program is included here in the following pages. It is assumed that the reader has familiarized himself with the language. Only the minimum amount of text necessary to follow the calculations is included within the body of the model. In order to preserve its form, additional explanations and comments are given here, followed by the model itself.

Page 1: PARAMETER VALUES

All the parameters relevant to the model run are concentrated on the first page. These include those needed for particle transport (density, viscosity, temperature and physical constants), modelling constants (particle size range, indices and unit multipliers), system parameters (enclosure dimensions, aperture dimensions, differential pressures and flow constants) and experimental parameters (turbulent dissipation parameters, empirical settling rates, cloud duration, exposure time, challenge spectral parameters and an optional challenge spectrum). The 'current test ID' is revised to indicate the test from which the data were taken. Of course, all parameters listed on the page can be altered for any run as long as their values reflect physical reality (recall the GIGO Syndrome).

Page 2: PRELIMINARY CALCULATIONS

Air flowrate, required for calculation of vapor and particulate transport, is calculated from the 'crack' equation with the differential pressure as the driving force. Note that differential pressure is an independent variable given five values from 1 to 3 mmWG in this run. Hence all calculations depending on it are vectors with the index j. All particle size-dependent calculations are indexed with i, the range of sizes from 0.1 to 10 microns defined at the beginning of the program. Cunningham's correction, terminal velocities, diffusion coefficients, settling parameters and the lognormal distribution function are calculated here for all future use. The Reynold's numbers for flow through the aperture are printed for reference, although not included in any calculations.

PENETRATION TRANSPORT - DEPOSITION BY MOLECULAR DIFFUSION

The empirical equations for transport through a rectangular channel mentioned in the literature search (Schwendiman and Sutter, 1977) are adopted for use here. In order to simplify the programming, if the condition $\beta < 0.1$ exists, and the alternative expression given should be used, the change is done manually later on. Values of this parameter along with selected values of the diffusion coefficient and the partial transport fraction are given on page 3 against particle size

m_o. These results should be examined at the first run with new parameters to determine if the alternative expression should be used.

Page 3: PENETRATION TRANSPORT - TURBULENT IMPACTION

As stated in the report, deposition velocities for narrow apertures and consideration of rough surfaces have not been treated here. The terminal velocities are used for now, resulting in minimum wall losses. Selected values of the results are printed for reference.

Page 4: PENETRATION TRANSPORT - GRAVITATIONAL SETTLING

The equation given in Schwendiman and Sutter (1977) is shown along with selected results.

TOTAL TRANSPORT FRACTION

The three mechanisms are combined into a final expression for the fraction of particles entering which are transported through the aperture. Note that the small square symbol after an equation written in Mathcad indicates that the expression is not included in the calculations, rather it is part of the text. The equation is essentially 'turned off'. At this point the user must chose the proper expression dependent on the value of β. The correct expression is 'turned on' and the alternate is 'turned off'.

Page 5: TOTAL PENETRATION TRANSPORT MATRIX

The total penetrating fractions are shown in a two-dimensional matrix as a function of particle sizes (rows) and differential pressures (columns). The particle size range is shown at the left for reference. Pressure values increase to the right in the matrix.

As noted in the comment, negative values of the transport fraction at the highest sizes and lowest pressures are liable to appear due to exaggerated losses by the combined mechanisms. This is, of course, not physically realized but rather due to the simplicity of the model. More detailed modelling of the deposition velocities in narrow crack flow are needed but is beyond the current scope of the program. The negative valued results are removed later.

The plot shows the transport fractions against particle size over the entire size range with the differential pressure as the parameter (pressure increases with the higher curves) .

Page 6: STIRRED SETTLING OF PARTICLES

The particle settling rates are calculated here using ther equation given by Chen, et al (1992). The two parameters, ke and ne, define the turbulent dissipation intensity. The resulting vector of theoretical settling rates (solid line) is plotted against particle size along with the empirical values supplied initially (dotted line). The extent of the goodness of fit for the theoretical values is clearly seen. This submodel may be used to manually optimize the two

parameters or to analyze their sensitivity. Automatic optimization was done separately with the ASYSTANT language. The best fit parameters have been used here. As is readily seen in the plot, the fit is not satisfactory in this instance. The size of minimum settling rate seen experimentally (0.55 microns) is reproduced and the settling rate gradient with increasing size is too great. No combination of parameter values was able to reproduce these results within the framework of the chosen model.

For this reason, empirical values are used in parallel with theoretical values for calculating the protection factors for solid aerosols. At some time it will have to be decided whether the sensitivity to the differences in the settling rates warrants further theoretical work on improving the published model for the scenarios to be researched at a later date.

Primarily as a tool for comparison of integral mass concentration data with theoretical results, settling rates have been weighted with the lognormal distribution of the challenge size spectrum. The proximity of the resulting weighted numbers shows that in this case the discrepancies may not be too severe. This aspect should be given attention in all cases where uncertainty is high before using the theoretical results further.

Page 7: PROTECTION FACTORS FOR THE EXPOSURE SCENARIO

The vapor protection factor is based on the air exchange rate, R_j, for each pressure differential value. This is calculated here based on the assumption of complete mixing in the enclosure. This assumptiom has been verified for the enclosure under like ventilation kinetics by the use of tracer gas. The flow rate calculated by the crack flow equation and displayed here in units of m^3/hr and l/min has been calibrated by direct measurement with a primary flow standard.

The total particulate removal rate, Rp_{ij}, includes the air exchange rate and the settling rate. Representative values at 0.1, 1.0 and 10 microns are displayed and can be compared to the vapor removal rate.

The protection factors are calculated next using the equations derived in Appendix 1. Negative results for the particulate protection factor due to exaggerated filtration of large particles at low pressure differentials are eliminated by setting them equal to the last positive result, making this occurence obvious in the final result tables.

Page 8: THEORETICAL PROTECTION FACTORS

This page shows a summary of the relevant parameters for the scenario and tables of the results. The vapor protection factors, Pv, are shown as a vector of results in order of ascending pressure values. The particulate protection factors, Pp, are shown as a two-dimensional matrix in particle sizes (rows) and presusres (columns). All the factors are displayed on the plot below. The vapor factors are straight lines, being independent of particle size. The influence of the particle-specific mechanisms are seen clearly at the lowest and highest size ranges. The y-axis of the plot has been cut off at 50 in order emphasize the effects at the lower values.

Page 9: WEIGHTED PROTECTION FACTORS FOR THE CHOSEN SIZE SPECTRUM

On the first page of the program, the option was given to provide a particle size spectrum, N_j, of any desired spectral distribution. This spectrum is now used to weigh the theoretical size-dependent protection factors accordingly. This weighting yields a single numerical value for the given challenge. These values, wPF_j, are plotted against the pressure differentials together with the corresponding vapor protection factors.

Page 10: WEIGHTED PROTECTION FACTORS FOR LOGNORMAL DISTRIBUTION

If the challenge size spectrum has been characterized by a lognormal distribution, whose parameters have been supplied at the beginning of the program, the results can be weighted by this optimum distribution. The distribution is shown in the small plot. A table of optional statistical definitions (Reist, 1984) is provided as a tool for visualizing other characteristics which may be of specific interest. Any definition, dp, can be calculated by chosing the corresponding parameter, p, from the table.

Since the theoretical distribution is asymptotic and the real spectrum is not, the weighting function is truncated to the end of the real spectrum by cutting off the index i. The protection factors are then weighted by the truncated distribution and diplayed in the plot along with the vapor protection factors.

Pages 11-12: PROTECTION FACTORS USING EMPIRICAL SETTLING DATA

Since the theoretical settling rate results may not be satisfactory, the protection factors are recalculated here using the empirical data supplied at the beginning. The data are plotted again for reference. The weighting factor, mult, is used to chose the correct level of turbulent dissipation for which the data are representative (see figure 18). The protection factors are again weighted by the lognormal distribution and displayed on page 12 with the theoretical factors and the vapor factors. Here the effect of the discrepancies between the empirical and the modelled settling rates is clearly seen. The decision can be taken at this point as to whether more effort should be invested in improving the model for a given enclosure and exposure scenario.

PROTECTION FACTORS FOR SOLID AEROSOL PENETRATION INTO SEALED ENCLOSURES

PFACDOC.MCD Version 19 Feb 93

Current test ID: 1221T1x

PARAMETER VALUES:

particle density $\rho = 2.7$ g/cm3 ORIGIN = 1

indices $a = 1..11$ $j = 1..5$
$x = 12..20$ $o = 1, 3..20$
$i = 1..20$

sizes microns: m_a m_x

m_a	m_x
.1	2
.2	3
.3	4
.4	5
.5	6
.6	7
.7	8
.8	9
.9	10
1	
1.5	

diff. press. $dpWG_j$

$dpWG_j$
1
1.5
2
2.5
3.

Exp. sizes N_i / Exp. decay exB_i

N_i	exB_i
1.56	2
8.53	1
.61	.7
0	.5
0	.4
0	.4
0	.425
0	.45
0	.5
0	.525
0	.7
0	.85
0	1
0	1.2
0	1.3
0	1.4
0	1.5
0	1.6
0	1.8
0	2

$exB_i = exB_i \cdot 10^{-3}$

sizes $d_i = m_i \cdot 10^{-4}$ cm

gravity acceleration $g = 980$ cm/sec2

air viscosity $\eta = 1.83 \cdot 10^{-4}$ g/cm/s

Boltzmann constant $k = 1.38 \cdot 10^{-16}$ erg/K

Temperature Temp = 288 deg K

flow exponent $n = .5$

flow coefficient $Cd = 1$

Turbulent dissipation parameters: ke = 1000 [1/sec] ne = 2.038

empirical multiplier: mult = .189

Dimensions of rectangular enclosure:

Height:	Length:	Width:	
L1 = 117	L2 = 213	L3 = 167	[cm]

aperture depth: height width: perimeter: area:
l = 4 h = 0.015 w = 80 $P = 2 \cdot (w + h)$ cm $Ar = w \cdot h$ cm2

smallest dimension: b = h

Cloud duration: T = .08333 Exposure time t = 0.5 [hours]

Lognormal spectrum parameters: Sigma: Geom. mean:
sigG = 2.284 meanG = 1.2

Appendix B

PRELIMINARY CALCULATIONS:

air flowrate: $Qr_j = 406 \cdot Cd \cdot Ar \cdot (dpWG_j)^n$ cm3/s

$$Vr_j = \frac{Qr_j}{Ar} \text{ cm/sec}$$

Cunningham's correction:

$$Fd_i = 1 + \frac{1.76 \cdot 10^{-5}}{d_i} + \frac{5.6 \cdot 10^{-6}}{d_i} \cdot \exp\left(-7.44 \cdot 10^{-4} \cdot d_i\right)$$

Terminal velocities: $$Ut_i = \frac{\rho \cdot g}{18 \cdot \eta} \cdot (d_i)^2 \cdot Fd_i$$

Diffusion coefficients: $$Db_i = \frac{k \cdot Temp}{3 \cdot \pi \cdot \eta \cdot d_i} \cdot Fd_i$$

Settling parameter: $$X1_i = \frac{\pi \cdot Ut_i}{ne \cdot \sin\left(\frac{\pi}{ne}\right) \cdot \left[ke \cdot (Db_i)^{ne-1}\right]^{\frac{1}{ne}}}$$

Reynold's numbers: $$Rn_j = b \cdot Vr_j \cdot 1.2 \cdot \frac{10^{-3}}{\eta}$$

Rn_j
40
49
56
63
69

Lognormal distribution:

$$lognorm_i = \left[\frac{1}{\left[\sqrt{(2 \cdot \pi)} \cdot \ln(sigG) \cdot m_i\right]}\right] \cdot \exp\left[\frac{\left(\left(\ln\left(\frac{m_i}{meanG}\right)\right)\right)^2}{\ln(sigG)} \over -2\right]$$

PENETRATION: TRANSPORT - DEPOSITION BY MOLECULAR DIFFUSION:

Under laminar flow conditions the deposition of particles is controlled by the diffusion coefficients, the length of the channel and the flow through the channel. The controlling parameter is then defined as:

$$\beta_{i,j} = \pi \cdot Db_i \cdot \frac{1}{Qr_j}$$

For transport through a rectangular channel:

$$f\alpha 5a_{i,j} = .819 \cdot \exp\left(-3.65 \cdot \beta_{i,j}\right) + .097 \cdot \exp\left(-22.3 \cdot \beta_{i,j}\right)$$

$$f\alpha 5b_{i,j} = .032 \cdot \exp\left(-57 \cdot \beta_{i,j}\right) + .027 \cdot \exp\left(-123 \cdot \beta_{i,j}\right) + .025 \cdot \exp\left(-750 \cdot \beta_{i,j}\right)$$

$$f\alpha 5DR_{i,j} = f\alpha 5a_{i,j} + f\alpha 5b_{i,j}$$

If $\beta < 0.1$ use:

$$f\alpha 6DR_{i,j} = 1 - 2.56 \cdot (\beta_{i,j})^{.667} + 1.2 \cdot \beta_{i,j} + .177 \cdot (\beta_{i,j})^{1.333}$$

m_o
0.1
0.3
0.5
0.7
0.9
1.5
3
5
7
9

mic.

Db_o
$7.65 \cdot 10^{-6}$
$1.36 \cdot 10^{-6}$
$6.75 \cdot 10^{-7}$
$4.38 \cdot 10^{-7}$
$3.22 \cdot 10^{-7}$
$1.77 \cdot 10^{-7}$
$8.28 \cdot 10^{-8}$
$4.82 \cdot 10^{-8}$
$3.4 \cdot 10^{-8}$
$2.63 \cdot 10^{-8}$

cm2/sec

$\beta_{1,j}$
$1.97 \cdot 10^{-7}$
$1.61 \cdot 10^{-7}$
$1.4 \cdot 10^{-7}$
$1.25 \cdot 10^{-7}$
$1.14 \cdot 10^{-7}$

$\beta_{19,j}$
$6.77 \cdot 10^{-10}$
$5.53 \cdot 10^{-10}$
$4.79 \cdot 10^{-10}$
$4.28 \cdot 10^{-10}$
$3.91 \cdot 10^{-10}$

cm-1

Selected transport fractions:

$f\alpha GDR_{(1,j)}$
$9.999 \cdot 10^{-1}$
$9.999 \cdot 10^{-1}$
$9.999 \cdot 10^{-1}$
$9.999 \cdot 10^{-1}$
$9.999 \cdot 10^{-1}$

$f\alpha 6DR_{(10,j)}$
1
1
1
1
1

$f\alpha 6DR_{(19,j)}$
1
1
1
1
1

$f\alpha 5DR_{(1,j)}$
1
1
1
1
1

$f\alpha 5DR_{(10,j)}$
1
1
1
1
1

$f\alpha 5DR_{(19,j)}$
1
1
1
1
1

PENETRATION TRANSPORT - TURBULENT IMPACTION:

Deposition will be determined by turbulent eddy transport and the inertial properties of the particles. The deposition velocity must be derived from considerations of Reynold's number and surface roughness. But using the terminal settling velocity, Ut, for now leads to minimum wall loss.

$$f\alpha TR_{i,j} = \exp\left(\frac{-P \cdot Ut_i \cdot l}{Ar \cdot Vr_j}\right)$$

Selected transport fractions:

m_o
0.1
0.3
0.5
0.7
0.9
1.5
3
5
7
9

microns

$f\alpha TR_{(1,j)}$
1
1
1
1
1

$f\alpha TR_{(10,j)}$
0.987
0.989
0.991
0.992
0.993

$f\alpha TR_{(19,j)}$
0.416
0.489
0.538
0.574
0.603

PENETRATION TRANSPORT - GRAVITATIONAL SETTLING:

Settling is dependent on leak rate, particle density and diameter, and channel dimensions.

Using Thomas' eqn. for gravity settling in a rectangular channel:

$$f\alpha GR_{i,j} = 1 - 1 \cdot Ut_i \cdot \frac{w}{Qr_j}$$

Selected transport fractions:

m_o microns	$f\alpha GR_{(1,j)}$	$f\alpha GR_{(10,j)}$	$f\alpha GR_{(19,j)}$
0.1	1	0.993	0.562
0.3	1	0.995	0.642
0.5	1	0.995	0.69
0.7	1	0.996	0.723
0.9	1	0.996	0.747
1.5			
3			
5			
7			
9			

TOTAL TRANSPORT FRACTION:

The total transport fraction is defined as the ratio of the total number of particles exiting the aperture to the number entering. The total number exiting will be, in terms of the above transport fractions, the number entering less the loss due to each process:

$$N_{out} := N_{in} - (1 - faD) \cdot N_{in} - (1 - f\alpha T) \cdot N_{in} - (1 - f\alpha G) \cdot N_{in}$$

The total transport fraction, Nout/Nin, reduces to:

$$f := f\alpha D + f\alpha T + f\alpha G - 2$$

For $\beta > 0.1$ use $\quad fR_{i,j} = f\alpha 6DR_{i,j} + f\alpha TR_{i,j} + f\alpha GR_{i,j} - 2$

For $\beta < 0.1$ use $\quad fR_{i,j} = f\alpha 5DR_{i,j} + f\alpha TR_{i,j} + f\alpha GR_{i,j} - 2$

Appendix B

TOTAL PENETRATION TRANSPORT MATRIX:

m_i

microns
0.1
0.2
0.3
0.4
0.5
0.6
0.7
0.8
0.9
1
1.5
2
3
4
5
6
7
8
9
10

$fR =$

0.999	1	1	1	1
0.999	0.999	0.999	0.999	0.999
0.997	0.998	0.998	0.998	0.999
0.996	0.997	0.997	0.997	0.998
0.994	0.995	0.996	0.996	0.997
0.992	0.994	0.994	0.995	0.995
0.99	0.992	0.993	0.993	0.994
0.987	0.989	0.991	0.992	0.992
0.984	0.987	0.989	0.99	0.991
0.981	0.984	0.986	0.988	0.989
0.959	0.967	0.971	0.974	0.976
0.93	0.943	0.951	0.956	0.96
0.852	0.878	0.894	0.905	0.913
0.747	0.791	0.818	0.837	0.85
0.621	0.685	0.725	0.752	0.773
0.477	0.563	0.617	0.654	0.682
0.319	0.428	0.497	0.544	0.58
0.152	0.283	0.366	0.425	0.469
-0.022	0.131	0.228	0.297	0.35
-0.2	-0.027	0.084	0.164	0.224

$dpWG_j$

mmWG
1
1.5
2
2.5
3

(Negative values reflect exaggerated loss of largest particles)

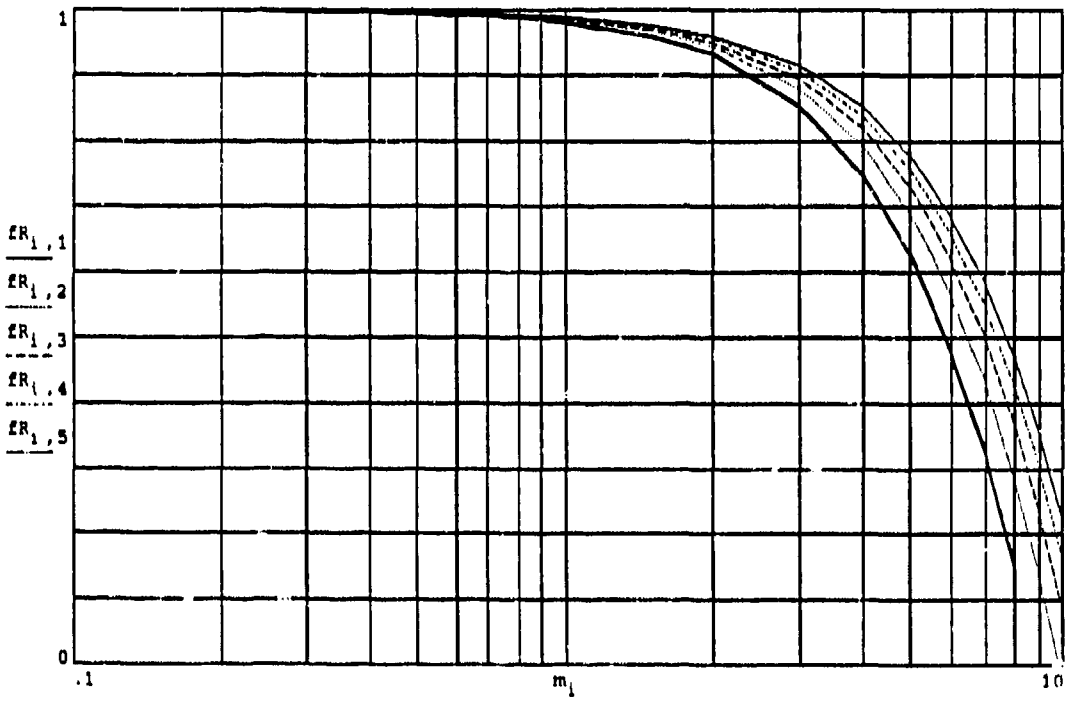

microns

(Differential pressure increases with higher curves)

Appendix B

STIRRED SETTLING OF PARTICLES:

N.B.- Turbulent eddy diffusion is defined by: $De = ke \cdot Y^{ne}$

Particle decay rates for rectangular chamber [1/sec]:

$$B_i = \frac{2 \cdot Ut_i}{X1_i} \cdot \left(\frac{1}{L2} + \frac{1}{L3}\right) + \left(\frac{Ut_i}{L1 \cdot \tanh\left(\frac{X1_i}{2}\right)}\right) \qquad ke = 1 \cdot 10^{3} \qquad ne = 2.038$$

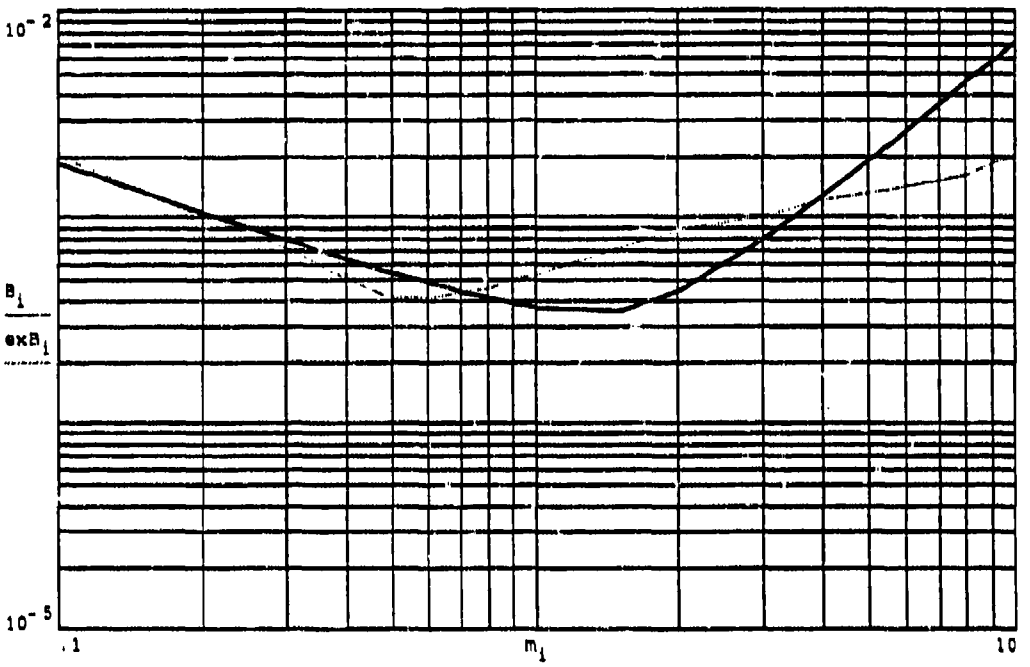

microns

Calculate theoretical lognormal-weighted decay rate:

$$lnB = \frac{\sum_i lognorm_i \cdot B_i \cdot m_i}{\sum_i lognorm_i \cdot m_i} \qquad lnB = 6.922 \cdot 10^{-4} \quad 1/sec$$

Calculate experimental lognormal-weighted decay rate:

(Experimental particle decay rates derived from 1204T7 test data)

$$wexB = \frac{\sum_i lognorm_i \cdot exB_i \cdot m_i}{\sum_i lognorm_i \cdot m_i} \qquad wexB = 6.692 \cdot 10^{-4} \quad 1/sec$$

Appendix 3

PROTECTION FACTORS FOR THE EXPOSURE SCENARIO:

Air infiltration rate: $R_j \equiv \frac{Qr_j \cdot 3600}{L1 \cdot L2 \cdot L3}$ [1/hour]

Total particulate removal: $Rp_{i,j} \equiv R_j + B_i \cdot 3600$ [1/hour]

Display air flowrates and selected removal rates:

$dpWG_j$	$Qr_j \cdot .0036$	$Qr_j \cdot .06$	R_j	$Rp_{(1,j)}$	$Rp_{(10,j)}$	$Rp_{(19,j)}$
1	1.754	29.232	0.421	7.019	1.709	21.161
1.5	2.148	35.802	0.516	7.113	1.804	21.256
2	2.48	41.34	0.596	7.193	1.884	21.336
2.5	2.773	46.22	0.666	7.263	1.954	21.406
3	3.038	50.631	0.73	7.327	2.018	21.47
mmWG	[m3/hr]	[l/min]	[1/hr]	[1/hr]	[1/hr]	[1/hr]
				0.1	1.0	10 microns

Calculate Protection Factors:

Vapor:

$$Pv_j \equiv \frac{R_j \cdot T}{R_j \cdot T + \exp(-R_j \cdot t) \cdot (1 - \exp(R_j \cdot T))}$$

Particulate:

$$Pp_{i,j} \equiv \frac{Rp_{i,j} \cdot T}{\left[Rp_{i,j} \cdot T + \exp(-Rp_{i,j} \cdot t) \cdot (1 - \exp(Rp_{i,j} \cdot T)) \right] \cdot \frac{fR_{i,j} \cdot R_j}{Rp_{i,j}}}$$

Eliminate negative values resulting from exaggerated filtration:

$$Pp_{i,j} \equiv \text{if}(Re(Pp_{i,j}) < 0, Pp_{i-1,j}, Pp_{i,j})$$

Appendix B

THEORETICAL PROTECTION FACTORS: 1221T1 talc/nozzle

$dpWG_j$

1
1.5
2
2.5
3

[mmWG]

ρ = 2.7 [g/cm3] Cd = 1 T = 0.083 [hr]

l = 4 [cm] n = 0.5 t = 0.5 [hr]

h = 0.015 [cm] ke = $1 \cdot 10^{3}$ ne = 2.038

w = 80 [cm]

Particles: Pp =

17.4	14.3	12.5	11.3	10.4
11.6	9.6	8.4	7.6	7
9.8	8.2	7.2	6.5	6
9	7.5	6.6	5.9	5.5
8.5	7.1	6.2	5.6	5.2
8.2	6.8	6	5.4	5
8	6.5	5.8	5.3	4.9
7.8	6.5	5.7	5.1	4.8
7.7	6.4	5.6	5.1	4.7
7.6	6.3	5.5	5	4.6
7.7	6.4	5.6	5.1	4.7
8.5	7	6.1	5.5	5
11.6	9.3	8	7.2	6.6
17.5	13.7	11.6	10.2	9.3
28.5	21.3	17.6	15.3	13.7
49.9	34.8	27.7	23.5	20.7
98.2	60.1	45.2	37.1	31.9
264.9	116.4	78.4	60.7	50.3
264.9	314.9	157.1	108.2	84.1
264.9	314.9	519.3	239.8	160

m_i

0.1
0.2
0.3
0.4
0.5
0.6
0.7
0.8
0.9
1
1.5
2
3
4
5
6
7
8
9
10

microns

Vapor:

Pv =

5.7
4.7
4.2
3.8
3.5

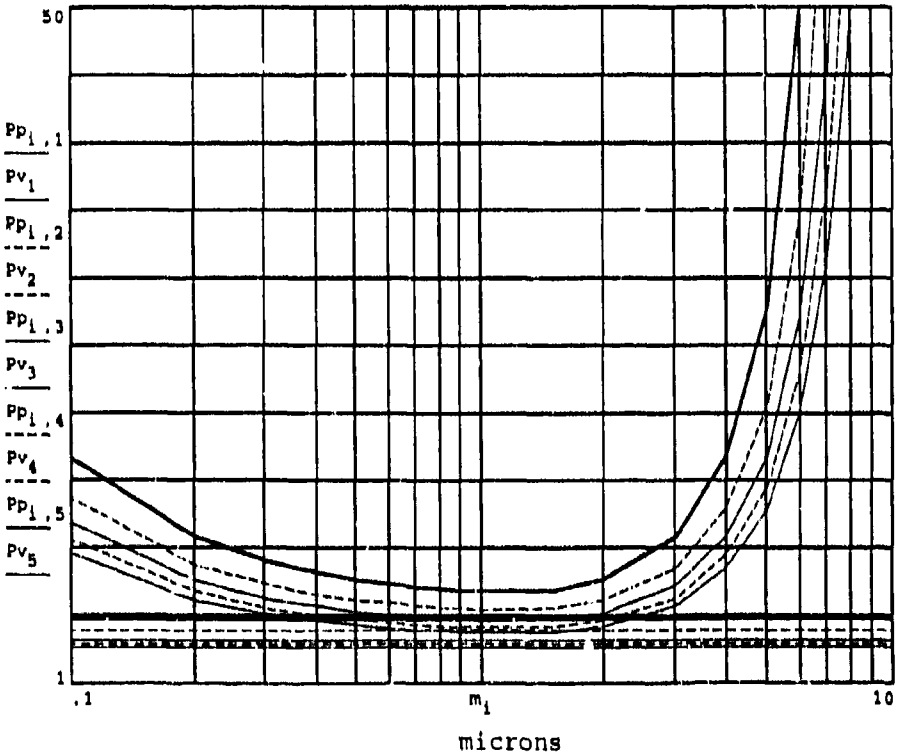

Appendix B

WEIGHTED PROTECTION FACTORS FOR THE GIVEN SIZE SPECTRUM:

m_i	N_i
0.1	1.56
0.2	8.53
0.3	0.61
0.4	0
0.5	0
0.6	0
0.7	0
0.8	0
0.9	0
1	0
1.5	0
2	0
3	0
4	0
5	0
6	0
7	0
8	0
9	0
10	0

microns

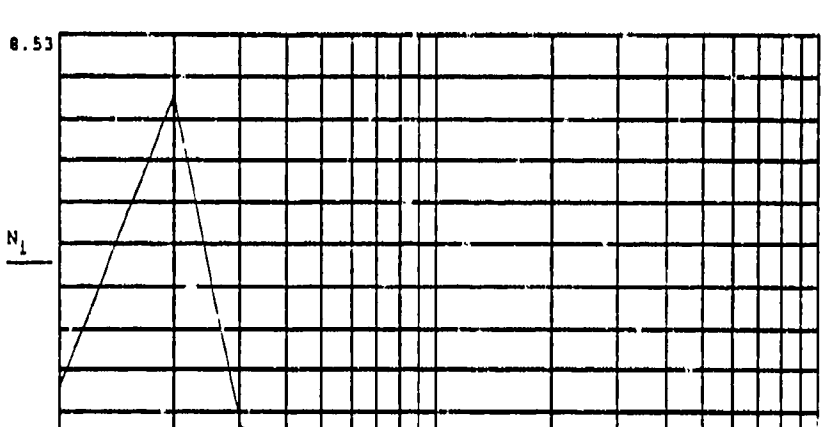

microns

$$wPF_j = \frac{\sum_i N_i \cdot Pp_{(i,j)} \cdot m_i}{\sum_i N_i \cdot m_i}$$

Weighted protection factors vs pressure

$dpWG_j$	wPF_j
1	11.9
1.5	9.8
2	8.6
2.5	7.8
3	7.2

mmWG

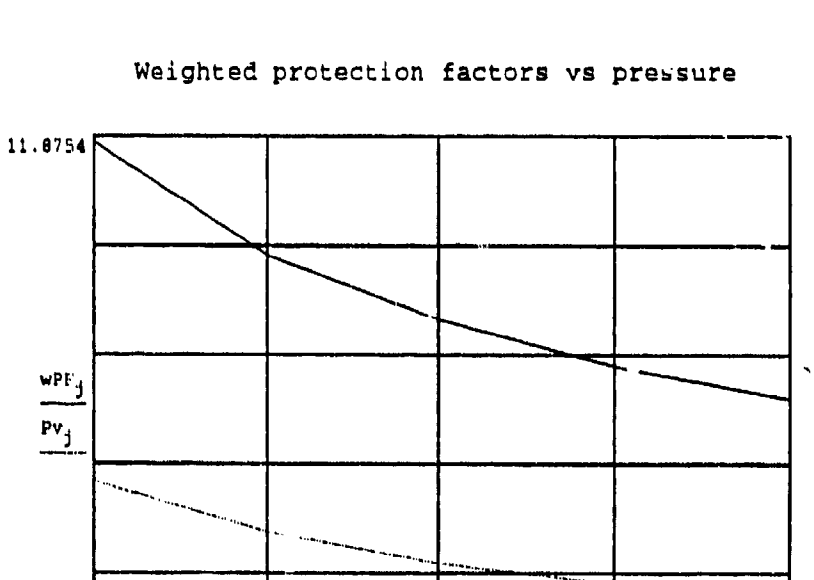

pressure [mmWG]

WEIGHTED PROTECTION FACTORS FOR LOGNORMAL DISTRIBUTION:

definition (dp)	p
Mode	-1
Geometric mean or mode	0
Arithmetic mean	0.5
Diameter of average area	1
Diameter of average mass	1.5
Surface median diameter	2
Surface mean diameter	2.5
Volume (mass) median diameter	3
Volume (mass) mean diameter	3.5

Distribution parameters

sigG = 2.284 meanG = 1.2

chosen p:

p = -1

$dp = meanG \cdot \exp\left(p \cdot \ln(sigG)^2\right)$

dp = 0.607 microns

m_o	$lognorm_o$
0.1	0.052
0.3	0.394
0.5	0.551
0.7	0.558
0.9	0.505
1.5	0.31
3	0.087
5	0.022
7	0.007
9	0.003

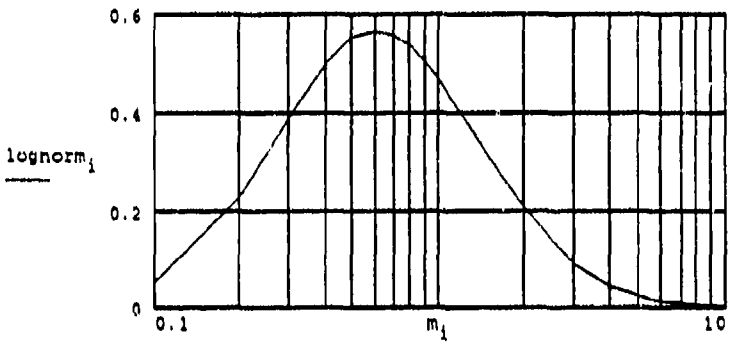

i = 1 .. 16 (truncate at m < 7 microns)

$$PFln_j = \frac{\sum_i lognorm_i \cdot Pp_{(i,j)} \cdot m_i}{\sum_i lognorm_i \cdot m_i}$$

Vapor: Particles:

$dpWG_j$	Pv_j	$PFln_j$
1	5.69	9.96
1.5	4.75	8.03
2	4.18	6.94
2.5	3.8	6.22
3	3.52	5.71

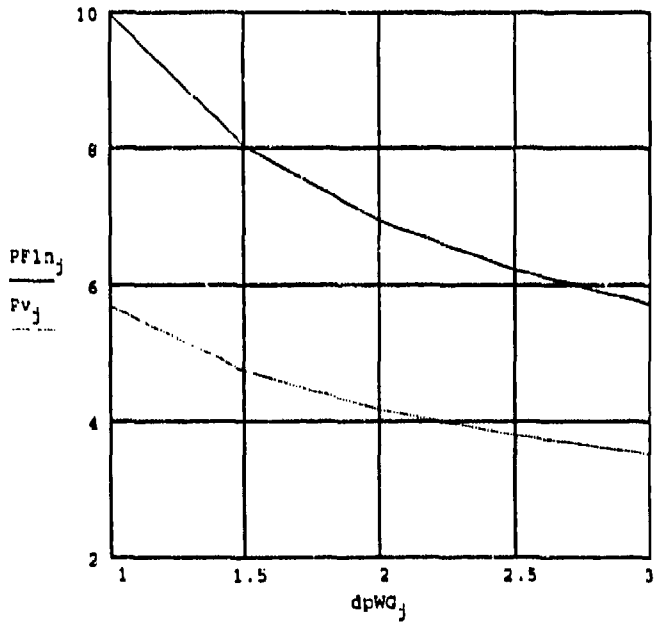

pressure differential [mmWG]

PROTECTION FACTORS USING EMPIRICAL SETTLING DATA:

Settling rate corrected relative to original data:

$$exRp_{i,j} := R_j + exB_i \cdot 3600 \cdot mult$$

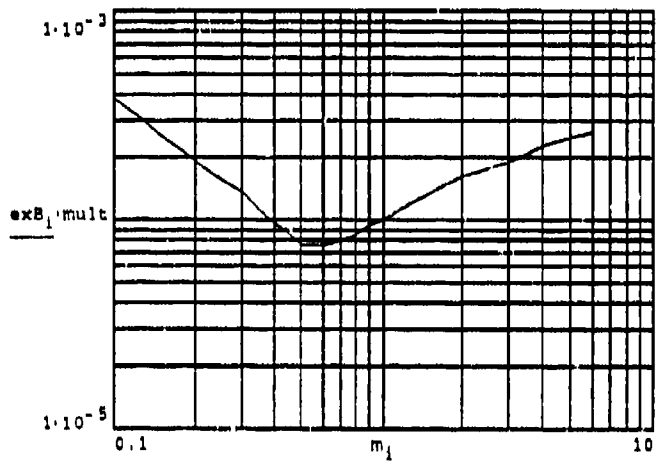

microns

$$exPp_{i,j} := \frac{exRp_{i,j} \cdot T}{\left[exRp_{i,j} \cdot T + \exp\left(-exRp_{i,j} \cdot t\right) \cdot \left(1 - \exp\left(exRp_{i,j} \cdot T\right)\right) \right] \cdot \frac{fR_{i,j} \cdot R_j}{exRp_{i,j}}}$$

Eliminate negative values from results:

$$exPp_{i,j} := if\left(Re\left(exPp_{i,j}\right) < 0, exPp_{i-1,j}, exPp_{i,j}\right)$$

Calculate experimental lognormal weighted protection factors:

$$exPFln_j := \frac{\sum_i lognorm_i \cdot exPp_{(i,j)} \cdot m_i}{\sum_i lognorm_i \cdot m_i}$$

Appendix B

Weighted protection factors using experimental settling rate data:

$dpWG_j$	vapor Pv_j	theoretical $PFln_j$	experimental $exPFln_j$
1	5.69	9.96	6.79
1.5	4.75	8.03	5.55
2	4.18	6.94	4.84
2.5	3.8	6.22	4.37
3	3.52	5.71	4.02

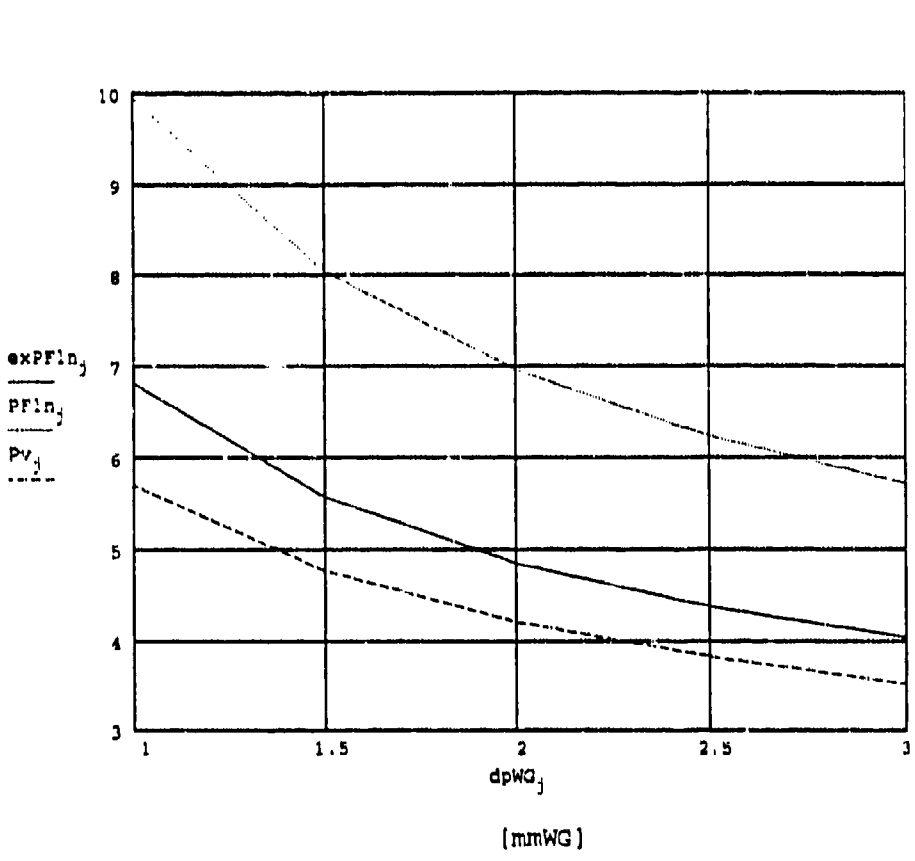

Appendix B

APPENDIX C

Utility Data Analysis Programs

C.1. LAS-X Net Particle Counts

Data acquisition from the LAS-X Aerosol Spectrometer is performed by a dedicated HP-85A personal computer and analysis program (Soderholm, 1984). Since data analysis will eventually be performed on an IBM-compatible machine, it was decided to transfer the data to a Mathcad program which would provide the functions of background subtraction, dilution correction and spectrum display. Later versions could be adapted for automated data acquisition and alternative spectral characteristics, such as lognormal fitting and mass-related fuctions. The LAS-X provides four size ranges, each comprising 15 individual bins, and an oversize bin for each range. The size ranges are as follows.

Range 3:	0.120 - 0.210	micron	interval = 0.006	micron
Range 2:	0.170 - 0.590	"	" 0.03	"
Range 1:	0.300 - 1.800	"	" 0.10	"
Range 0:	1.500 - 7.500	"	" 0.40	"

The size intervals of the ranges differ widely one from the other, hence it is difficult to visually grasp spectra which span several ranges. A utility program was written in Mathcad language to facilitate LAS-X data analysis by compressing the background- and dilution-corrected counts from each range into new intervals which are easier to visualize. Results are displayed in a new spectrum comprising 42 bins instead of 60. The compression ratios of the smaller size bins can be easily adjusted to account for any spectra of interest in the future. The following program, named LASXDOC.MCD, is provided with minimum comments in the body of the text. Additional comments are provided here.

Page 1:

The program is initialized with identifying numbers for the test. TID and BID are the sampling times automatically printed on the LAS-X outputs with each run. The dilution factor x20 is included if the TSI Diluter was used in the run. If not, the number 1 is written. The indices i through q determine the subdivisions of the ranges that are to be compressed. They can be changed to tailor the program for specific solid aerosols.

INPUT BACKGROUND DATA OF THE FOUR SIZE RANGES:

The dx_j vectors are the fixed sizes of each bin in the four ranges. The $bkgdx_j$ vectors are the raw data counts from each bin printed out by the HP-85A program. They are replaced by the new data at each run. If the same background run is used repeatedly for a series of runs, they do not have to be altered.

CORRECT FOR x20 DILUTION AND EFFICIENCY IF APPLICABLE

This segment corrects each background range for the dilution factor if dil=20. The highest size range, $bkgd0_i$, includes a correction factor for the efficiency of the diluter at these sizes. The manufacturer's efficiency curve was previously fit to a polynomial function using the ASYSTANT curve fitting option.

Page 2:

CALCULATE COMPRESSED BINS FOR RANGE 3:

Range 3 is compressed into three bins, each including five original bins as determined by the indices j, k and l. The interval size is now 0.018 micron.

DEFINE NEW BIN SIZES FOR THE COMPRESSED RANGE 3:

These constants are the new mid-point sizes redefined for the compressed range 3.

CALCULATE COMPRESSED BINS FOR THE SECOND HALF OF RANGE 1:

This segment compresses the range 1.0-1.7 microns to provide a smoother transition to the highest range 0.

DEFINE NEW SIZE BINS FOR THE COMPRESSED RANGE 1:

These constants are the new mid-points redefined for the compressed range 1.

PLOT THE COMPRESSED BACKGROUND DATA COUNTS:

The plot shows the smoothed background spectrum after compression of range 3. Ambient background at the test site is always below 0.5 micron so that range 0 is not affected.

Page 3:

INPUT EXPERIMENTAL DATA:

The four $datax_i$ vectors are the raw count data of the test run itself. They correspond to the size ranges appearing on page 1. They are replaced by new data vectors for each run whether or not the background data had to be changed. Recall that the test identification number and the aerosol name are to be updated for each run. It is useful to also change the file name each time to indicate the nature of the run and to save results individually.

CORRECT DATA FOR DILUTION FACTOR AND EFFICIENCY IF APPLICABLE:

As for the background data, the test data is adjusted for dilution, if needed.

CALCULATE COMPRESSED BINS FOR RANGE 3/ SECOND HALF OF RANGE 1:

As for the background data, the test data are compressed in a like manner. The sizes of the new bins were calculated previously.

Page 4:

PLOT COMPRESSED DATA COUNTS:

The test data are displayed with the new size bins. Note that there is still overlap between ranges, but the plot is smoother than the original uncompressed version.

CALCULATE NET COUNTS ABOVE BACKGROUND/PLOT NET COUNTS:

Background counts in the compressed ranges are subtracted from the data counts to provide net counts in each range and plotted.

Page 5:

The compressed net counts in the new bins are tabulated alongside the newly defined sizes.

LASXDOC.MCD

CALCULATION OF NET PARTICLE COUNTS FROM LAS-X SPECTROMETER DATA

version 23 Sept 92

This program accepts raw size count data from the PMS LAS-X Laser Aerosol Spectrometer and converts them to a compressed background- and dilution-corrected spectrum.

Aerosol: TiO2 Tiona Test identification TID := 150540

Input dilution factordil := 20 Background identification BID := 131130

i := 1..15 j := 1..5 k := 6..10 l := 11..15 m := 1..3

n := 1..6 o := 7..9 p := 10..12 q := 13..15 ORIGIN = 1

INPUT BACKGROUND DATA OF THE FOUR SIZE RANGES:

$d3_i :=$	$bkgd3_i :=$	$d2_i :=$	$bkgd2_i :=$	$d1_i :=$	$bkgd1_i :=$	$d0_i :=$	$bkgd0_i :=$
.120	125	.17	451	.3	11	1.5	0
.126	120	.20	258	.4	3	1.9	0
.132	112	.23	168	.5	1	2.3	0
.138	129	.26	64	.6	0	2.7	0
.144	109	.29	36	.7	0	3.1	0
.150	119	.32	18	.8	0	3.5	0
.156	136	.35	11	.9	1	3.9	0
.162	121	.38	6	1.0	0	4.3	0
.168	116	.41	1	1.1	0	4.7	0
.174	84	.44	1	1.2	1	5.1	0
.180	97	.47	1	1.3	0	5.5	0
.186	89	.50	0	1.4	0	5.9	0
.192	70	.53	0	1.5	0	6.3	0
.198	65	.56	1	1.6	0	6.7	0
.204	66	.59	0	1.7	0	7.1	0
micron	counts	micron	counts	micron	counts	micron	counts

CORRECT FOR x20 DILUTION AND EFFICIENCY IF APPLICABLE:

$bkgd3_i := if(dil - 20, bkgd3_i, bkgd3_i \cdot dil)$ $bkgd2_i := if(dil - 20, bkgd2_i, bkgd2_i \cdot dil)$

$bkgd1_i := if(dil - 20, bkgd1_i, bkgd1_i \cdot dil)$

$bkgd0_i := if\left[dil - 20, bkgd0_i, bkgd0_i \cdot dil \cdot \left[1.06 - .024 \cdot d0_i - .002 \cdot (d0_i)^2\right]\right]$

CALCULATE COMPRESSED BINS FOR RANGE 3:

$$bkgd3x_1 := \sum_j bkgd3_j \qquad bkgd3x_2 := \sum_k bkgd3_k \qquad bkgd3x_3 := \sum_l bkgd3_l$$

DEFINE NEW BIN SIZES FOR THE COMPRESSED RANGE 3:

$$d3x_1 := .132 \qquad d3x_2 := .162 \qquad d3x_3 := .192$$

CALCULATE COMPRESSED BINS FOR THE SECOND HALF OF RANGE 1:

$$bkgd1x_1 := \sum_o bkgd1_o \qquad bkgd1x_2 := \sum_p bkgd1_p \qquad bkgd1x_3 := \sum_q bkgd1_q$$

DEFINE NEW BIN SIZES FOR THE COMPRESSED RANGE 1:

$$d1x_1 := 1.0 \qquad d1x_2 := 1.3 \qquad d1x_3 := 1.6$$

PLOT THE COMPRESSED BACKGROUND DATA COUNTS:

BID = 131130

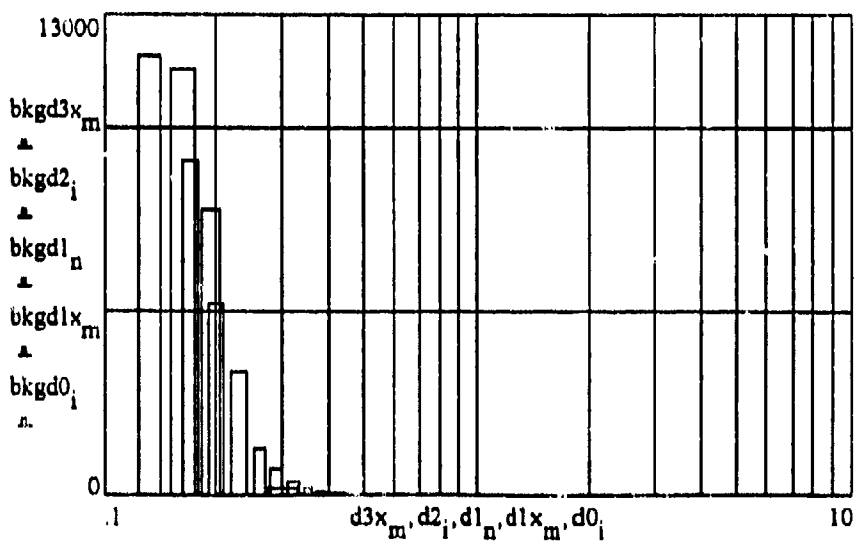

INPUT EXPERIMENTAL DATA:

$data3_i :=$	$data2_i :=$	$data1_i :=$	$data0_i :=$
557	1855	3375	3379
369	1052	3567	1454
285	769	9237	638
308	755	10969	332
269	654	6386	176
270	674	4441	109
282	568	3261	43
294	558	2632	31
218	471	1982	18
292	518	1556	10
205	507	1306	12
226	611	959	2
236	935	691	2
196	1430	558	3
205	2076	441	2
counts	counts	counts	counts

CORRECT DATA FOR DILUTION FACTOR AND EFFICIENCY IF APPLICABLE:

$$data3_i := if(dil - 20, data3_i, data3_i \cdot dil) \qquad data2_i := if(dil - 20, data2_i, data2_i \cdot dil)$$

$$data1_i := if(dil - 20, data1_i, data1_i \cdot dil)$$

$$data0_i := if\left[dil - 20, data0_i, data0_i \cdot dil \cdot \left[1.06 - .024 \cdot d0_i - .002 \cdot (d0_i)^2\right]\right]$$

CALCULATE COMPRESSED BINS FOR RANGE 3:

$$data3x_1 := \sum_j data3_j \qquad data3x_2 := \sum_k data3_k \qquad data3x_3 := \sum_l data3_l$$

CALCULATE COMPRESSED BINS FOR SECOND HALF OF RANGE 1:

$$data1x_1 := \sum_o data1_o \qquad data1x_2 := \sum_p data1_p \qquad data1x_3 := \sum_q data1_q$$

PLOT COMPRESSED DATA COUNTS:

TID = 150540

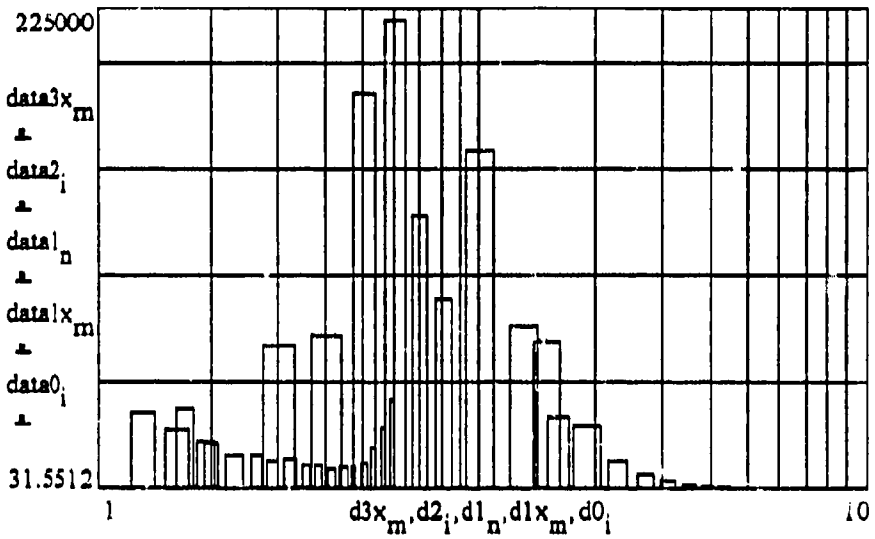

microns

CALCULATE NET COUNTS ABOVE BACKGROUND:

$net3_m := data3x_m - bkgd3x_m$ $net2_i := data2_i - bkgd2_i$

$net1_n := data1_n - bkgd1_n$ $net1x_m := data1x_m - bkgd1x_m$ $net0_i := data0_i - bkgd0_i$

PLOT NET COUNTS:

TID = 150540 TiO2 Tiona

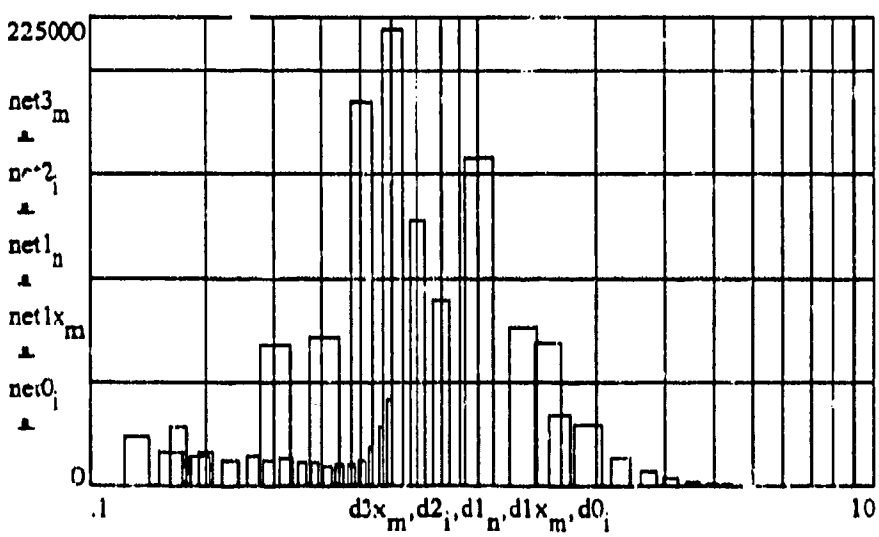

microns

DISPLAY COMPRESSED NET COUNTS:

$d3x_m$	$net3_m$
0.132	23860
0.162	15600
0.192	13620
micron	counts

$d2_i$	$net2_i$
0.17	28080
0.2	15880
0.23	12020
0.26	13820
0.29	12360
0.32	13120
0.35	11140
0.38	11040
0.41	9400
0.44	10340
0.47	10120
0.5	12220
0.53	18700
0.56	28580
0.59	41520
micron	counts

$d1_n$	$net1_n$
0.3	67280
0.4	71280
0.5	184720
0.6	219380
0.7	127720
0.8	88820
micron	counts

$d1x_m$	$net1x_m$
1	157480
1.3	76400
1.6	33800
microns	counts

$d0_i$	$net0_i$
1.5	68898
1.9	29289
2.3	12686
2.7	6511
3.1	3402
3.5	2074
3.9	805
4.3	570
4.7	325
5.1	177
5.5	208
5.9	34
6.3	33
6.7	49
7.1	32
microns	counts

C.2. Exponential Decay Rate Calculation

The estimation of exponential decay rates, whether from tracer gas concentration or solid aerosol settling in a stirred enclosure, is done by least squares fit of the logarithm of the concentration data against time. A utility program written in Mathcad, LASXRATE.MCD shown on the next page, serves all applications of this nature.

The example shown is for the settling of particles from a certain size bin of LAS-X data. First, the number of data points, N, is specified. A time vector, $time_k$, is inputted corresponding to the measurements, $count_k$. Background counts, if constant over the measurement, are inputted as $bkgd_k$. If the measurement is of long duration, such that the background is changing as well, a function can be inputted instead.

Net counts are calculated and normalized by the first value for simplicity. Mathcad functions INTERCEPT and SLOPE then calculate values for the zero intercept, exp(u), and the slope, v. The correlation coefficient is calculated by Mathcad function CORR. The decay rate in units of sec^{-1}, in this case. The normalized data points and the fitted function are plotted together.

The utility program may be used for any exponentially decaying data set as long as consistent time units are maintained.

EXPONENTIAL DECAY RATE CALCULATION

LASXRATE.MCD

data: 1204t7 bin 3.90-4.30 micron

Data index: $N := 14$ points $k := 1..N$ Background: $bkgd_k := 0$ counts

$time_k :=$	$count_k :=$
0	37
4	27
8	25
12	17
16	18
20	17
24	12
28	10
32	8
36	8
40	6
44	4
48	2
52	1

Calculate net counts and normalize:

$$c_k := \frac{count_k - bkgd_k}{count_1} \qquad lnC_k := \ln c_k$$

Calculate best fit to exponential function:

$u := intercept(time, lnC)$ $u = 0.12$

$\exp(u) = 1.128$

$v := slope(time, lnC)$ $v = -0.0573$

Calculate correlation coefficient:

$corr(time, lnC) = -0.95857$

Calculate decay rate in 1/seconds:

$$rate := \frac{-v}{60} \qquad rate = 9.55 \cdot 10^{-4} \qquad sec\text{-}1$$

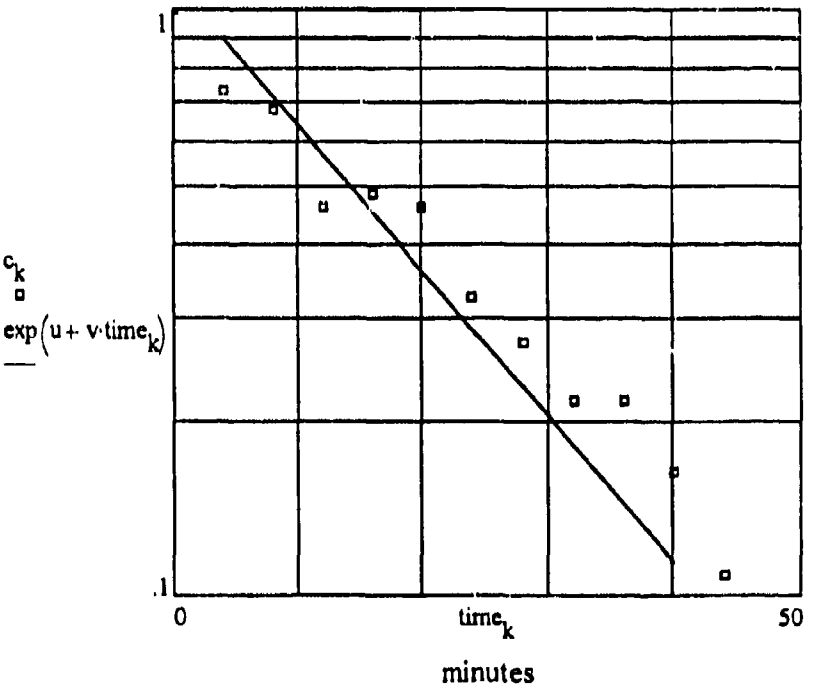

C.3. Theoretical Settling Rate Calculation

In order to study the theoretical model of particle settling in a stirred enclosure independently, the utility programs SETTLENEDOC.MCD and SETTLEN.DOC were compiled. These are essentially the same as the submodel that is integrated into the protection factor model program but used separately to allow parameter sensitivity tests with the turbulent dissipation intensity, k_e, and the exponent, n. as an independent parameters. Any other parameter can be tested if the appropriate changes in the indices are made. Sample runs of the two programs folow.

The dimensions of the rectangular enclosure are those of the test exposure chamber. The remaining parameter values given are typical. The particle settling rates are calculated in a two-dimensional matrix as a function of size and the chosen parameter vector.

Results are plotted on Page 2 of each run. Terminal velocities and diffusion coefficients are plotted for reference. In the first run, the settling rate matrix for varying turbulent intensity, k_e, (with constant exponent n=2.0) is plotted below with the five runs clearly delineated. Note that below 1 micron the settling rate varies by a factor of about 3 for a change in k_e of 10. Above 3 microns the settling rate is insensitive to the turbulent dissipation rate. The second run shows the effect of changing n with a fixed value of k_e. A strong sensitivity to the exponent n is evident as the settling rate below 1 micron varies by about an order of magnitude for a change in n from 2 to 2.8, the range in which published values have been noted. Again, the settling rate above 3 microns is insensitive to this parameter. In this region, gravitational settling predominates. The particle size with the minimum settling rate is very sensitive to the parameter.

MODEL EQUATIONS FOR STIRRED SETTLING OF PARTICLES (SETTLEKE.MCD)

Dimensions of rectangular chamber:

height- $L1 = 117$ length- $L2 = 213$ width- $L3 = 167$ cm

indices: $i = 1..32$ $p = 24$ $q = 1..5$ $j = 1..p$ $l = p..32$

sizes: m_i

m_i
.05
.06
.07
.08
.09
.1
.125
.15
.175
.2
.25
.3
.4
.5
.6
.7
.8
.9
1
1.2
1.4
1.6
1.8
2
2.5
3
3.5
4
5
6
8
10

microns

Parameter values:

$\rho = 1$	g/cm3	$T = 298$	deg K
$g = 980$	cm/sec2	$n = 2.0$	
$\eta = 1.83 \cdot 10^{-4}$	g/cm/s	$d_i = m_i \cdot 10^{-4}$	(conversion to cm.)
$k = 1.38 \cdot 10^{-16}$	erg/K		

ke_q

ke_q
100
250
500
750
1000

sec-1

Cunningham's corrections:

$$Fd_i = 1 + \frac{1.76 \cdot 10^{-5}}{d_i} + \frac{5.6 \cdot 10^{-6}}{d_i} \cdot \exp\left(-7.44 \cdot 10^{-4} \cdot d_i\right)$$

Terminal velocities:

$$Ut_i = \frac{\rho \cdot g}{18 \cdot \eta} \cdot \left(d_i\right)^2 \cdot Fd_i$$

Diffusion coefficients:

$$Db_i = \frac{k \cdot T}{3 \cdot \pi \cdot \eta \cdot d_i} \cdot Fd_i$$

Settling Parameter:

$$Xl_{i,q} = \frac{\pi \cdot Ut_i}{n \cdot \sin\left(\frac{\pi}{n}\right) \cdot \left[ke_q \cdot \left(Db_i\right)^{n-1}\right]^{\frac{1}{n}}}$$

Particle settling rates for rectangular chamber [1/sec]:

$$\beta_{i,q} = \frac{2 \cdot Ut_i}{Xl_{i,q}} \cdot \left(\frac{1}{L2} + \frac{1}{L3}\right) + \left(\frac{Ut_i}{L1 \cdot \tanh\left(\frac{Xl_{i,q}}{2}\right)}\right)$$

Terminal Velocities and Diffusion Coefficients

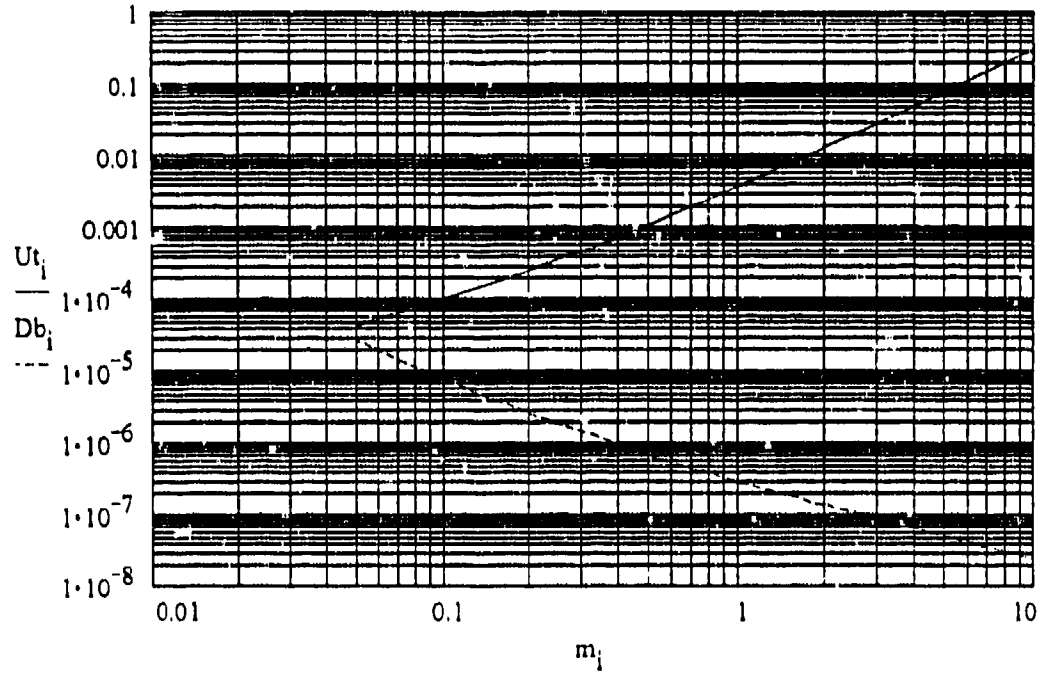

Settling Rates [1/sec]

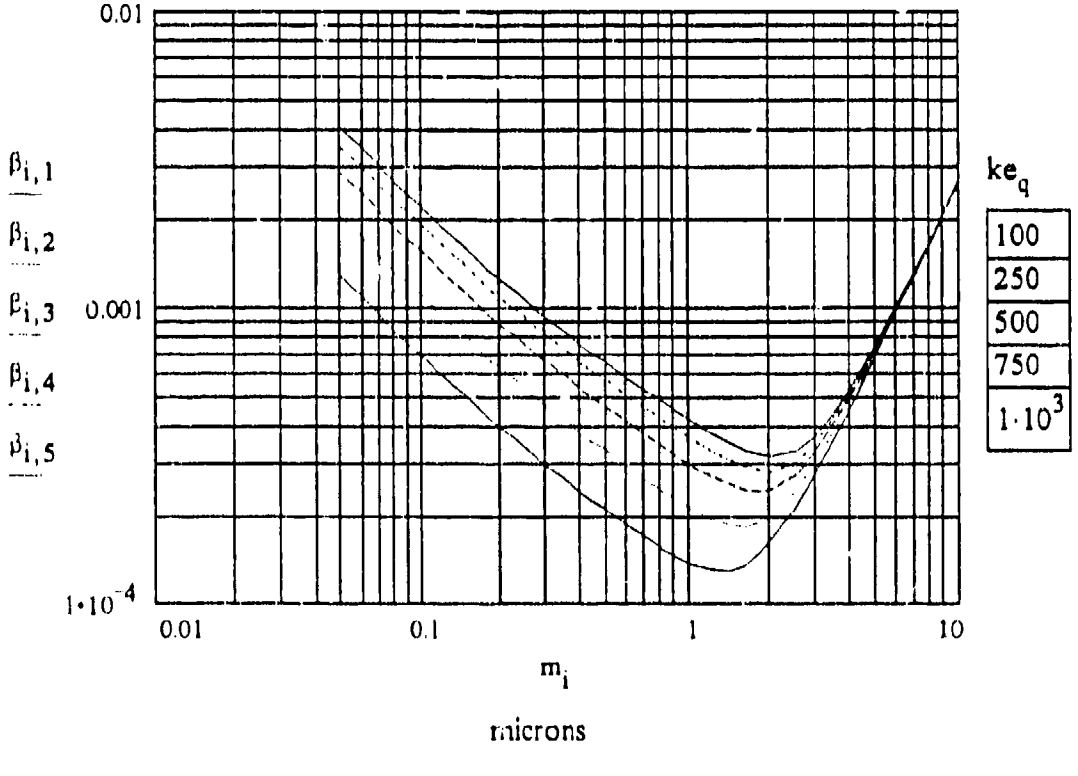

Appendix C

MODEL EQUATIONS FOR STIRRED SETTLING OF PARTICLES
(SETTLEN.MCD)

Dimensions of rectangular chamber:

height- $L1 := 117$ length- $L2 := 213$ width- $L3 := 167$ cm

indices: $i := 1..32$ $p := 24$ $q := 1..5$ $j := 1..p$ $l := p..32$

Parameter values:

$\rho := 1$ g/cm3 $T := 298$ deg K

$g := 980$ cm/sec2 $ke := 1000$

$\eta := 1.83 \cdot 10^{-4}$ g/cm/s $d_i := m_i \cdot 10^{-4}$ (conversion to cm.)

$k := 1.38 \cdot 10^{-16}$ erg/K

n_q

2
2.2
2.4
2.6
2.8

Cunningham's corrections:

$$Fd_i := 1 + \frac{1.76 \cdot 10^{-5}}{d_i} + \frac{5.6 \cdot 10^{-6}}{d_i} \cdot \exp\left(-7.44 \cdot 10^{-4} \cdot d_i\right)$$

Terminal velocities: $$Ut_i := \frac{\rho \cdot g}{18 \cdot \eta} \cdot (d_i)^2 \cdot Fd_i$$

Diffusion coefficients: $$Db_i := \frac{k \cdot T}{3 \cdot \pi \cdot \eta \cdot d_i} \cdot Fd_i$$

Settling Parameter:

$$X1_{i,q} := \frac{\pi \cdot Ut_i}{n_q \cdot \sin\left(\frac{\pi}{n_q}\right) \cdot \left[ke \cdot (Db_i)^{n_q - 1}\right]^{\frac{1}{n_q}}}$$

Particle settling rates for rectangular chamber [1/sec]:

$$\beta_{i,q} := \frac{2 \cdot Ut_i}{X1_{i,q}} \cdot \left(\frac{1}{L2} + \frac{1}{L3}\right) + \left(\frac{Ut_i}{L1 \cdot \tanh\left(\frac{X1_{i,q}}{2}\right)}\right)$$

sizes: m_i

.05
.06
.07
.08
.09
.1
.125
.15
.175
.2
.25
.3
.4
.5
.6
.7
.8
.9
1
1.2
1.4
1.6
1.8
2
2.5
3
3.5
4
5
6
8
10

microns

Terminal Velocities and Diffusion Coefficients

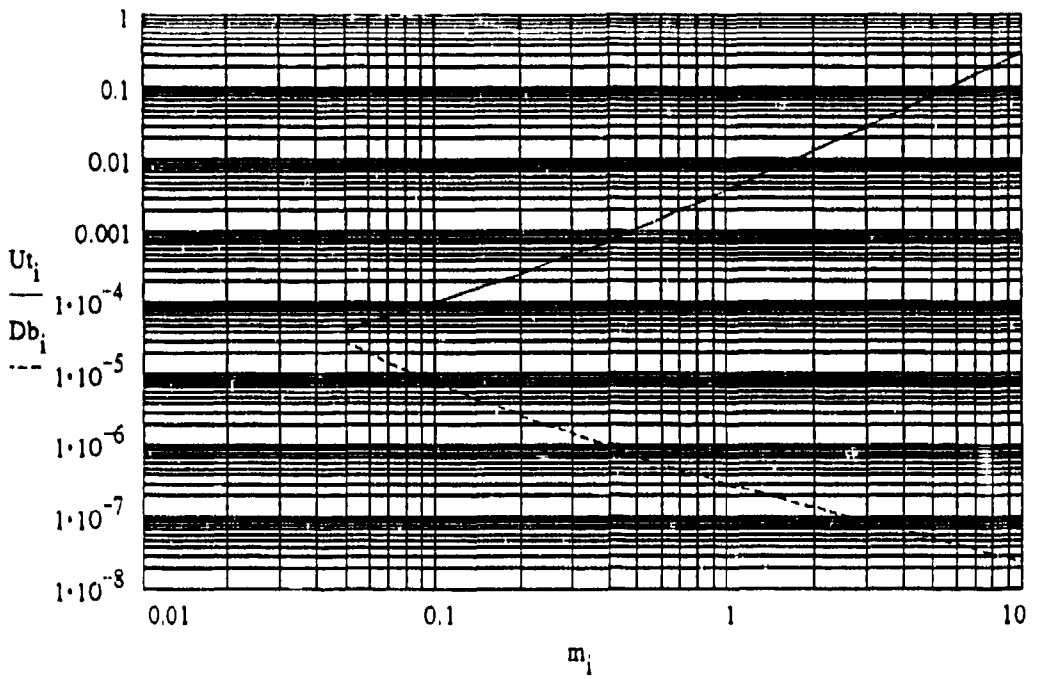

microns

Settling Rates [1/sec]

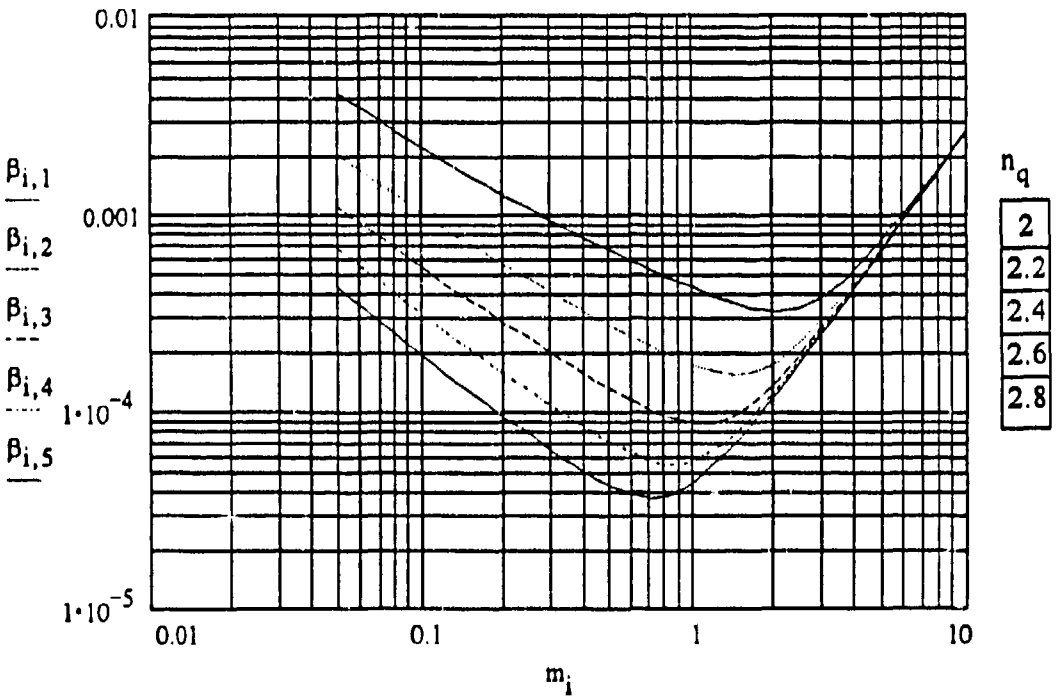

microns

C.4. Theoretical Settling Rate Optimization

Sample results of the attempts to optimize the two parameters of the turbulent dissipation coefficient were given in the text. The optimization was performed using the Asystant scientific software. Aside from the option to define user functions, the program is entirely menu-driven. In order to insert the settling rate model for curve-fitting against the data, the equations were defined as a five-stage nested user fuction. On the following two pages the screen prints showing the user function definitions, parameters and variables are shown. Fourteen experimental data points were inserted in variable Y against their sizes, inserted in variable Z. Prior to the optimization, Z and Y are placed on the stack followed by the final function, F7. The result of the calculation was stored in variable B, labelled beta.

The nested function definitions are as follows:

F1 - Cunningham's correction
F2 - Terminal velocity
F3 - Diffusion coefficient
F4 - Settling rate parameter (X1)
F7 - Settling rates

At the bottom of the second page is the screen for chosing the fit of the experimental data (variable Y with the sizes Z), against the curve calculated by function F7 with two independent parameters, A and B, whose initial values are given in the left-hand column.

The third page shows screens for three results given in the text. Note that for widely varying k_e parameter values ($1000<A<10000$), similar values of n ($2.038<B<2.301$) yield essentially identical, and rather unsatisfactory, fits to the experimental data. This is despite the fact that the least squares fit correlation coefficient, R^2, is excellent in all cases ($0.9335<R^2<0.9361$). The model as posed is ill-conditioned for fit through these two parameters against the measured data.

Although the model, in this case, does not result in satisfactory results, the use of Asystant as a tool in quantitative sensitivity analysis is demonstrated as a useful time-saver for whatever models may be developed in the future.

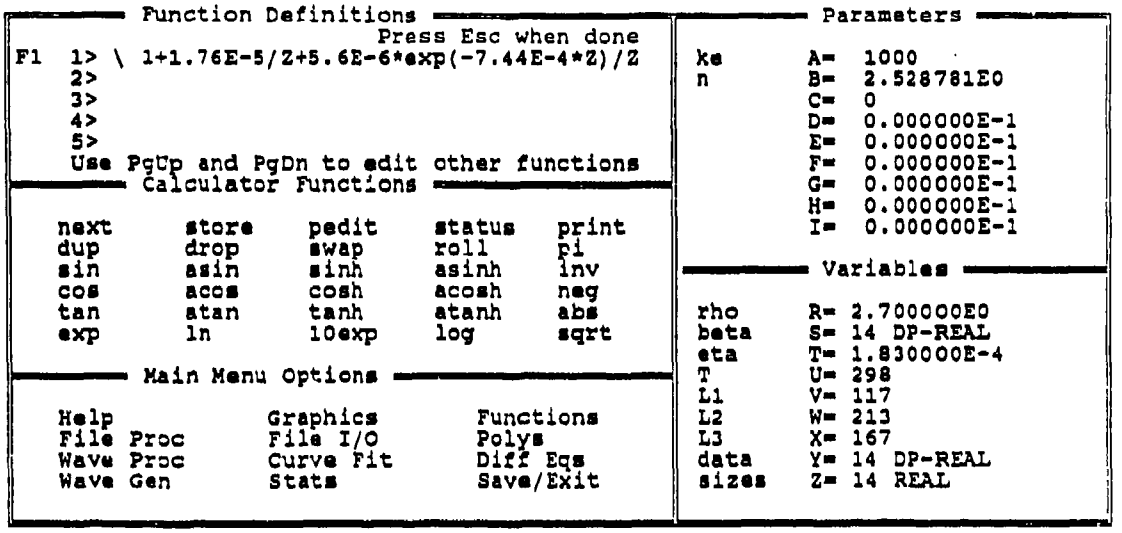
Function Definitions
Press Esc when done
F1 1> \ 1+1.76E-5/Z+5.6E-6*exp(-7.44E-4*Z)/Z
2>
3>
4>
5>
Use PgUp and PgDn to edit other functions
Calculator Functions
next store pedit status print
dup drop swap roll pi
sin asin sinh asinh inv
cos acos cosh acosh neg
tan atan tanh atanh abs
exp ln 10exp log sqrt
Main Menu Options
Help Graphics Functions
File Proc File I/O Polys
Wave Proc Curve Fit Diff Eqs
Wave Gen Stats Save/Exit
Parameters
ke A= 1000
n B= 2.528781E0
C= 0
D= 0.000000E-1
E= 0.000000E-1
F= 0.000000E-1
G= 0.000000E-1
H= 0.000000E-1
I= 0.000000E-1
Variables
rho R= 2.700000E0
beta S= 14 DP-REAL
eta T= 1.830000E-4
T U= 298
L1 V= 117
L2 W= 213
L3 X= 167
data Y= 14 DP-REAL
sizes Z= 14 REAL

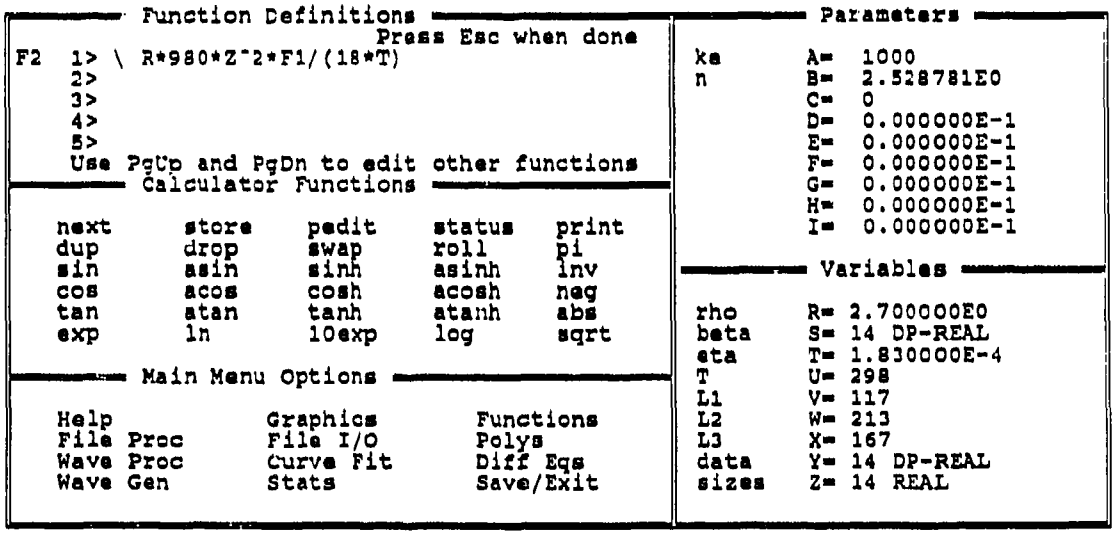
Function Definitions
Press Esc when done
F2 1> \ R*980*Z^2*F1/(18*T)
2>
3>
4>
5>
Use PgUp and PgDn to edit other functions
Calculator Functions
next store pedit status print
dup drop swap roll pi
sin asin sinh asinh inv
cos acos cosh acosh neg
tan atan tanh atanh abs
exp ln 10exp log sqrt
Main Menu Options
Help Graphics Functions
File Proc File I/O Polys
Wave Proc Curve Fit Diff Eqs
Wave Gen Stats Save/Exit
Parameters
ke A= 1000
n B= 2.528781E0
C= 0
D= 0.000000E-1
E= 0.000000E-1
F= 0.000000E-1
G= 0.000000E-1
H= 0.000000E-1
I= 0.000000E-1
Variables
rho R= 2.700000E0
beta S= 14 DP-REAL
eta T= 1.830000E-4
T U= 298
L1 V= 117
L2 W= 213
L3 X= 167
data Y= 14 DP-REAL
sizes Z= 14 REAL

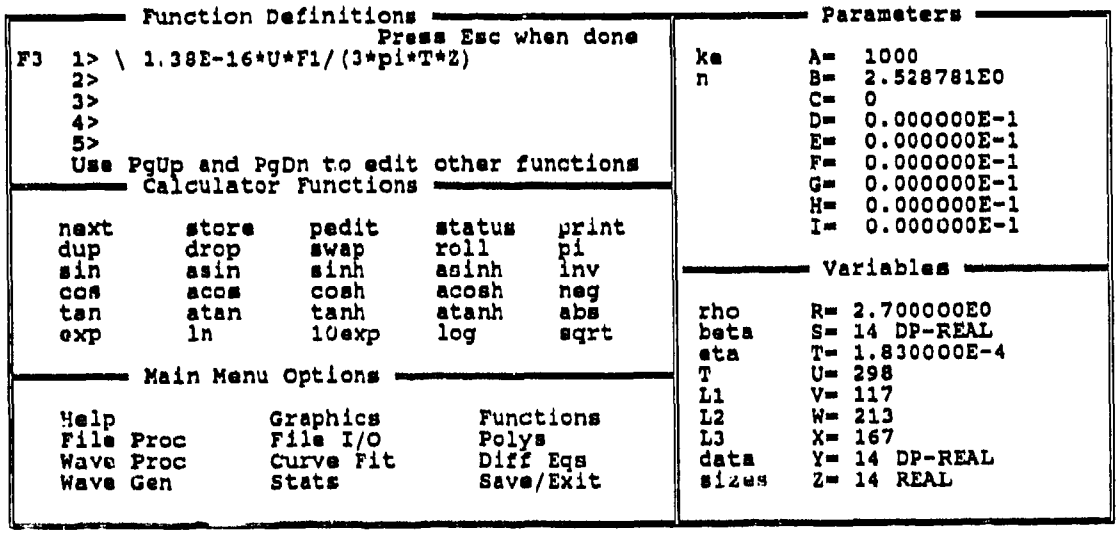
Function Definitions
Press Esc when done
F3 1> \ 1.38E-16*U*F1/(3*pi*T*Z)
2>
3>
4>
5>
Use PgUp and PgDn to edit other functions
Calculator Functions
next store pedit status print
dup drop swap roll pi
sin asin sinh asinh inv
cos acos cosh acosh neg
tan atan tanh atanh abs
exp ln 10exp log sqrt
Main Menu Options
Help Graphics Functions
File Proc File I/O Polys
Wave Proc Curve Fit Diff Eqs
Wave Gen Stats Save/Exit
Parameters
ke A= 1000
n B= 2.528781E0
C= 0
D= 0.000000E-1
E= 0.000000E-1
F= 0.000000E-1
G= 0.000000E-1
H= 0.000000E-1
I= 0.000000E-1
Variables
rho R= 2.700000E0
beta S= 14 DP-REAL
eta T= 1.830000E-4
T U= 298
L1 V= 117
L2 W= 213
L3 X= 167
data Y= 14 DP-REAL
sizes Z= 14 REAL

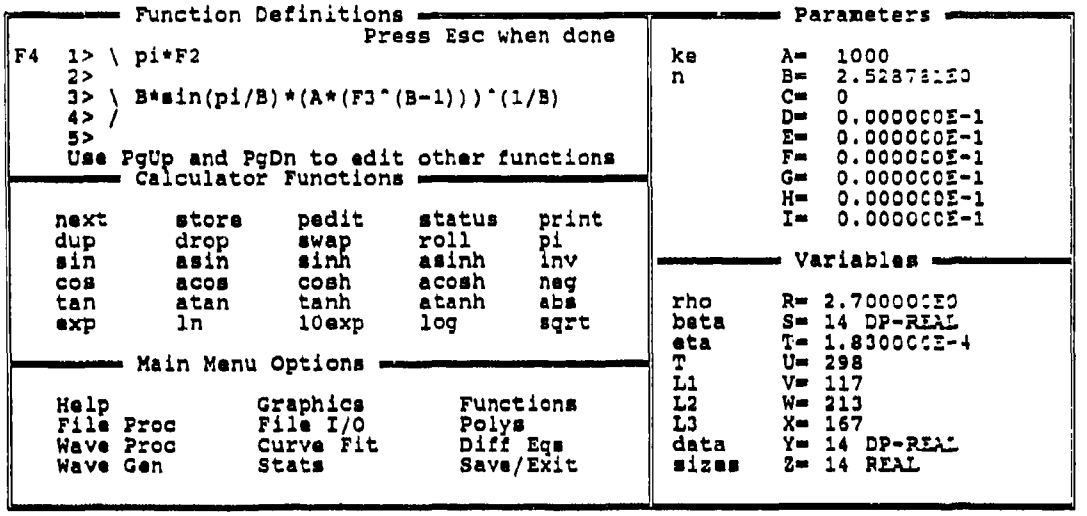
Function Definitions
Press Esc when done
F4 1> \ pi*F2
2>
3> \ B*sin(pi/B)*(A*(F3^(B-1)))^(1/B)
4> /
5>
Use PgUp and PgDn to edit other functions
Calculator Functions
next store pedit status print
dup drop swap roll pi
sin asin sinh asinh inv
cos acos cosh acosh neg
tan atan tanh atanh abs
exp ln 10exp log sqrt
Main Menu Options
Help Graphics Functions
File Proc File I/O Polys
Wave Proc Curve Fit Diff Eqs
Wave Gen Stats Save/Exit
Parameters
ke A= 1000
n B= 2.528781E0
C= 0
D= 0.000000E-1
E= 0.000000E-1
F= 0.000000E-1
G= 0.000000E-1
H= 0.000000E-1
I= 0.000000E-1
Variables
rho R= 2.700000E0
beta S= 14 DP-REAL
eta T= 1.830000E-4
T U= 298
L1 V= 117
L2 W= 213
L3 X= 167
data Y= 14 DP-REAL
sizes Z= 14 REAL

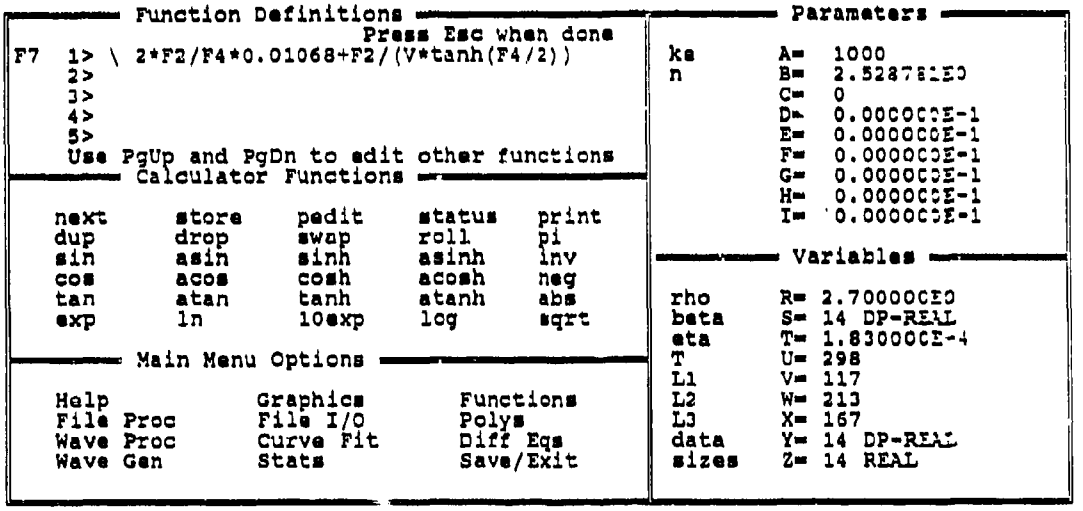
Function Definitions
Press Esc when done
F7 1> \ 2*F2/F4*0.01068+F2/(V*tanh(F4/2))
2>
3>
4>
5>
Use PgUp and PgDn to edit other functions
Calculator Functions
next store pedit status print
dup drop swap roll pi
sin asin sinh asinh inv
cos acos cosh acosh neg
tan atan tanh atanh abs
exp ln 10exp log sqrt
Main Menu Options
Help Graphics Functions
File Proc File I/O Polys
Wave Proc Curve Fit Diff Eqs
Wave Gen Stats Save/Exit
Parameters
ke A= 1000
n B= 2.528781E0
C= 0
D= 0.000000E-1
E= 0.000000E-1
F= 0.000000E-1
G= 0.000000E-1
H= 0.000000E-1
I= 0.000000E-1
Variables
rho R= 2.700000E0
beta S= 14 DP-REAL
eta T= 1.830000E-4
T U= 298
L1 V= 117
L2 W= 213
L3 X= 167
data Y= 14 DP-REAL
sizes Z= 14 REAL

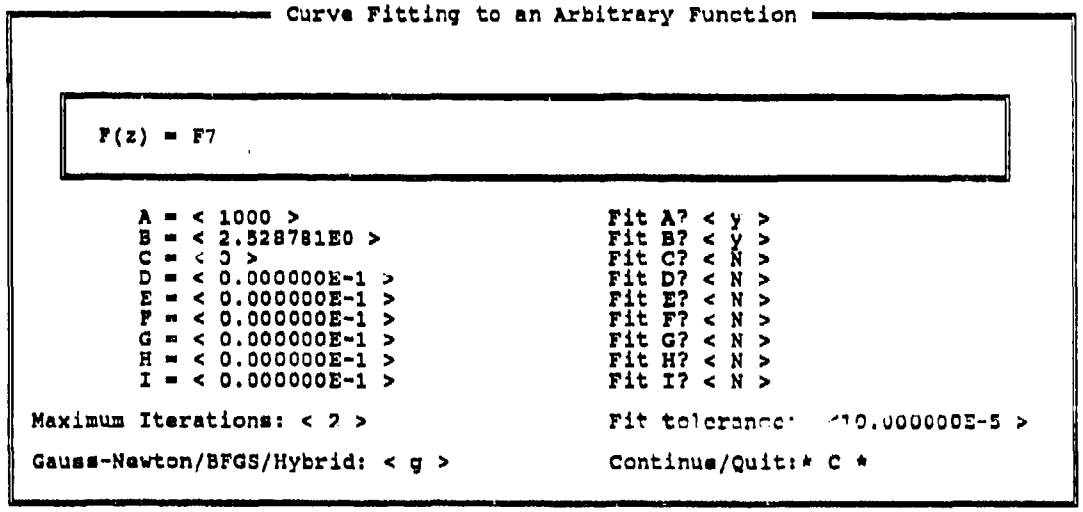
Curve Fitting to an Arbitrary Function
F(z) = F7
A = < 1000 >
B = < 2.528781E0 >
C = < 0 >
D = < 0.000000E-1 >
E = < 0.000000E-1 >
F = < 0.000000E-1 >
G = < 0.000000E-1 >
H = < 0.000000E-1 >
I = < 0.000000E-1 >
Fit A? < y >
Fit B? < y >
Fit C? < N >
Fit D? < N >
Fit E? < N >
Fit F? < N >
Fit G? < N >
Fit H? < N >
Fit I? < N >
Maximum Iterations: < 2 >
Fit tolerance: < 0.000000E-5 >
Gauss-Newton/BFGS/Hybrid: < g >
Continue/Quit:* C *

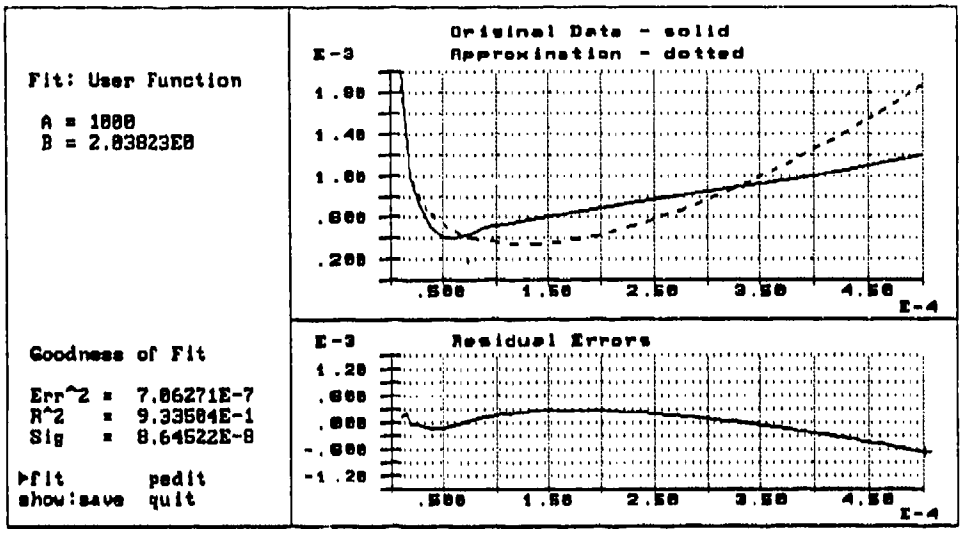
Fit: User Function
A = 1000
B = 2.83823E0
Goodness of Fit
Err^2 = 7.86271E-7
R^2 = 9.33504E-1
Sig = 8.64522E-8
▸fit pedit
show:save quit
Original Data - solid
Approximation - dotted
E-3
1.80
1.40
1.00
.600
.200
.500
1.50
2.50
3.50
4.50
E-4
Residual Errors
1.20
.600
.000
-.600
-1.20

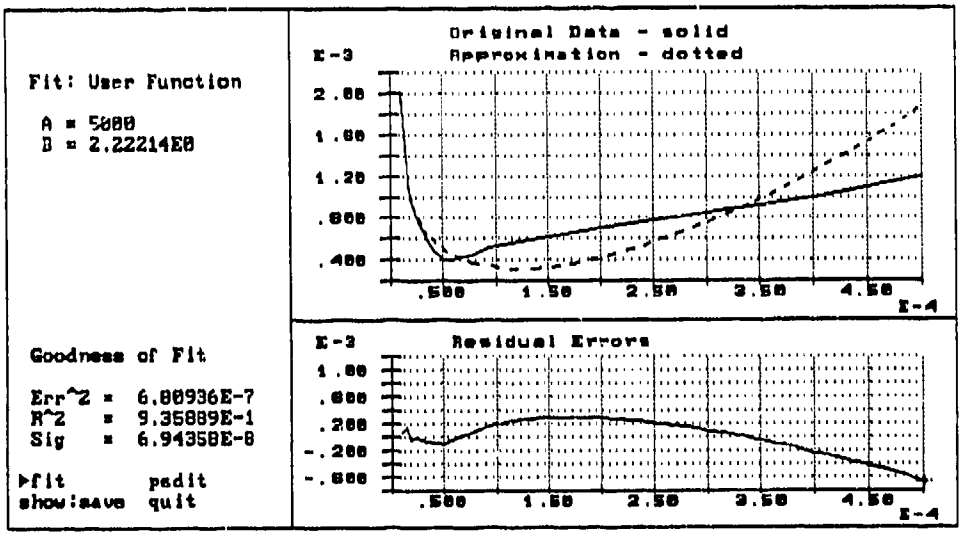
Fit: User Function
A = 5000
B = 2.22214E0
Goodness of Fit
Err^2 = 6.80936E-7
R^2 = 9.35889E-1
Sig = 6.94358E-8
▸fit pedit
show:save quit
Original Data - solid
Approximation - dotted
E-3
2.00
1.60
1.20
.800
.400
.500
1.50
2.50
3.50
4.50
E-4
Residual Errors
1.00
.600
.200
-.200
-.600

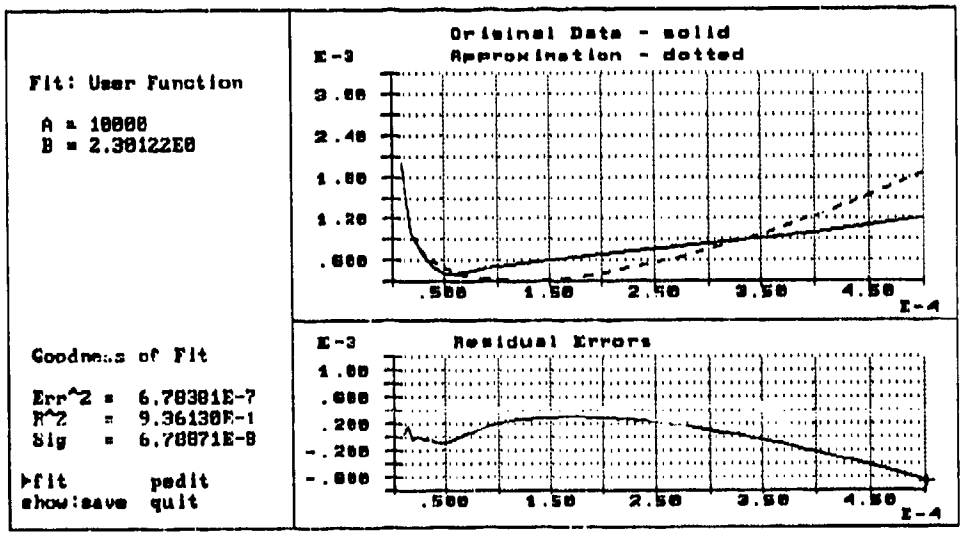
Fit: User Function
A = 10000
B = 2.30122E0
Goodness of Fit
Err^2 = 6.78381E-7
R^2 = 9.36130E-1
Sig = 6.78871E-8
▸fit pedit
show:save quit
Original Data - solid
Approximation - dotted
E-3
3.00
2.40
1.80
1.20
.600
.500
1.50
2.50
3.50
4.50
E-4
Residual Errors
1.00
.600
.200
-.200
-.600

Appendix C

C.5. MIE Sensor Response Weighting

The MIE, Inc. monitoring instruments, RAM-1 and RAS-2 are very nonlinear in their particle size-dependent response. In order to correct the measured mass response for specific size spectra the manufacturer-supplied calbration curve must be used. If a mono-disperse challenge is being used, then a relative response may be read directly from the curve. However, we are involved for the time being with various poly-dispersed challenges and size-dependent penetration effects. Hence the nominal broad-spectrum response of the instruments must be corrected for the nonlinear response.

A Mathcad utility program, MIE.MCD, has been written whose purpose is to weigh a given challenge spectrum by the manufacturer's response curve and correct the nominal analog output accordingly. The program, shown in the next two pages, allows two different methods of presenting the challenge spectrum: either by direct input of the spectrum by size bins or by lognormal distribution parameter estimates.

The program first plots the MIE calibration distribution given as the em_i vector against the particle sizes, d_i. Below the calibration plot is the particle size spectrum, given as vector n_i. After the size-weighted efficiency, eff, is calculated, the nominal millivolt responses of the instruments is calculated. These are the values supplied by the manufacturer. Their validity must be checked periodically for each instrument by gravimetric calibration with well-defined particles.

The RAS-2 sensor has a nominal analog output of 16 mv/mg/m^3 when calibrated to the manufacturer's specifications. The RAM-1 monitor has three panel scale settings at 0-2, 0-20 and 0-200 mg/m^3 with 0-10 volt output. In order to prevent confusion, the program supplies all three numbers.

The option of using the lognormal distribution is shown on the second page. The distribution parameter estimates are initially user-supplied. This program segment may be used as a rough tool for manually optimizing the parameters against empirical data by comparing peak position, width, intercept and slope values. The distribution is shown in the plot. Additional statistics based on the lognormal parameter estimates are available from the Hatch-Choate conversion table (Reist, 1984). As in the first segment, the instrument sensitivities are corrected by the weighted efficiency and displayed in the final table.

MIE SENSOR EFFICIENCY CALIBRATION
MIE.MCD

$i = 0 .. 25$

particle size spectrum

d_i	em_i	n_i
.1	.1	1
.15	.1	1
.175	.13	2
.2	.17	2
.25	.3	5
.3	.54	25
.4	1.2	30
.5	2.	35
.6	2.65	30
.7	2.45	20
.8	2.3	18
.9	2.05	15
1.	1.68	12
1.25	1.15	10
1.5	1	9
1.75	.9	8
2.	.65	8
2.5	.41	7
3	.32	6
3.5	.22	5
4.	.18	4
4.5	.16	3
5.	.16	2
5.5	.2	1
6.	.17	0
7	.12	0
8	.115	0
9	.1	0
10	.1	0

RAS Monodisperse Response Curve

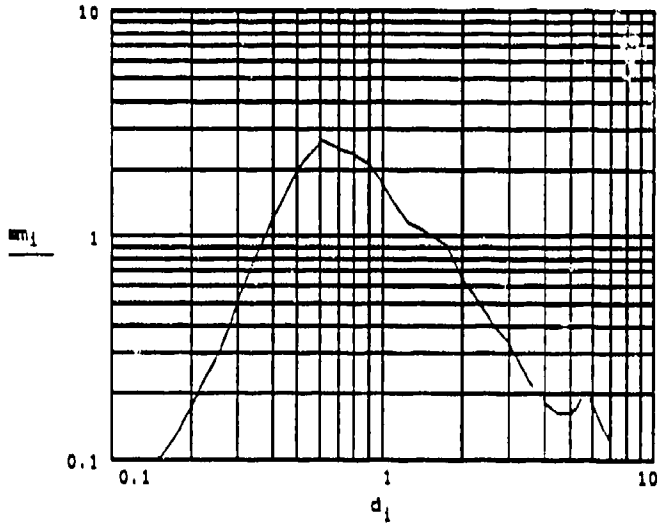

microns

Particle Size Spectrum

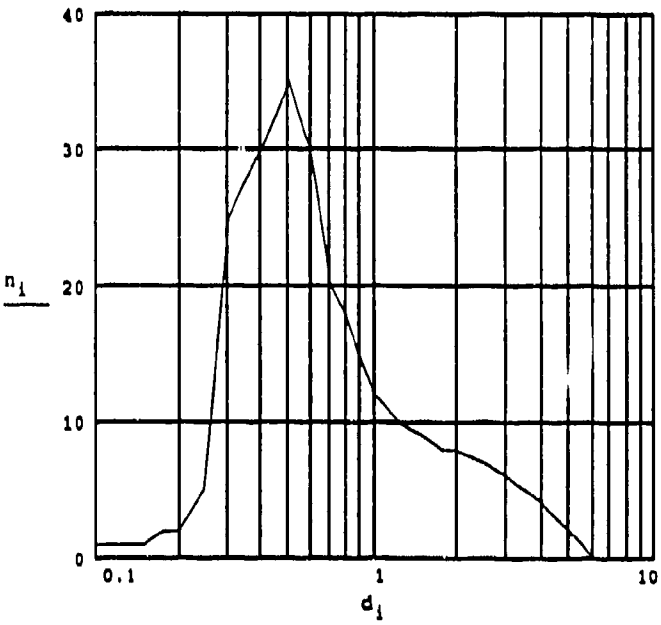

microns

Size-Weighted Efficiency

$$eff = \frac{\sum_i n_i \cdot em_i \cdot d_i}{\sum_i n_i \cdot d_i}$$

eff = 1.102

RAS-2 Sensor: (16mv/mg/M3) RAS2 = eff·16 RAS2 = 17.6 mv/mg/m3

RAS-1 Monitor: scale(mg/m3)

0-2	RAS12 = eff·5000	RAS12 = 5512.3	"
0-20	RAS120 = eff·500	RAS120 = 551.2	"
0-200	RAS1200 = eff·50	RAS1200 = 55.1	"

Approximation for lognormal distribution:

Data identification:
Talc nozzle/inside
for 1221T2

Hatch-Choate conversions:

definition (dp)	p
Mode	-1
Geometric mean or mode	0
Arithmetic mean	0.5
Diameter of average area	1
Diameter of average mass	1.5
Surface median diameter	2
Surface mean diameter	2.5
Volume (mass) median diameter	3
Volume (mass) mean diameter	3.5

Distribution parameters:

sigG = 2.15 meanG = .995

chosen p: p = 3

$dp = meanG \cdot \exp\left(p \cdot \ln(sigG)^2\right)$

dp = 5.771 microns

lognormal distribution calculation:

$$lnorm_i = \left[\frac{1}{\left[\sqrt{(2\cdot\pi)}\cdot\ln(sigG)\cdot d_i\right]}\right]\cdot\exp\left[\frac{\left(\left(\ln\left(\frac{d_i}{meanG}\right)\right)\right)^2}{\ln(sigG)}\right]$$

d_i	$lnorm_i$
0.1	0.058
0.15	0.164
0.175	0.226
0.2	0.29
0.25	0.409
0.3	0.509
0.4	0.641
0.5	0.696
0.6	0.698
0.7	0.67
0.8	0.626
0.9	0.574
1	0.521
1.25	0.399
1.5	0.301
1.75	0.227
2	0.172
2.5	0.101
3	0.061
3.5	0.039
4	0.025
4.5	0.017
5	0.011
5.5	0.008
6	0.006
7	0.003

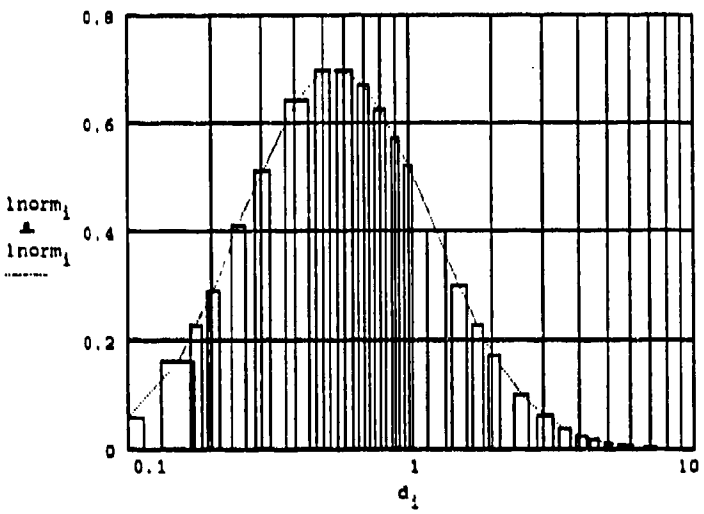

$$eff = \frac{\sum_i lnorm_i \cdot sm_i \cdot d_i}{\sum_i lnorm_i \cdot d_i}$$

eff = 1.388

RAS2 = eff·16	RAS2 = 22.2	mv/mg/m3
RAS12 = eff·5000	RAS12 = 6940	"
RAS120 = eff·500	RAS120 = 694	"
RAS1200 = eff·50	RAS1200 = 69.4	"

C.6. Aperture Flow Characteristics

The air exchange rate of the enclosure during a test is determined by the flowrate of air through the aperture. In some cases the flowrate may be measured directly by any suitable instrument. If no instrument is available for the range involved, it may be estimated using the crack flow equation:

$$Q = C \cdot A_e \cdot (dp)^n$$

Use of the equation requires estimation of the effective leakage area and the exponent n. A Mathcad program has been written to estimate these parameters from given flowrate and pressure differential data. The utility program is applicable to any test for which the flow through leaks must be estimated, whether a single leak or a combination of leaks in an unknown configuration such as may be encountered with a vehicle or shelter.

In the program QPDOC.MCD on the following page, the above equation is applied to finding the parameters for the 0.1mm x 40mm x 840mm aperture used in the verification tests. Since the equation is more familiar with American units, the constant value 4005 has been retained and the units adjusted for liters/minute and mmWG. The natural logarithms of the flowrate and the pressure differential are fitted by the linear least squares optimization function to provide estimates of the intercept, m, and slope, n. The correlation coefficient is also calculated (corr). The effective area is then calculated and given in cm^2. Dividing by the length of the aperture gives an effective height, assuming zero residual leakage area in the enclosure.

Measurements of flowrate and differential pressure in the very low range of interest were carried out using the Gillibrator Primary Flow calibrator. The blower was not capable of overcoming resistances in the flow line with any other available flowmeter so maesurements were done very accurately in the range 0.37-0.57 mmWG and results were extrapolated to -1 mmWG.

A slope of n=0.512 with a correlation coefficient of 0.992 was calculated. The effective area of 1.24 cm^2 indicated an effective aperture height of 0.148 mm. Under the assumption of zero residual leakage, this difference from the nominal 0.1 mm height could include some surface roughness and inaccuracy in the simple feeler gauge measurement which served to fix the aperture height. These optimized parameters were then used in the protection factor model to calculate the air exchange rate.

CALCULATION OF LEAKAGE AREA CHARACTERISTICS

QPDOC.MCD

Characteristic curve for nominal 0.1 mm x 40 mm x 840 mm aperture1215T1 data

Number of data points $N := 5$ $i := 0..N - 1$

data values:

$Q_i :=$

21
19.5
20.5
17.4
22

lpm

$Pmm_i :=$

0.55
0.47
0.52
0.37
0.57

mmWG

convert flow to cfm: $Q_i := \frac{Q_i}{28.3}$

Convert pressure to in H2O: $P_i := \frac{Pmm_i}{25.4}$

$lnQ_i := \ln(Q_i)$ $lnP_i := \ln(P_i)$

calculate slope and intercept:

$m := intercept(lnP, lnQ)$ $m = 1.676$

$n := slope(lnP, lnQ)$ $n = 0.512$

$corr(lnP, lnQ) = 0.992$

calculate effective area:

$area := \exp(m - \ln(4005)) \cdot 144 \cdot 6.452$ $area = 1.24$ sq. cm.

calculate effective height:

$height := \frac{area}{84}$ $height = 0.0148$ cm.

extrapolate flow to -1 mmWG:

$Qex := \exp(m) \cdot 0.03937^{n} \cdot 28.3$ The flow is $Qex = 28.839$ lpm at 1mmWG

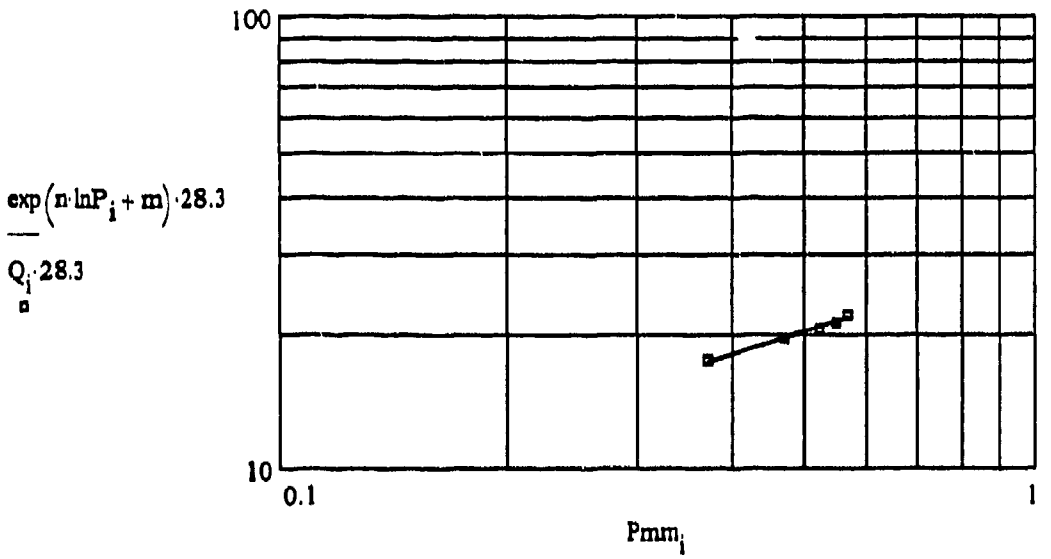

APPENDIX D

Piezoresistive Pressure Transducer Calibration Setup

The piezoresistive pressure transducers acquired for the experimental setup provide stable, linear voltage outputs over a wide range of differential pressures with exceptionally high frequency response. Their characteristics are presented on the following two pages. With the maximum amplification provided by the Endevco Model 106 Piezoresistive Conditioner, the tranducers could be used at a sensitivity of about 70 mv/mmWG differential pressure.

Since the transducers are intended for use at very low pressure differentials (from 1 mmWG) it is necessary to calibrate them against a reliable standard. The water-filled U-tube can be considered a primary standard, by definition. An inclined water manometer can be used for the lowest pressure range. In order to readily calibrate the transducers over the nominal range of the transducers (1 psig) without recourse to a standards laboratory, a simple setup was constructed as shown in the following schematic diagram. The U-tube is about 900 cm. in length, filled halfway with water. A rubber tube leads from one arm of the tube to a T-junction. One end of the junction is firmly attached to the threaded sleeve supplied by the manufacturer which seals onto the body of the transducer with a rubber O-ring. The other arm of the junction is connected to a rubber bulb. The transducer is connected to the conditioner according to the manufacturer's instructions and allowed to warm up.

Constant pressure on the rubber bulb, maintained by a laboratory clamp, produces a change in the water level, measured with a metric ruler, and the corresponding change in the transducer output, indicated on a millivoltmeter. A calibration chart for the range of interest can readily be constructed directly in terms of the standard pressure unit.

ENDEVCO®

PRESSURE TRANSDUCER TEST REPORT

MODEL 8510B-1 **SERIAL #** AAAA7

Range	1	psig
Sensitivity	242.9	mV/psi
Excitation	10.00	Vdc
Zero Pressure Output	-1	mV
Full Scale Output	243	mV
Non-Linearity	.51	%FSO
Hysteresis	.07	%FSO
Non-Repeatability	.08	%FSO
Combined Lin., Hyst., & Rep.*	.52	%FSO
Thermal Zero Shift	.16	%FSO
Zero Shift After 3X FSO	.01%	3XFSO
Thermal Sensitivity Shift	.93	%
Input Resistance	1930.2	Ω
Output Resistance	1682.6	Ω
Isolation Resistance	>100	MΩ

*RSS

All calibrations are traceable to the National Institute of Standards and Technology and in accordance with MIL-STD-45662

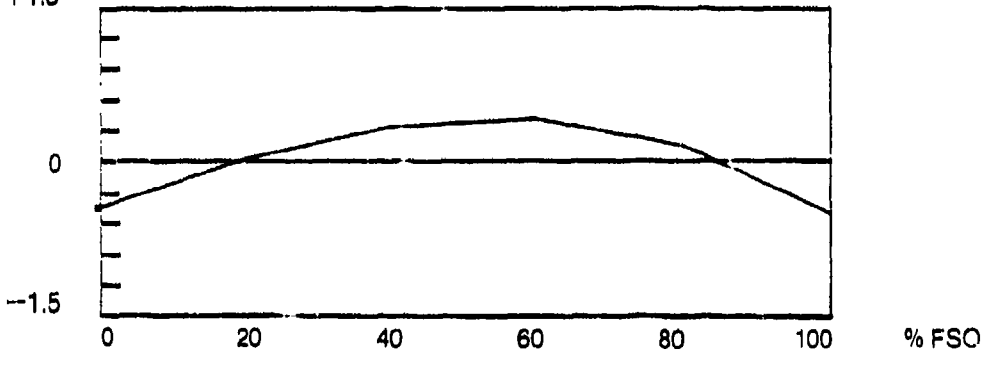

NON-LINEARITY (% FSO)

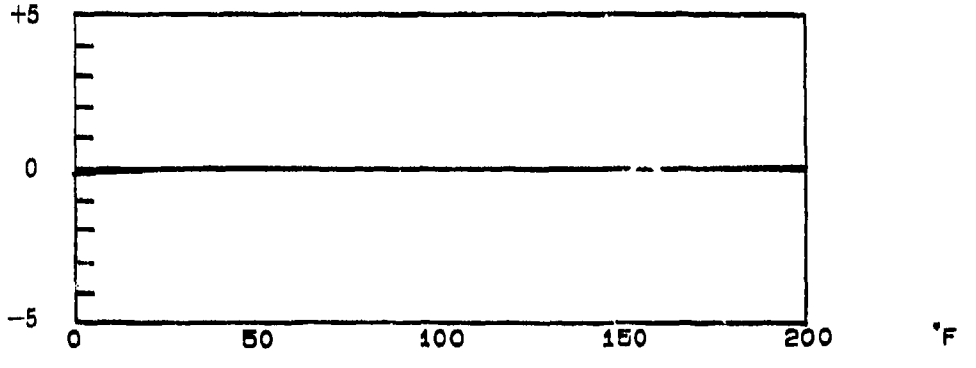

THERMAL ZERO SHIFT (% FSO)

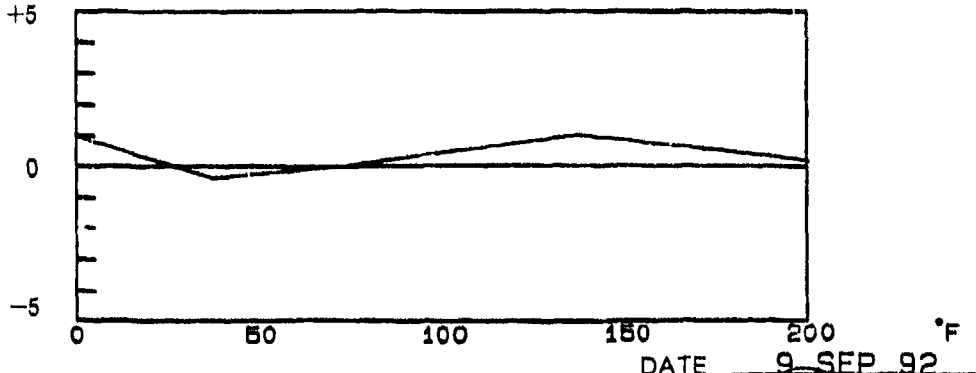

THERMAL SENSITIVITY SHIFT (%)

DATE 9 SEP 92

BY [signature]

2nd SEP 11 '92

Allied-Signal Aerospace Company

Allied Signal

Endevco Corporation
30700 Rancho Viejo Road
San Juan Capistrano, CA 92675
(714) 493-8181

ENDEVCO'

PRESSURE TRANSDUCER TEST REPORT

MODEL 8510B-1 **SERIAL #** AAAA8

Range	1	psig
Sensitivity	282.7	mV/psi
Excitation	10.00	Vdc
Zero Pressure Output	1	mV
Full Scale Output	283	mV
Non-Linearity	1.36	%FSO
Hysteresis	.04	%FSO
Non-Repeatability	.05	%FSO
Combined Lin., Hyst., & Rep.*	1.36	%FSO
Thermal Zero Shift	.94	%FSO
Zero Shift After 3× FSO	0%	3×FSO
Thermal Sensitivity Shift	2.78	%
Input Resistance	1412.8	Ω
Output Resistance	1304.8	Ω
Isolation Resistance	>100	MΩ

*RSS

All calibrations are traceable to the National Institute of Standards and Technology and in accordance with MIL-STD-45662

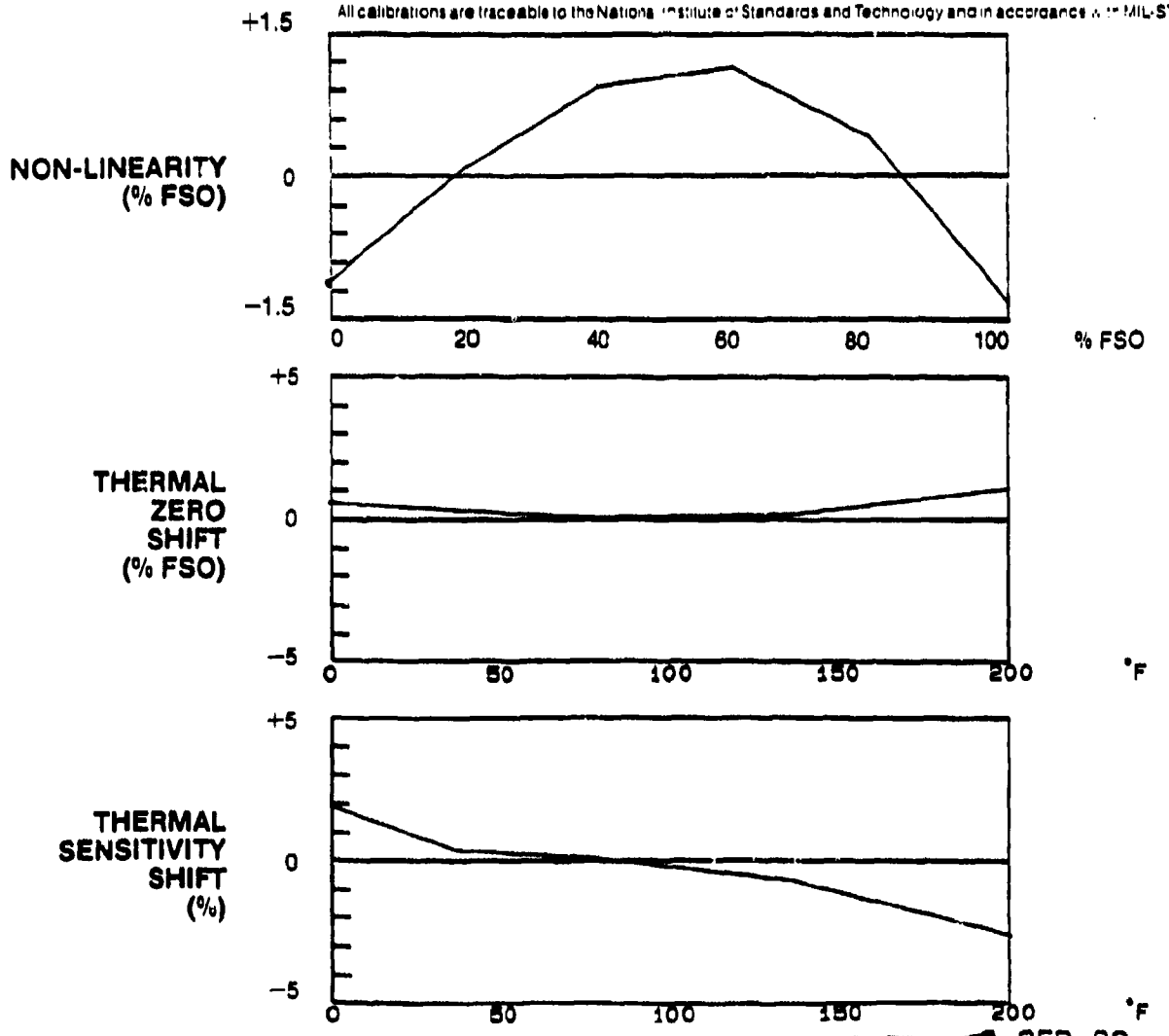

DATE 9 SEP 92

BY

SEP 11 '92

Allied-Signal Aerospace Company

Allied Signal

Appendix D

Form 26707

Endevco Corporation
30700 Rancho Viejo Road
San Juan Capistrano, CA 92675
(714) 493-8181

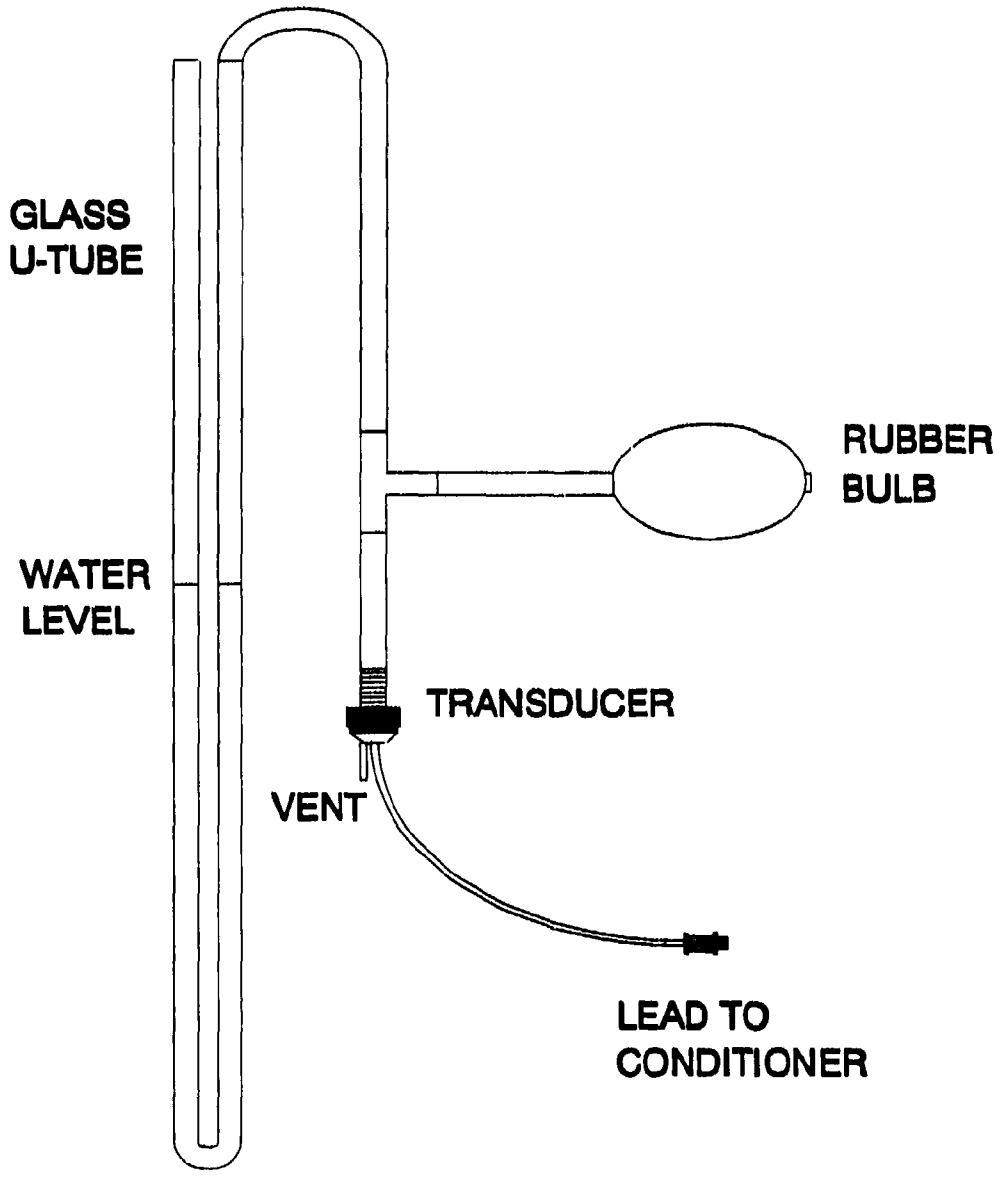

PRESSURE TRANSDUCER CALIBRATION SETUP

APPENDIX E

TSI 3302 Diluter Operation with the LAS-X Laser Spectrometer

In certain instances the challenge cloud concentration is liable to be too great for the LAS -X Laser Spectrometer to handle without distorting the data. This being so, a TSI 3302 Diluter with x20 dilution has been adapted for this purpose. The diluter is an accessory to the TSI APS 33 Aerodynamic Particle Sizer using a 5 lpm total flowrate supplied by the sizer. The diluter works in a closed system where a small sample of the aerosol is diluted with filtered air from the input air flow. The aerosol flow is monitored by the pressure drop across a laminar flow capillary tube. The dilution ratio is determined by a valve in the clean air flow stream. The diluter is normally placed on top of the APS 33 with the particle flow stream facing downwards.

In order to use the diluter with the LAS-X, an adaptor had to be devised which would feed the LAS-X input stream isokinetically from the diluter outflow stream. The LAS-X samples at 5 cc/sec whereas the diluter operates at 5 lpm. Hence the diluter output flow diameter had to be adjusted to match the flow velocity into the LAS-X as closely as possible. The diagram on the next page schematically depicts the arrangement devised to overcome this problem.

The solution is based on a 1/8" I.D. plastic tube suspended within a 5/16" I.D. plastic tube. A teflon T-junction supports the inner tube and permits the diluted, reduced flow to be sampled by the LAS-X internal pump. The excess flow is pumped out of the third arm by the main diaghram pump which is adjusted to maintain the proper flow through the diluter. This function normally is fulfilled by the APS 33.

This is obviously a temporary solution, but it is effective. Particle count reduction of factor 20-22 were obtained by carefully adjusting the diluter pressure ratio according to the manufacturer's specifications. It should be noted that the pressure ratio is very sensitive to the air sampling geometry at the inlet of the diluter. If a long sampling tube is used, the pressure ratio must be adjusted carefully to the new situation.

As noted in the text, the penetration efficiency as a function of particle size of the diluter capillary is given as a graph in the manufacturer's instruction manual. The graph is normally stored in the APS software for automatic use. In order to make use of the correction curve in our utility programs, the curve was fitted to a polynomial function with ASYSTANT. The resulting best fit parameters are included in the LAS-X data analysis program. The best fit equation for the x20 diluter is as follows:

$$E = 1.06 - 0.024 \cdot D - 0.002 \cdot D^2$$

where E is the penetration efficiency and D is the particle diameter in microns. Penetration degradation begins at approximately 2 microns and reaches 60% efficiency at 10 microns.

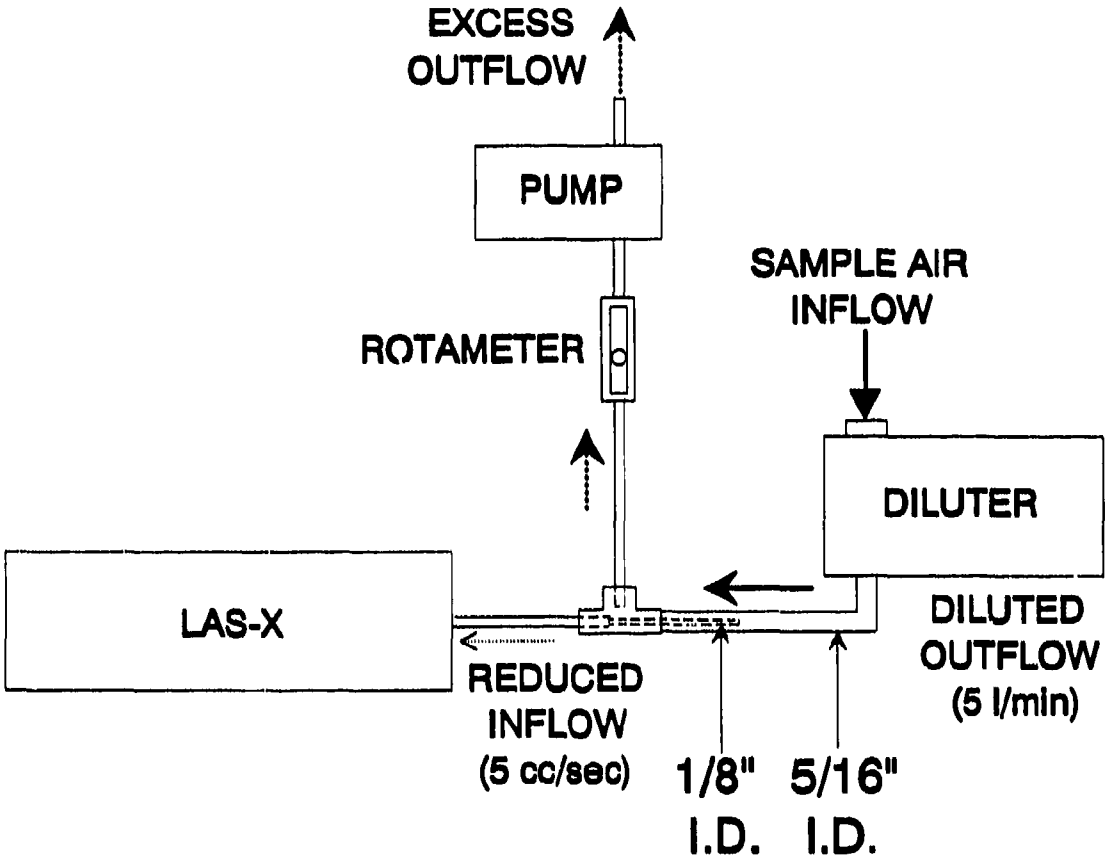

ADAPTATION OF TSI 3302 DILUTER TO LAS-X SAMPLING

APPENDIX F

Solid Aerosol Test Facility Photographs

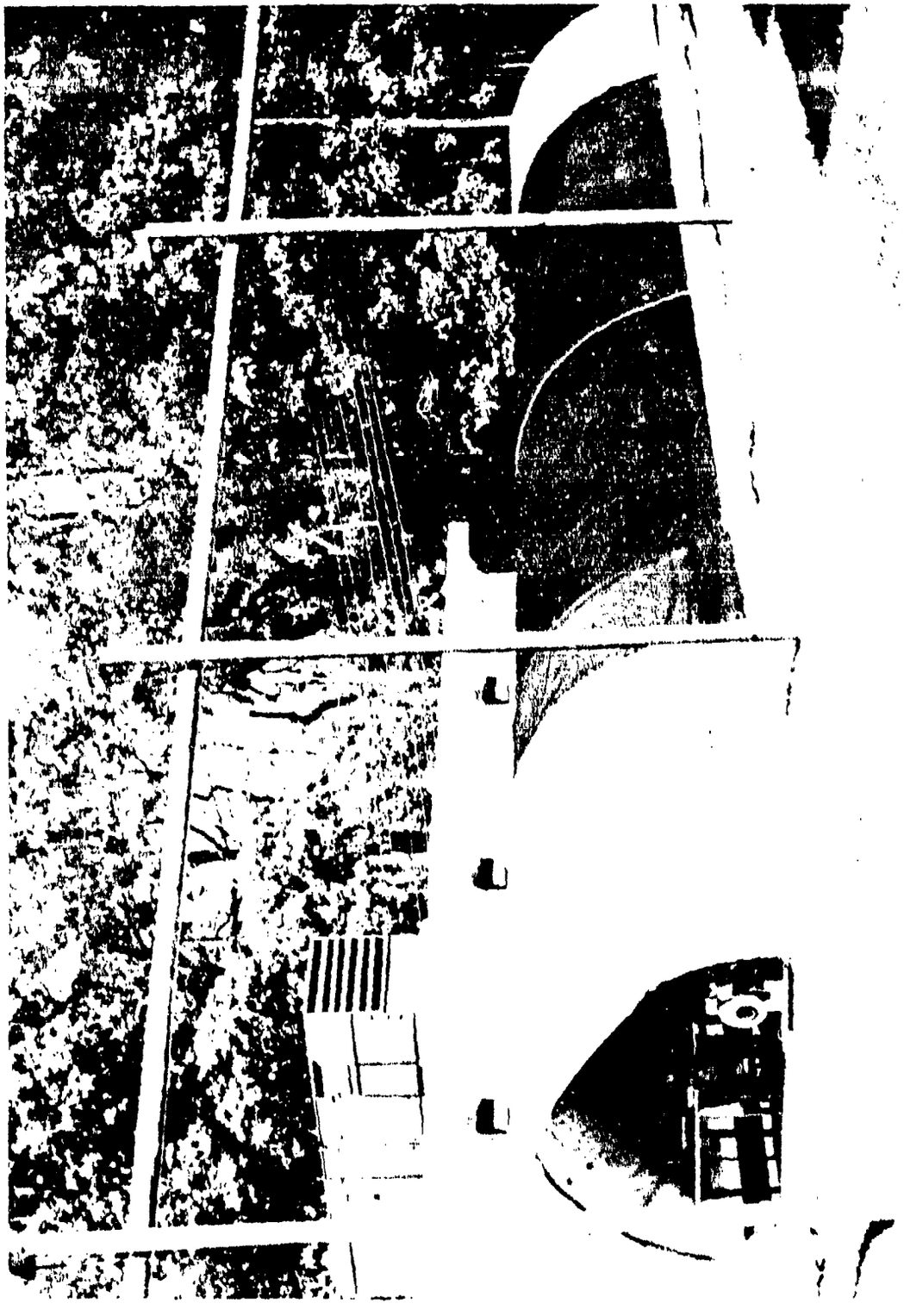

Figure F.1. Solid Aerosol Test Facility

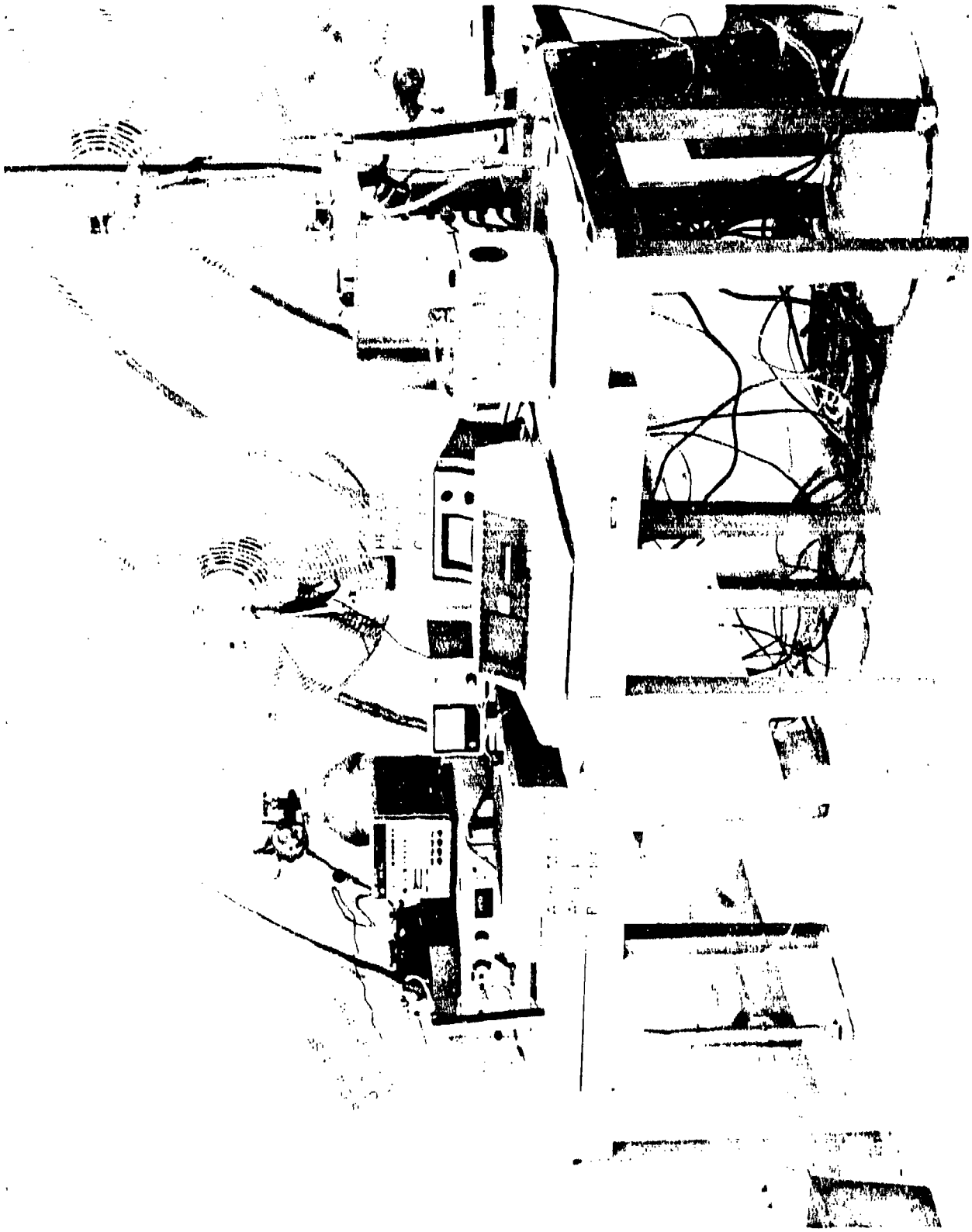

Figure F.2. Dissemination Control Table

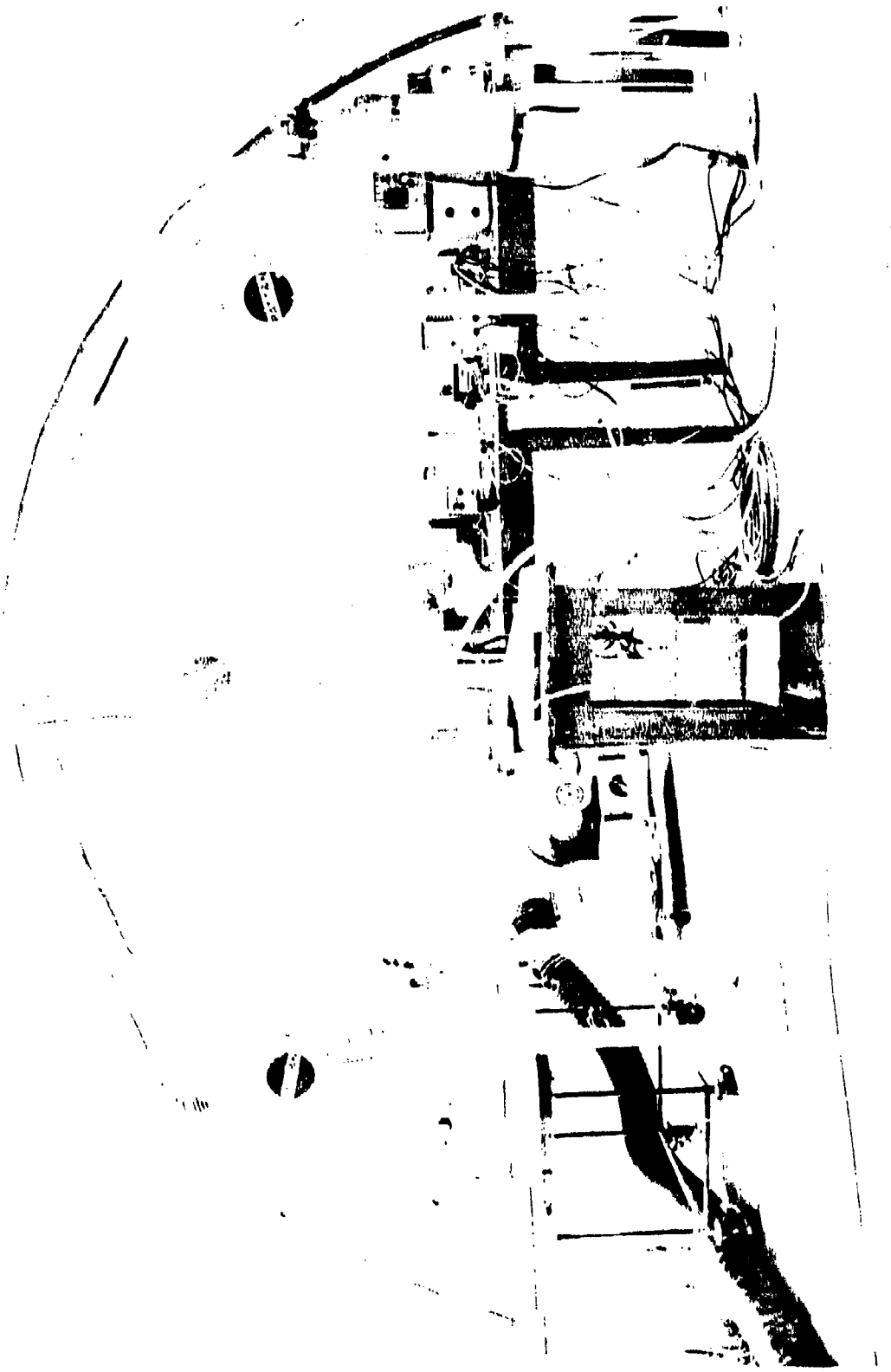

Figure F.3. Powder Dissemination System: Inside View

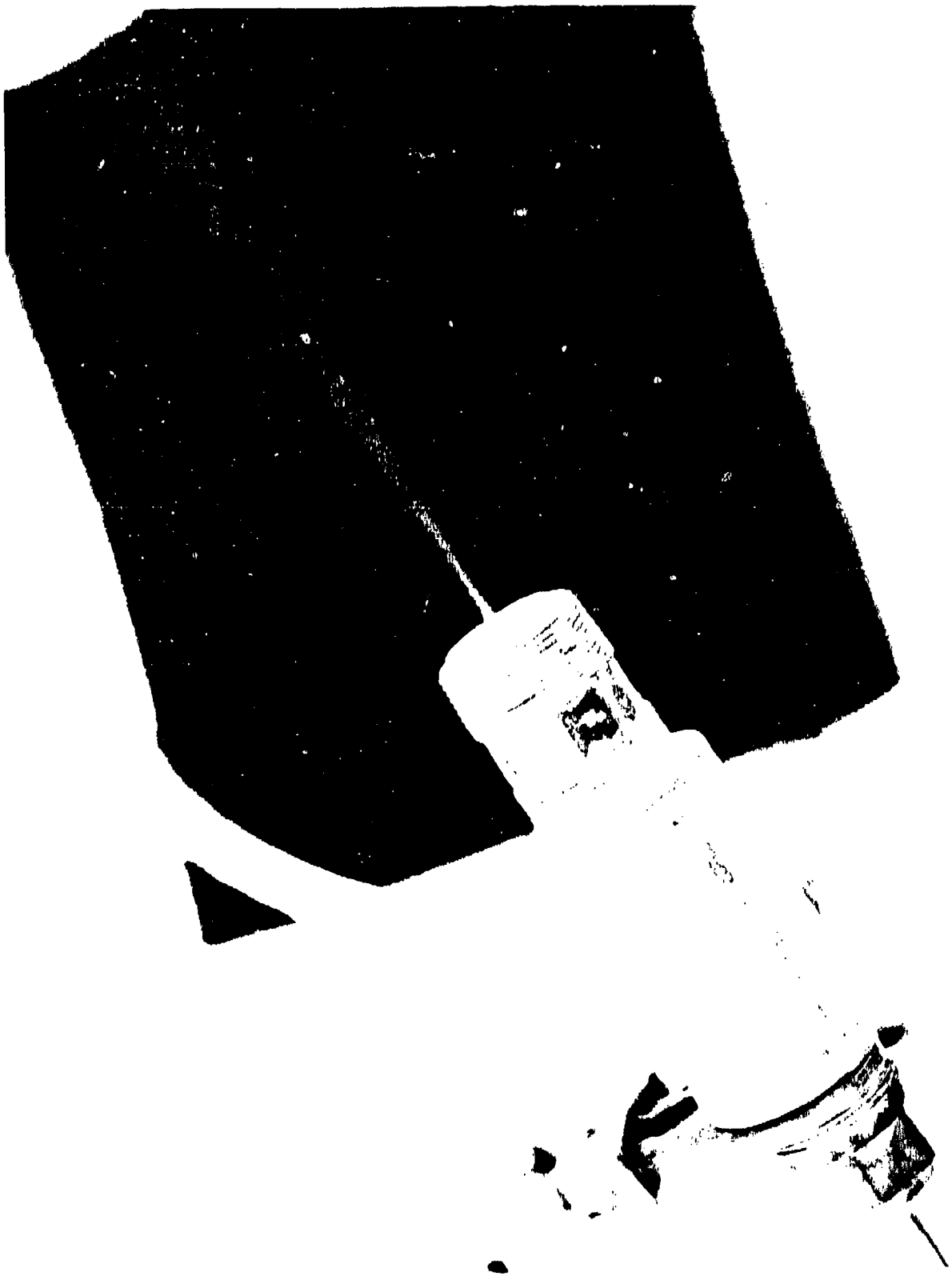

Figure F.4. Sonic Nozzle Disseminating Talc

Figure F.5. Test Enclosure at Far End of Facility

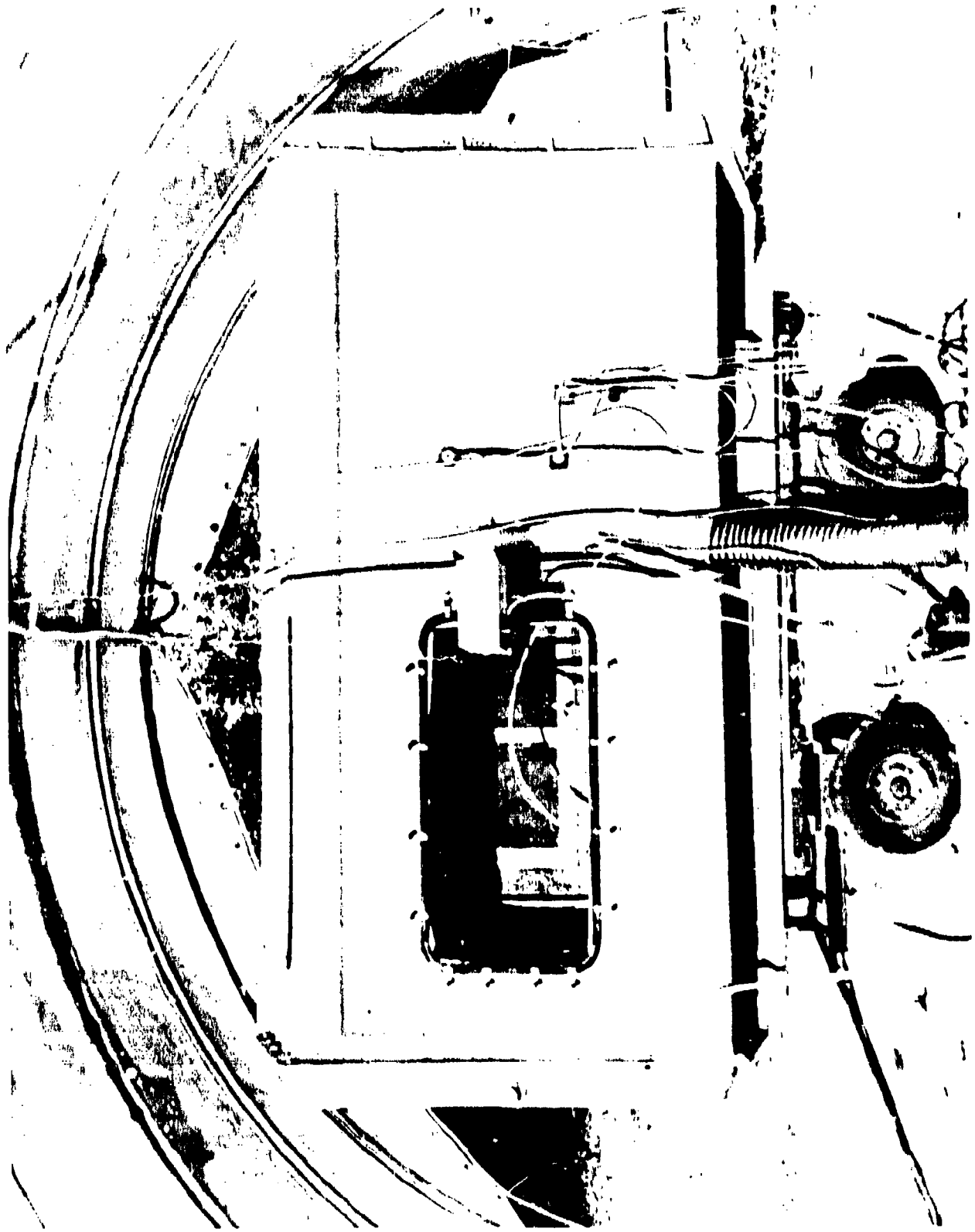

Figure F.6. Test Enclosure View from Within Facility

Figure F.7. Enclosure Window: 10mm Thick Perspex Plates

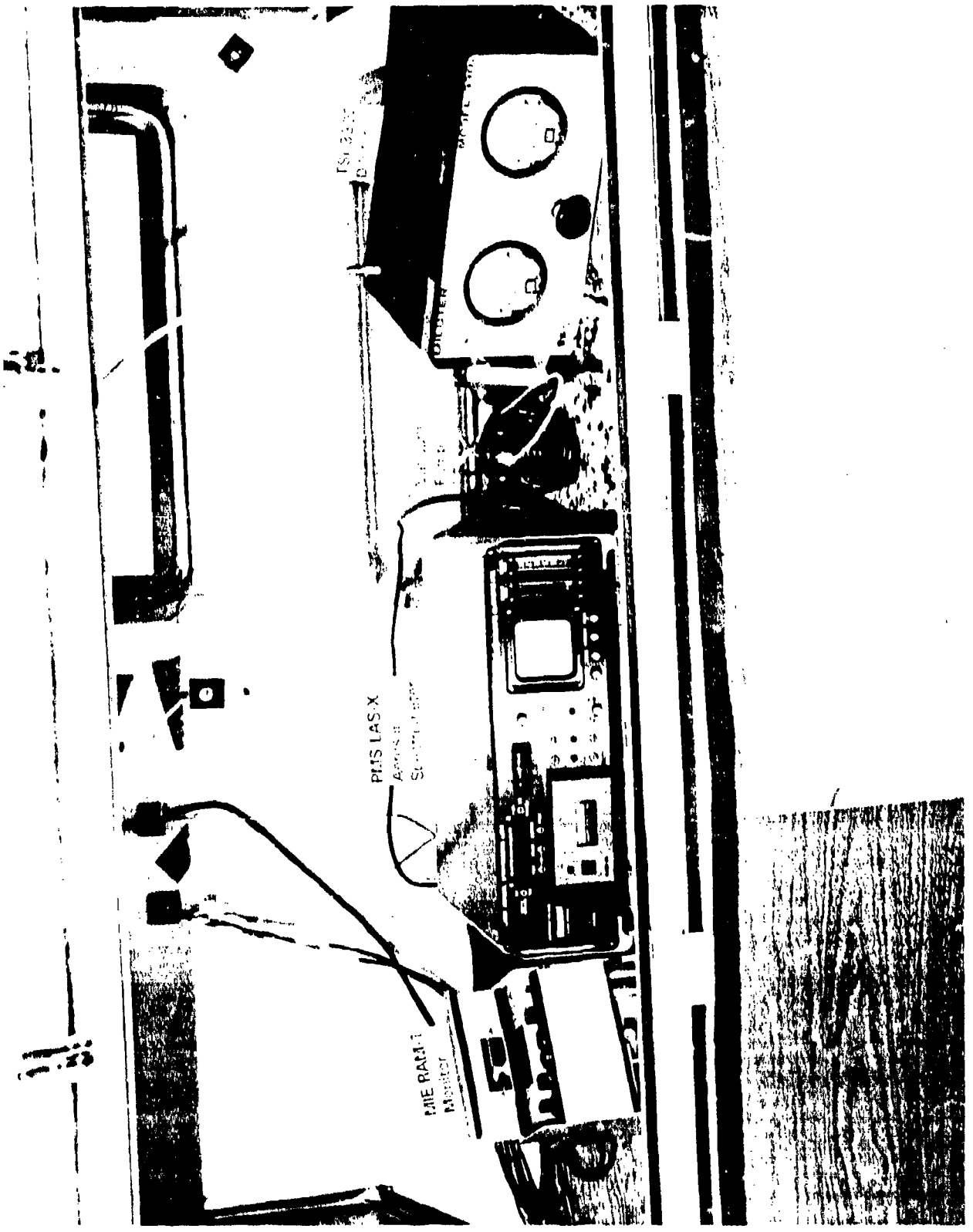

Figure F.8. Test Instrumentation Inside Enclosure